UNIVERSITÀ DI PARMA

UNIVERSITÀ DEGLI STUDI DI PARMA

DOTTORATO DI RICERCA IN FISICA
CICLO XXXV

in CO-TUTELA con
INSTITUT QUÌMIC DE SARRIÀ,
UNIVERSITAT RAMON LLULL

PROTEIN-BASED TARGETED DELIVERY SYSTEMS FOR ANTIMICROBIAL PHOTODYNAMIC INACTIVATION

SISTEMI DI TRASPORTO BASATI SU PROTEINE E DOTATI DI CAPACITÀ DI INDIRIZZAMENTO PER L'INATTIVAZIONE FOTODINAMICA DI MICROORGANISMI

Coordinatore: Chiar.mo Prof. STEFANO CARRETTA

Tutore: Chiar.mo Prof. CRISTIANO VIAPPIANI
Tutore: Chiar.mo Prof. SANTI NONELL MARRUGAT

Dottorando: ANDREA MUSSINI

Anni accademici 2019/2020 – 2021/2022

TESI DOCTORAL

Títol	**Protein-Based Targeted Delivery Systems for Antimicrobial Photodynamic Inactivation**
Realitzada per	**Andrea Mussini**
en el Centre	**Institut Químic de Sarrià, School of Engineering**
i en el Departament	**Química Analítica i Aplicada**
Dirigida per	**Prof. Santi Nonell Marrugat** **Prof. Cristiano Viappiani**

C. Claravall, 1-3 | 08022 Barcelona | Tel. 93 602 22 00 | Fax 93 602 22 49 | info@url.edu | www.url.edu

Ringrazio infinitamente i miei genitori.
Non potrò mai ripagarvi né ringraziarvi abbastanza per tutto ciò che avete fatto per me e che mi avete dato. Senza di voi non sarei mai potuto arrivare fin qui ed è grazie a voi che oggi sono ciò che sono.
A mamma e papà: grazie per il vostro amore, supporto e incoraggiamento.

«**It is not difficult** to make microbes resistant to penicillin in the laboratory by exposing them to concentrations not sufficient to kill them, and the same thing has occasionally happened in the body. The time may come when penicillin can be bought by anyone in the shops. Then there is the danger that the ignorant man may easily underdose himself and by exposing his microbes to non-lethal quantities of the drug make them resistant.»

Sir Alexander Fleming, *Nobel Lecture in Physiology or Medicine*, 11 December 1945

«**This is our fault**. Doctors over-prescribing antibiotics. Got a cold? Take some penicillin. Sniffles? No problem. Have some Azithromycin. Is that not working anymore? Well, got your Levaquin. Antibacterial soaps in every bathroom. We'll be adding Vancomycin to the water supply soon. We bred these super bugs. They're our babies. Now they're all grown up and they've got body piercings and a lot of anger.»

Dr. House – Medical Division, season 1, episode 4. *FOX*, 2004.

«The time for talk has passed—it's time to act. The "bad bugs, no drugs" problem is growing more severe, and patients are suffering. […]
New drugs are desperately needed to treat serious as well as common infections (e.g., blood, heart, and urinary tract infections; pneumonia; childhood middle-ear infections; boils; food poisoning; gonorrhea; sore throat, etc.). The bacteria that cause these infections are becoming increasingly resistant to the antibiotics that for years have been considered standard of care, and the list of resistant pathogens keeps growing. It is not possible to predict when an epidemic of drug-resistant bacteria will occur— but we do know **it will happen**.»

Bad bugs, no drugs: as antibiotic discovery stagnates, a public health crisis brews. Alexandria, VA: *Infectious Diseases Society of America*, 2004

«Antimicrobial resistance (AMR), and in particular resistance of bacteria to antibiotics (antibiotic resistance), is an urgent public health and socio-economic problem that has a profound effect on the world […]. The impact of drug resistance could affect people anywhere. Moreover, inappropriate use of antibiotics further exacerbates AMR. […] Although the risks of AMR are shared by all countries globally, low- and middle-income countries bear a more significant burden of infectious disease and will be most adversely affected by AMR. Building on previous G7 commitments, alongside those in the WHO AMR Global Action Plan, we acknowledge AMR as a shared responsibility and we commit to intensifying our activities and to take further urgent and tangible action in order to address AMR. We are convinced that **the time to act is now**.
We acknowledge that AMR further emerges and spreads at the human, animal, plant and environment interface and requires an integrated One Health approach.»

G7 Health Ministers' Communiqué. 20 May 2022, Berlin

Contents

Acronyms

AMR: antimicrobial resistance.
aPDT: antimicrobial photodynamic therapy.
CD: circular dichroism.
DMSO: dimethyl sulfoxide.
DOL: degree of labeling.
EITC: eosin isothiocyanate.
FCS: fluorescence correlation spectroscopy.
Ig: immunoglobulin.
IgG: immunoglobulin G.
LB: Luria-Bertani (liquid media).
LFP: laser flash photolysis.
MB: methylene blue.
NIR: near-infrared.
PBS: phosphate-buffered saline.
PDT: photodynamic therapy.
PIT: photoimmuno therapy.
PS: photosensitizer.
ROS: reactive oxygen species.
STED: stimulated emission depletion.
STORM: stochastic optical reconstruction microscopy.
TCSPC: time-correlated single photon counting.
TSB: tryptic soy broth.
UV: Ultraviolet.

Foreword

This thesis reports the studies of antimicrobial PDT that we have conducted through the construction of supramolecular modular complexes.
During the PhD, however, we also conducted other studies always related to PDT:

- We studied the interaction between hypericin and SARS-CoV-2 viral particles and the phototoxic action caused by the PS.
- We evaluated the applications of antibodies in anti-tumor PDT.

1 Summary

Since the introduction of antibiotics, microorganisms have started to develop resistance to them and nowadays, due to the abuse of these drugs and the lack of discovery of new classes of antibiotics, antimicrobial resistance is one of the most pressing threats for world public health [1].

Among microorganisms, bacterial resistance to antibiotics is a "silent pandemic" that in 2019 led to the deaths of nearly 5 million people [2] and, without actions and innovations, in 2050 the death rate will rise to 10 million [3]. From this point of view, one of the most worrying bacteria is *S. aureus*, classified by the WHO as a high priority bacterium.

The aim of this project is to develop supramolecular complexes for targeted antimicrobial photodynamic therapy (aPDT) against bacteria, in particular *S. aureus*.

aPDT is a promising technique for countering antibiotic resistance [4] thanks to its fast action and its ability to target different biomolecules. Therefore, microorganisms are not expected to develop resistance to aPDT. PDT is based on the use of photosensitizers (PS), i.e. molecules that can be excited by visible light of appropriate wavelength and, from the excited states, generate reactive oxygen species that are toxic for the target cell. After photoexcitation to an electronically excited state, a PS normally undergoes transition to the triplet state, which can interact with molecular oxygen in two different ways, by electron transfer (type I) or by energy transfer (type II), leading to the formation of reactive oxygen species (radicals and singlet oxygen, respectively). These highly reactive species have a cytotoxic action, through damage to biological macromolecules present in cells, leading to cell death.

Using a modular approach, in this work, we developed supramolecular complexes that are able to deliver the PS to the target cell. These complexes are formed by three components: the PS, the junction system and the targeting system. The PS elicits the photocytotoxic action when exposed to visible light, and the junction system, formed by streptavidin (a tetrameric protein) and biotin (a vitamin), connect the PS to the targeting system which allows to drive the photoactive unit towards the target cells.

We chose this approach because it is inherently flexible. PSs can be modified by adding to them an appropriate chemical group that is reactive towards amino acid side chains (Lys, Cys, …) and thus allows binding them to proteins, in our case streptavidin. Depending on the target molecule/cell type, it is possible to choose an appropriate targeting protein that can be functionalized with biotin. Finally, by exploiting the high affinity between streptavidin and biotin, it is possible to link the two parts (PS-streptavidin and biotinylated targeting molecule) to form the supramolecular complex.

We have created and characterized two different complexes (**Figure 1**): one that has eosin as PS and the antibody Immunoglobulin G (IgG) as targeting system and one that contains methylene blue as a PS, and the protein concanavalin A (ConA) as the targeting system.

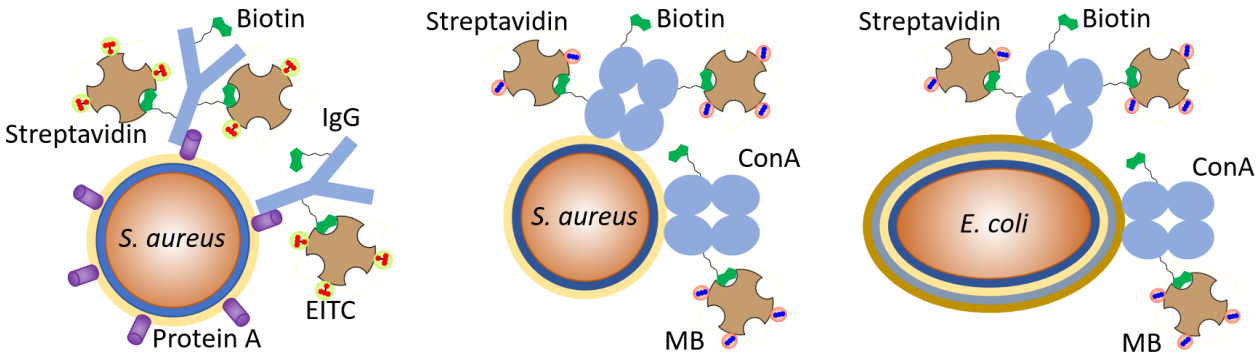

Figure 1. Cartoon representation of the complexes developed in this work. We labelled streptavidin with a PS (EITC or MB) and the targeting molecule (IgG or ConA) with biotin, then exploited the high affinity between streptavidin and biotin to form the complex.

Using fluorescence anisotropy and FCS we confirmed that both the PSs (EITC and MB, respectively) are bound to streptavidin.

We characterized some photophysical properties of EITC-streptavidin and MB-streptavidin, and in both cases, we observed that when the PS is bound to the protein, all quantum yields (of fluorescence, triplet state formation and singlet oxygen formation) decrease. Furthermore, with the EITC-labeled streptavidin we noticed that the quantum yields decrease as the number of PS molecules present on the same protein increase.

Using FCS we confirmed that labeled streptavidin bound to biotinylated targeting system (IgG and ConA, respectively) and that the latter is required to target bacteria; this was further confirmed by the photoinactivation where in absence of the targeting system the cell death was orders of magnitude lower (around 4 logs).

Microscopy measurements showed that the first complex selectively target *S. aureus*, while the second one target both *S. aureus* and *E. coli*.

Finally, performing photoinactivation tests we obtained an efficiently cell death against *S. aureus* with the first complex (8 logs with 2 µM of EITC and 50 J/cm^2) and an equivalent cell death for both *S. aureus* and *E. coli* with the second complex (4 logs with 5 µM of MB and 200 J/cm^2).

1.1 Sommario

Dall'introduzione degli antibiotici, i microrganismi hanno iniziato a sviluppare resistenza ad essi e oggigiorno, a causa dell'abuso di questi farmaci e della mancata scoperta di nuove classi di antibiotici, la resistenza antimicrobica è una delle minacce più urgenti per la salute pubblica mondiale [1].

Tra i microrganismi, la resistenza batterica agli antibiotici è una “pandemia silenziosa” che nel 2019 ha portato alla morte di quasi 5 milioni di persone [2] e, senza azioni e innovazioni, nel 2050 il tasso di mortalità salirà a 10 milioni [3]. Da questo punto di vista, uno dei batteri più preoccupanti è *S. aureus*, classificato dall'OMS come batterio ad alta priorità.

Lo scopo di questo progetto è lo sviluppo di complessi supramolecolari per la terapia fotodinamica antimicrobica mirata (aPDT) contro i batteri, in particolare *S. aureus*.

La aPDT è una tecnica promettente per contrastare la resistenza agli antibiotici [4] grazie alla sua rapida azione e alla sua capacità di bersagliare diverse biomolecole. Pertanto, non si prevede che i microrganismi sviluppino resistenza alla aPDT.
La PDT si basa sull'utilizzo di fotosensibilizzatori (PSs), cioè molecole che possono essere eccitate dalla luce visibile di opportuna lunghezza d'onda e, dagli stati eccitati, generare specie reattive dell'ossigeno tossiche per la cellula bersaglio. Dopo la fotoeccitazione a uno stato elettronico eccitato, un PS normalmente subisce la transizione allo stato di tripletto, che può interagire con l'ossigeno molecolare in due modi diversi, per trasferimento di elettroni (tipo I) o per trasferimento di energia (tipo II), portando alla formazione di specie reattive dell'ossigeno (radicali e ossigeno singoletto, rispettivamente). Queste specie altamente reattive hanno un'azione citotossica, tramite il danneggiamento delle macromolecole biologiche presenti nelle cellule, portando alla morte cellulare.

Utilizzando un approccio modulare, in questo lavoro, abbiamo sviluppato complessi supramolecolari in grado di trasportare il PS alla cellula bersaglio. Questi complessi sono formati da tre componenti: il PS, il sistema di giunzione e il sistema di indirizzamento. Il PS provoca l'azione fotocitotossica quando viene esposto alla luce visibile, e il sistema di giunzione, formato da streptavidina (una proteina tetramerica) e biotina (una vitamina), collega il PS al sistema di indirizzamento che permette di portare l'unità fotoattiva verso le cellule bersaglio.

Abbiamo scelto questo approccio perché è intrinsecamente flessibile. I PSs possono essere modificati aggiungendo ad essi un gruppo chimico appropriato che sia reattivo nei confronti delle catene laterali degli amminoacidi (Lys, Cys, …) e permetta quindi di legarli alle proteine, nel nostro caso la streptavidina. A seconda del tipo di molecola/cellula bersaglio, è possibile scegliere una proteina di indirizzamento appropriata che può essere funzionalizzata con la biotina. Infine, sfruttando l'elevata affinità tra streptavidina e biotina, è possibile legare le due parti (PS-streptavidina e molecola bersaglio biotinilata) per formare il complesso supramolecolare.

Abbiamo realizzato e caratterizzato due diversi complessi (**Figura 1**): uno che ha l'eosina come PS e l'anticorpo immunoglobulina G (IgG) come sistema di indirizzamento e uno che sfrutta il blu di metilene come PS e la proteina concanavalina A (ConA) come sistema di indirizzamento.

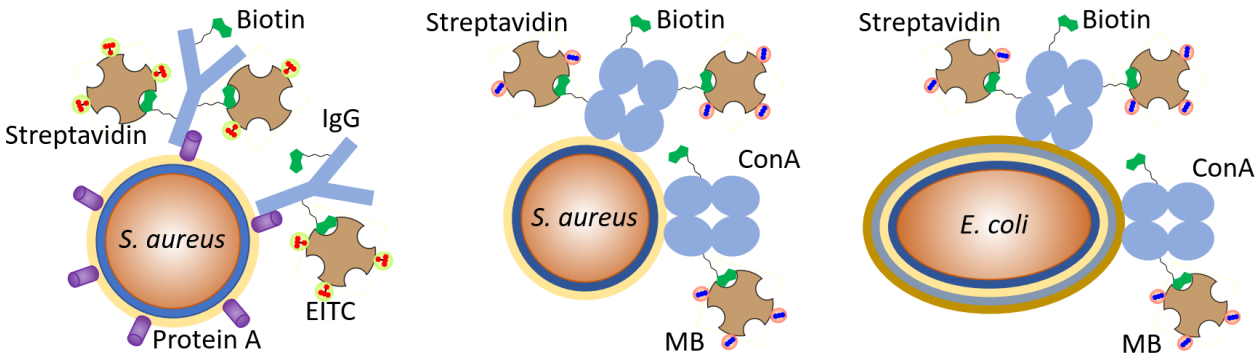

Figura 1. Rappresentazione a cartoon dei complessi sviluppati in questo lavoro. Abbiamo marcato la streptavidina con un PS (EITC o MB) e la molecola di indirizzamento (IgG o ConA) con la biotina, quindi abbiamo sfruttato l'elevata affinità tra streptavidina e biotina per formare il complesso.

Usando anisotropia di fluorescenza e FCS abbiamo confermato che entrambi i PS (EITC e MB, rispettivamente) sono legati alla streptavidina.

Abbiamo caratterizzato alcune proprietà fotofisiche di EITC-streptavidina e MB-streptavidina e, in entrambi i casi, abbiamo osservato che quando il PS è legato alla proteina, tutte le rese quantiche (di fluorescenza, formazione dello stato di tripletto e formazione di ossigeno singoletto) diminuiscono. Inoltre, con la streptavidina marcata con EITC abbiamo notato che le rese quantiche diminuiscono all'aumentare del numero di molecole di PS presenti sulla stessa proteina.

Usando FCS abbiamo confermato che la streptavidina marcata si lega al sistema di indirizzamento biotinilato (IgG e ConA, rispettivamente) e che quest'ultimo è necessario per bersagliare i batteri; ciò è stato ulteriormente confermato dalla fotoinattivazione in cui in assenza del sistema di indirizzamento la morte cellulare era ordini di grandezza inferiore (circa 4 log).

Le misurazioni al microscopio hanno mostrato che il primo complesso bersaglia selettivamente *S. aureus*, mentre il secondo bersaglia sia *S. aureus* che *E. coli*.

Infine, eseguendo test di fotoinattivazione abbiamo ottenuto una morte cellulare efficiente contro *S. aureus* con il primo complesso (8 log con 2 μM di EITC e 50 J/cm^2) e una morte cellulare equivalente sia per *S. aureus* che per *E. coli* con il secondo complesso (4 log con 5 μM di MB e 200 J/cm^2).

1.2 **Resum**

Des de la introducció dels antibiòtics, els microorganismes han començat a desenvolupar resistència a ells i, avui dia, a causa de l'abús d'aquests fàrmacs i la manca de descobriment de noves classes d'antibiòtics, la resistència antimicrobiana és una de les amenaces més urgents per a la salut pública mundial [1].

Entre els microorganismes, la resistència bacteriana als antibiòtics és una “pandèmia silenciosa” que el 2019 va provocar la mort de gairebé 5 milions de persones [2] i, sense accions i innovacions, el 2050 la taxa de mortalitat pujarà a 10 milions [3]. Des d'aquest punt de vista, un dels bacteris més preocupants és **S. aureus**, classificat per l'OMS com a bacteri d'alta prioritat.

L'objectiu d'aquest projecte és desenvolupar complexos supramoleculars per a la teràpia fotodinàmica antimicrobiana dirigida contra bacteris (aPDT), en particular *S. aureus*.

La PDT és una tècnica prometedora per oposar la resistència als antibiòtics [4] gràcies a la seva ràpida acció i capacitat per apuntar diferents biomolècules. Per tant, no s'espera que els microorganismes desenvolupin resistència a la aPDT.
La PDT es basa en l'ús de fotosensibilitzadors (PSs), és a dir, molècules que poden ser excitades per la llum visible d'una longitud d'ona adequada i, a partir dels estats excitats, generar espècies reactives d'oxigen tòxiques per a la cèl·lula objectiu. Després de la fotoexcitació a un estat electrònic excitat, un PS normalment pateix la transició a l'estat triplet, que pot interactuar amb l'oxigen molecular de dues maneres diferents, per transferència d'electrons (tipus I) o per transferència d'energia (tipus II), fet que porta a la formació d'espècies reactives d'oxigen (radicals i oxigen singlet, respectivament). Aquestes espècies altament

reactives tenen una acció citotòxica, en danyar les macromolècules biològiques presents a les cèl·lules, cosa que porta a la mort cel·lular.

Usant un enfocament modular, en aquest treball, hem desenvolupat complexos supramoleculars capaços de transportar el PS a la cèl·lula objectiu. Aquests complexos consten de tres components: el PS, el sistema d'unió i el sistema d'orientació. El PS provoca una acció fotocitotòxica quan s'exposa a la llum visible, i el sistema d'unió, format per estreptavidina (una proteïna tetramèrica) i biotina (una vitamina), connecta el PS al sistema d'orientació que permet que la unitat fotoactiva sigui transportada cap a les cèl·lules objectiu.

Triem aquest enfocament perquè és inherentment flexible. Els PSs poden modificar-se afegint-los un grup químic apropiat que sigui reactiu amb les cadenes laterals dels aminoàcids (Lys, Cys, …) i per tant els permeti unir-se a les proteïnes, en el nostre cas l'estreptavidina. Depenent del tipus de molècula/cèl·lula objectiu, es pot triar una proteïna d'encaminament adequada que es pot funcionalitzar amb la biotina. Al final, aprofitant l'alta afinitat entre l'estreptavidina i la biotina, és possible unir les dues parts (PS-estreptavidina i molècula diana biotinilada) per formar el complex supramolecular.

Hem construït i caracteritzat dos complexos diferents (**Figura 1**): un que té l'eosina com a PS i l'anticòs immunoglobulina G (IgG) com a sistema d'orientació i un altre que explota el blau de metilè com a PS i la proteïna concanavalina A (ConA) com a sistema d'orientació.

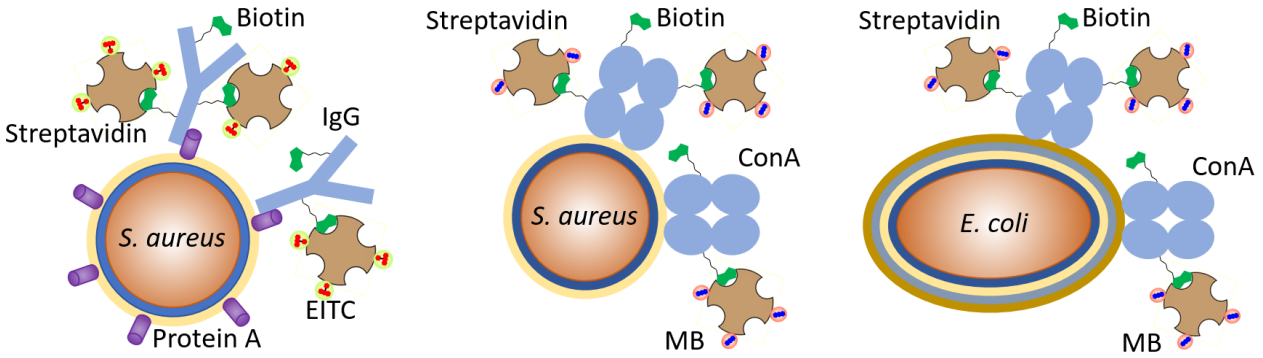

Figura 1. Representació cartoon dels complexos desenvolupats en aquest treball. Vam etiquetar l'estreptavidina amb un PS (EITC o MB) i la molècula d'orientació (IgG o ConA) amb biotina, després vam aprofitar l'alta afinitat entre l'estreptavidina i la biotina per formar el complex.

Usant anisotropia de fluorescència i FCS, confirmem que tots dos els PSs (EITC i MB, respectivament) estan units a estreptavidina.

Caracteritzem algunes propietats fotofísiques d'EITC-estreptavidina i MB-estreptavidina i, en tots dos casos, observem que quan el PS s'uneix a la proteïna, tots els rendiments quàntics (de fluorescència, formació d'estat triplet i formació d'oxigen singlet) disminueixen. A més, amb l'estreptavidina marcada amb EITC notem que els rendiments quàntics disminueixen amb l'augment del nombre de molècules de PS presents a la mateixa proteïna.

Usant FCS, confirmem que l'estreptavidina marcada s'uneix al sistema d'adreçament biotinilat (IgG i ConA, respectivament) i que aquest últim és necessari per apuntar els bacteris; això es va confirmar a més mitjançant la fotoinactivació en què, en absència del sistema d'orientació, la mort cel·lular va ser ordres de magnitud menor (al voltant de 4 log).

Els mesuraments microscòpics van mostrar que el primer complex apunta selectivament a *S. aureus*, mentre que el segon apunta tant a *S. aureus* com a *E. coli*.

Al final, en realitzar proves de fotoinactivació, vam obtenir una mort cel·lular eficient contra *S. aureus* amb el primer complex (8 log amb EITC 2 µM i 50 J/cm^2) i una mort cel·lular equivalent tant per a *S. aureus* com per a *E. coli* amb el segon complex (4 log amb 5 µM de MB i 200 J/cm^2).

1.3 **Resumen**

Desde la introducción de los antibióticos, los microorganismos han comenzado a desarrollar resistencia a ellos y, hoy en día, debido al abuso de estos fármacos y a la falta de descubrimiento de nuevas clases de antibióticos, la resistencia antimicrobianaes una de las amenazas más urgentes para la salud pública mundial [1].

Entre los microorganismos, la resistencia bacteriana a los antibióticos es una "pandemia silenciosa" que en 2019 provocó la muerte de casi 5 millones de personas [2] y, sin acciones e innovaciones, en 2050 la tasa de mortalidad ascenderá a 10 millones [3]. Desde este punto de vista, una de las bacterias más preocupantes es *S. aureus*, clasificado por la OMS como bacteria de alta prioridad.

El objetivo de este proyecto es el desarrollo de complejos supramoleculares para la terapia fotodinámica antimicrobiana dirigida contra bacterias (aPDT), en particular *S. aureus*.

La PDT es una técnica prometedora para opondrar la resistencia a los antibióticos [4] gracias a su rápida acción y su capacidad para apuntar diferentes biomoléculas. Por lo tanto, no se espera que los microorganismos desarrollen resistencia a la aPDT.
La PDT se basa en el uso de fotosensibilizadores (PSs), es decir, moléculas que pueden ser excitadas por la luz visible de una longitud de onda adecuada y, a partir de los estados excitados, generar especies reactivas de oxígeno tóxicas para la célula diana. Después de la fotoexcitación a un estado electrónico excitado, un PS normalmente sufre la transición al estado triplete, que puede interactuar con el oxígeno molecular de dos maneras diferentes, por transferencia de electrones (tipo I) o por transferencia de energía (tipo II), lo que lleva a la formación de especies reactivas de oxígeno (radicales y oxígeno singlete, respectivamente). Estas especies altamente reactivas tienen una acción citotóxica, al dañar las macromoléculas biológicas presentes en las células, lo que lleva a la muerte celular.

Usando un enfoque modular, en este trabajo, hemos desarrollado complejos supramoleculares capaces de transportar el PS a la célula diana. Estos complejos constan de tres componentes: el PS, el sistema de empalme y el sistema de direccionamiento. El PS provoca una acción fotocitotóxica cuando se expone a la luz visible, y el sistema de empalme, formado por estreptavidina (una proteína tetramérica) y biotina (una vitamina), conecta el PS al sistema de direccionamiento que permite que la unidad fotoactiva sea transportada hacia las células diana.

Elegimos este enfoque porque es inherentemente flexible. Los PSs pueden modificarse añadiéndoles un grupo químico apropiado que sea reactivo con las cadenas laterales de los aminoácidos (Lys, Cys, …) y por

tanto los permita unirse a las proteínas, en nuestro caso la estreptavidina. Dependiendo del tipo de molécula/célula diana, se puede elegir una proteína de direccionamiento adecuada que se puede funcionalizar con la biotina. En el final, aprovechando la alta afinidad entre la estreptavidina y la biotina, es posible unir las dos partes (PS-estreptavidina y molécula diana biotinilada) para formar el complejo supramolecular.

Hemos construido y caracterizado dos complejos diferentes (**Figura 1**Figura 1): uno que tiene la eosina como PS y el anticuerpo inmunoglobulina G (IgG) como sistema de direccionamiento y otro que explota el azul de metileno como PS y la proteína concanavalina A (ConA) como sistema de direccionamiento.

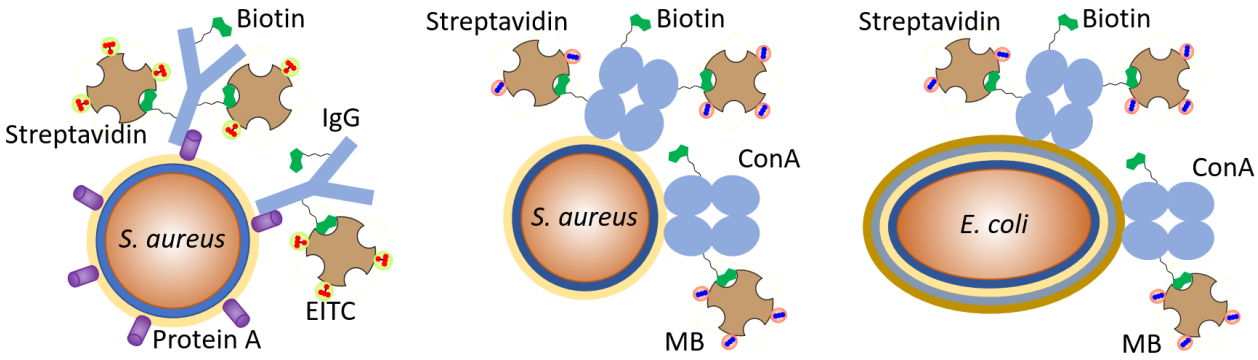

Figura 1. Representación cartoon de los complejos desarrollados en este trabajo. Marcamos la estreptavidina con un PS (EITC o MB) y la molécula de direccionamiento (IgG o ConA) con biotina, luego explotamos la alta afinidad entre la estreptavidina y la biotina para formar el complejo.

Usando anisotropía de fluorescencia y FCS, confirmamos que ambos los PSs (EITC y MB, respectivamente) están unidos a estreptavidina.

Caracterizamos algunas propiedades fotofísicas de EITC-estreptavidina y MB-estreptavidina y, en ambos casos, observamos que cuando el PS se une a la proteína, todos los rendimientos cuánticos (de fluorescencia, formación de estado triplete y formación de oxígeno singlete) disminuyen. Además, con la estreptavidina marcada con EITC notamos que los rendimientos cuánticos disminuyen con el aumento del número de moléculas de PS presentes en la misma proteína.

Usando FCS, confirmamos que la estreptavidina marcada se une al sistema de direccionamiento biotinilado (IgG y ConA, respectivamente) y que este último es necesario para apuntar las bacterias; esto se confirmó además mediante la fotoinactivación en la que, en ausencia del sistema de direccionamiento, la muerte celular fue órdenes de magnitud menor (alrededor de 4 log).

Las mediciones microscópicas mostraron que el primer complejo apunta selectivamente a *S. aureus*, mientras que el segundo apunta tanto a *S. aureus* como a *E. coli*.

En el final, al realizar pruebas de fotoinactivación, obtuvimos una muerte celular eficiente contra *S. aureus* con el primer complejo (8 log con EITC 2 µM y 50 J/cm^2) y una muerte celular equivalente tanto para *S. aureus* como para *E. coli* con el segundo complejo (4 log con 5 µM de MB y 200 J/cm^2).

2 Introduction

The treatment of bacterial infections was mainly revolutionized in 1928 by the discovery of penicillin [5]. The following years were the golden age for antibiotics, in fact the development of new antibiotics helped to further reduce the mortality caused by infectious diseases [6].
Unfortunately, this era is coming to an end: the abuse and misuse of antibiotics has led to an explosion of antimicrobial resistance (AMR) [7]. The characteristic of antibiotic-resistant bacteria is their ability to evade the targeted action of the antibiotic.
A microorganism is defined as resistant to a particular therapy if the probability of the treatment failing is high. From a quantitative point of view, however, there is no universally accepted definition; clinically a microorganism is defined as resistant to a given antibiotic if, in all strains, the minimum inhibitory concentration is higher than a previously defined limit (breakpoint) [8] which definition, however, varies over time [9].
Bacteria can develop resistance to antibiotics thanks to the appearance of gene mutations or by horizontal transfer (conjugation mediated by plasmids, transformation mediated by bacteriophages, transduction with absorption of extracellular DNA) [10]. Furthermore, the genes that allow them to survive diffuse and propagate easily among bacteria living in the same environment [10].
At the level of a single nucleotide the probability of a mutation occurring in a bacterium, thanks to which the microorganism is resistant, is about 10^{-9}-10^{-7} per replication [8]. Although this probability is small, it is still more than sufficient for the generation of resistant microorganisms.
Bacteria containing genes that provide antibiotic resistance may exhibit different resistance mechanisms, which can be grouped as following [10]:

- Inhibit the entry of the antibiotic by reducing the permeability of the cell membrane.
- Increase efflux, i.e. by transporting the antibiotic out of the cell using an efflux pumps.
- Modify the molecular target recognized by the antibiotic, so that the drug has a lower affinity for the target but still guaranteeing the latter to perform its biological functions. This modification can occur through a mutation of the genetic sequence of the target or through a subsequent chemical modification.
- Inactivate the antibiotic through enzymes that degrade or modify it.

Antibiotic resistance comes from the natural selective pressure to which bacteria are subjected from treatments in which antibiotics are used [8]. These resistance mechanisms put in place by bacteria, however, were not born due to antibiotics, in fact they already existed before and derive from millions of years of evolution that bacteria have undergone due to the constant competition for environmental resources [11].
In recent years, antibiotic resistance originates in three areas [12] (**Figure 2**): in the hospital setting; on animal farms (where antibiotics are also used to promote the growth of livestock); and in the environment that can be "contaminated" with antibiotics in various ways (agriculture, excretions, wastewater, especially in aerial sewage, and inadequate disposal of drugs). Moreover, the environment allows the evolution of resistance but above all its transmission via contaminated food, water and surfaces [11].
For these reasons it is necessary to use the One Health approach which «recognizes the inextricable link between humans, animals, and the environment to achieve better community health and well-being» [13].

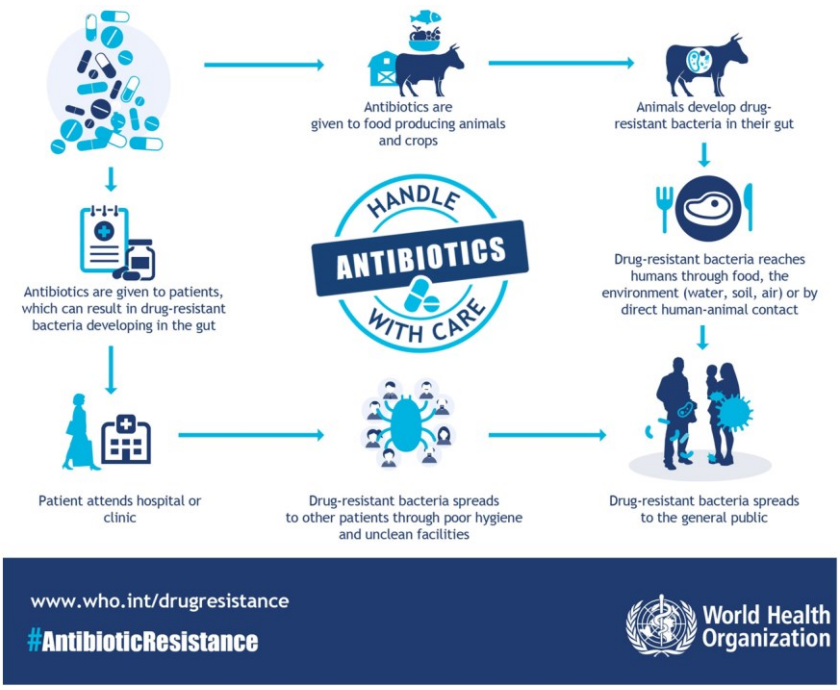

Figure 2. Spread of antibiotic resistance. Antimicrobial resistance arises and spreads in farms, hospitals and the environment.

As reported by the World Economic Forum Global Risks, antibiotic resistance is one of the biggest and most pressing global health problems [10]. In fact, the appearance and the increase of resistance negatively affects the possibility of treating infections and compromises the effectiveness of immunosuppressive treatments [8].

The principal bacteria that have developed drug resistance and that therefore are of greatest concern are: methicillin-resistant *Staphylococcus aureus* (MRSA), vancomycin-resistant *Enterococcus faecalis* (VRE), carbapenem-resistant *Klebsiella*, *Escherichia coli* and some mycobacteria [14].

According to estimates [10], due to antibiotic-resistant bacteria, every year in Europe 25,000 people die (for an economic cost of 1.5 billion €) and 23,000 in the USA.

The most comprehensive research to date on bacterial resistance has recently been conducted [2] comprising 204 countries, 23 bacterial strains and 88 pathogen-antibiotic combinations. This study [2] estimates that in 2019 there were 4.95 million deaths related to antibiotic-resistant bacteria and of these 1.27 million are directly attributable to them. By comparison, worldwide this number of deaths is comparable to the sum of deaths caused by malaria (627,000) and HIV (680,000) and, considering the deaths caused by infections, it is second only to those caused by tuberculosis and COVID-19 [15].

Without interventions, it is estimated [3] that by 2050 antibiotic-resistant microorganisms could cause 10 million deaths each year and that this economic burden is about 100 trillion $; in comparison, antibiotic-resistant bacteria would cause more deaths than cancers in 2050.

Of all these 4.95 million deaths, 73.4% are due to just six bacterial strains: *Escherichia coli*, *Staphylococcus aureus*, *Klebsiella pneumoniae*, *Streptococcus pneumoniae*, *Acinetobacter baumannii*, *Pseudomonas aeruginosa* [2].

The WHO categorizes antibiotic-resistant bacteria according to the level of priority for research and development of new antibiotics [12]: critical priority (*Acinetobacter baumannii*, *Pseudomonas aeruginosa*, *Enterobacteriaceae* (*Klebsiella pneumoniae*, *Escherichia coli*, *Enterobacter* spp., *Serratia* spp., *Proteus* spp., *Providencia* spp., *Morganella* spp.)), high priority (*Enterococcus faecium*, *Staphylococcus aureus*, *Helicobacter*

pylori, *Campylobacter* spp., *Salmonella* spp., *Neisseria gonorrhoeae)*, medium priority (*Streptococcus pneumoniae*, *Haemophilus influenzae*, *Shigella* spp.).

In the high-income GBD (Global Burden of Disease) super-region about half of all deaths are caused by just two bacteria: *S. aureus* (with 25.4% resistance-related deaths) and *E. coli* (with 24.3%) [2].
Geographically, the distribution of bacteria and their resistance is very varied. For example, in the GBD region of Australasia 28 deaths out of 100,000 are related to antibiotic-resistant bacteria (of which 6.5 are directly attributable to them) while in the region of western sub-Saharan Africa deaths related to antibiotic-resistant bacteria are 114.8 (of which 27.3 directly attributable to them) [2].

Among resistance developing bacteria, *S. aureus* is of special interest.
S. aureus is a Gram-positive bacterium belonging to the group of cocci, bacteria that have a spherical shape. In humans, *S. aureus* is a bacterium that can be found in the nasal cavities, on the skin and in the intestines. It is a commensal microorganism that is found in about 20-30% of the population [16] but it also acts as an opportunistic pathogen that can cause various diseases: mild skin infections, food poisoning, severe respiratory infections and life-threatening diseases (such as pneumonia, meningitis, osteomyelitis, endocarditis, toxic shock syndrome, bacteremia and sepsis) [17], [18].
Its infections can come from farms, from the ingestion of contaminated food, from contaminated surfaces (often plastics on which it is found in form of biofilm) or it can act in an opportunistic way causing a secondary infection [19]. *S. aureus* is among the five most common causes of nosocomial infections and often infects wounds after surgery. Each year in the United States, approximately 500,000 patients in hospitals are infected with this bacterium [115] and up to 50,000 deaths are attributable to the infections it causes [116].

An additional problem with *S. aureus* is that it can easily develop resistance to antibiotics [20], such as penicillin, methicillin and vancomycin.
S. aureus is defined as methicillin resistant (MRSA) when it has a modification of the penicillin-binding antigens which causes its lower affinity for that antibiotic and other β-lactam antibiotics. Given the lower efficacy of these antibiotics against MRSA, this bacterium is recognized as a worldwide problem in clinical medicine [21] and one of the most widespread bacteria with multidrug resistance (for penicillin, methicillin, vancomycin and others) in both hospitals and the general population [22], [23].
It is estimated [2] that in 2019 MRSA caused more than 100,000 deaths and that its distribution in the world is uneven (from 60% to 80% in the countries of North Africa and Middle East and less than 5% in several countries of Europe and sub-Saharan Africa).

To infect the host, *S. aureus* has a wide variety of virulence factors available. In fact, on its surface, it has different types of proteins that allow it to adhere to tissues, escape or inactivate the immune system and secrete toxins that destroy cells [16].
Among these virulence factors, there are some proteins exploited by *S. aureus* [16]:

- Hemolysins (α-, β-, γ-, δ-), they cause the formation of pores on the host cells and induce their lysis.
- Panton-valentine leukocidin (PVL), it induces lysis of white blood cells.
- Phenol-soluble modulins (PSMα, PSMβ), they cause the formation of pores on host cells inducing their lysis and favoring the formation of biofilms.
- Epidermal cell differentiation inhibitor exotoxins (EDIN-A, EDIN-B), they cause the formation of dilated pores in the host cells, compromising their integrity.
- Exfoliative toxins (ET-A, ET-B, ET-C, ET-D), they destroy the adhesion between cells causing them to dissociate.

- Staphylococcal enterotoxins (SE-A – SE-IV), they induce food poisoning and are linked to inflammatory molecules.
- Toxic shock syndrome toxin 1 (TSST-1), stimulates the release of cytokines which can cause toxic shock syndrome.
- Staphylococcal protein A (SpA), inhibits the host's immune response by binding IgG.

As mentioned, *S. aureus* can alter the activity of the host's immune system and it can use opsonization inhibition to do so because, on its surface, *S. aureus* has three types of proteins that allow it to bind the Fc domains of Ig: protein A (SpA), *S. aureus* binder of IgG (Sbi), staphylococcal superantigen-like protein 10 (SSL10) [19].
Furthermore, *S. aureus* has the ability to produce several proteins that inhibit the complement system [19], a non-specific defense mechanism that allows to eliminate components not belonging to the organism.
Given their key role in evasion of both innate and adaptive immunity, many virulence factors are used as targets for immunization strategies and vaccines. Unfortunately, however, these approaches have often failed in clinical trials or have not yet been approved for clinical use. As reported in a study [24] the reasons why classical antibody-based approaches against *S. aureus* are failing may be:

- Only one antigen present on the cell wall is targeted. However, *S. aureus* has several extracellular factors and simply targeting only one of these antigens is difficult to damage this bacterium.
- *S. aureus* may have developed many virulence factors specific to humans but few to other species. In fact, therapies that have been shown to be effective in mice have not shown as much protection in humans.
- Since high levels of antibodies against S. aureus are naturally present in human serum, it is possible that increasing the amount of antibodies does not significantly increase the phagocytosis of the bacterium. In fact, unlike what has been demonstrated in preclinical studies on mice, there is no increase in opsonization in humans.

Bacteria are often found in environments where they are exposed to sub-inhibitory concentrations of antibiotics. Being in an unfavorable environment which, however, is not able to destroy them, the bacteria undergo alterations in their cellular morphology and in their virulence.
In vitro, in the presence of sub-inhibitory concentrations of antibiotics, *S. aureus* can undergo some main changes [25]. A morphological change can be due to the cell deformation, the modification of the constituents of the cell membrane or the rupture of the cell wall. Adhesiveness and invasiveness may change, and their change depends on the considered bacterium and host cell; an increase in adhesion does not always imply a better cellular invasiveness. The virulence factors can be altered, the use of different antibiotics leads to an increase or a decrease in the expression of virulence factors. Small colonies variant (SCV, slow-growing bacteria exhibit unusual metabolism and form atypical colonies) can be formed and, in general, is favored; in the case of *S. aureus* these SCV are involved in small persistent and recurrent infections; SCV formation is generally favored. Biofilm formation (microorganisms that grow on a surface adhere to each other) can be favored or inhibited, depending on the bacterium considered and the stage of development of the biofilm.

Among the main strategies to combat antimicrobial resistance there are [2]: prevention and control, limiting the use of antibiotics for the non-treatment of human diseases and for purposes not aimed at improving human health, intensifying efforts and research for the development of new antibiotics, use of the One Health approach.
Unfortunately, one of the main limitations in the fight against antibiotic-resistant bacteria is the lack and difficulty in developing new types of antibiotics [10].

The possibility of prevention through vaccines is also subject to many adversities so much that, among the most lethal and with a higher priority bacteria, vaccination is available only for *S. pneumoniae* [26].

The difficulty in dealing with antibiotic-resistant bacteria has been declared by the WHO as one of the most pressing global threats to human health in the 21st century [27]. Therefore, efforts must be renewed to seek new approaches to combat these microorganisms and it should be done so that they cannot develop antibiotic resistance.

3 Photodynamic therapy

In the context of antibiotic resistance, a promising strategy for fighting antibiotic-resistant bacteria is antimicrobial Photodynamic Therapy (aPDT), also called antimicrobial photodynamic inactivation (PDI).
PDT is a selective, non-invasive therapy that can be used to destroy target cells by affecting the integrity of a variety of molecular components by photo-oxidative damages. Thanks to this mechanism, bacteria are unlikely to develop resistance to aPDT [4], [28].

More than a quarter of a century ago PDT was approved for the clinical treatment of certain cancers and today its range of applications has expanded enormously to include fields such as cardiology, urology, immunology, ophthalmology, dentistry, dermatology and cosmetics [29]. PDT is successfully used also for the treatment of viral (antiviral PDT) [30] and fungal infections [31] , for the sterilization and the sanitation of water sources and surfaces [32].

PDT is based on the simultaneous presence of three independently non-toxic components: a photosensitizer (PS), molecular oxygen and visible (or near infrared) light [33]. After being excited with light of an appropriate wavelength, the electronically excited state of the PS interacts with molecular oxygen and generates singlet oxygen and reactive oxygen species (ROS) in the target cells, leading to cell death [34]. The phototoxic properties of PDT have been shown to be caused by the oxidation of different types of biomolecules present in cells (including nucleic acids, lipids and proteins) which can lead to alterations of their structural and functional properties, in cell signaling processes, or in the regulation of gene expression [34].

3.1 Photophysics of photosensitizers

A PS is a molecule that when irradiated with light of suitable wavelength undergoes a transition from the ground state S_0 to an excited electronic state (S_n). After non-radiative relaxation to the lowest excited electronic state S_1, the molecule may undergo intersystem crossing to the triplet state T_1 through spin inversion (**Figure 3**). This process is competitive with fluorescence emission and internal conversion S_1-S_0. The triplet state T_1 decays to S_0 through intersystem crossing or phosphorescence emission.

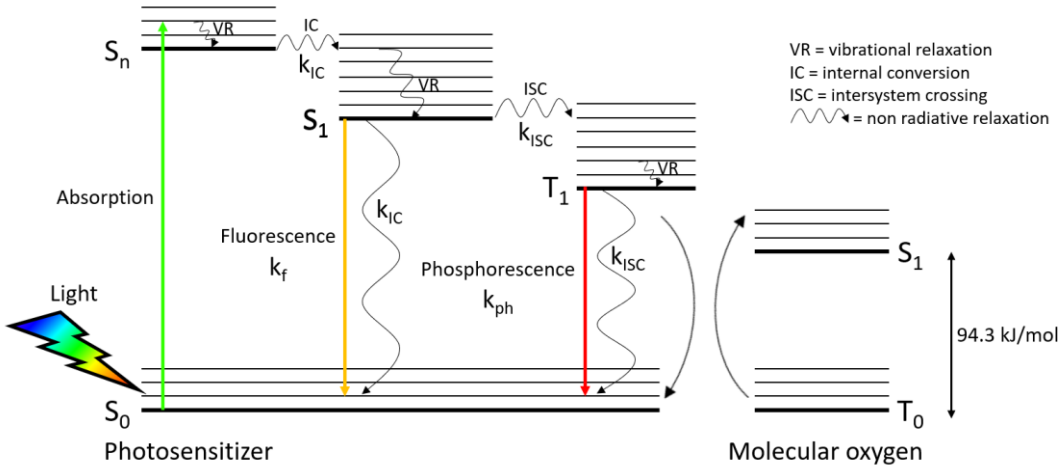

Figure 3. Jablonski diagram of a PS in presence of molecular oxygen. After photoexcitation PS reaches the triplet state, which can interact with molecular oxygen leading to the formation of molecular oxygen in the singlet state.

The lifetime τ of an excited state is given by the inverse of the sum of the rate constants k_i that characterize the de-excitation processes: $\tau = \frac{1}{\sum_i k_i}$.

For a PS the lifetime of the singlet state S_1 is:

$$\tau_S = \frac{1}{k_{decay}^S} = \frac{1}{k_f + k_{IC} + k_{ISC}^S} \qquad \textbf{Equation 1}$$

In the absence of oxygen, the lifetime of the triplet state of a PS is:

$$\tau_T = \frac{1}{k_{decay}^T} = \frac{1}{k_{ph} + k_{ISC}^T} \qquad \textbf{Equation 2}$$

While in the presence of oxygen, i.e. in the presence of a further de-excitation path but neglecting other mechanisms that may proceed from the triplet state (such as photoinduced electron transfer), the lifetime of the triplet state is:

$$\tau_T = \frac{1}{k_{ph} + k_{ISC}^T + k_q[O_2]} \qquad \textbf{Equation 3}$$

Thus, the rate constant of the triplet state can be written as:

$$k_{obs} = k_{decay}^T + k_q[O_2] \qquad \textbf{Equation 4}$$

Where k_q is the rate constant of the bimolecular quenching by molecular oxygen and is of the order of 10^9-10^{10} $M^{-1}s^{-1}$ [35].

A fundamental parameter to characterize the photoactivation and de-excitation processes is the quantum yield Φ which, at the kinetic level, is defined as $\Phi = \frac{k_{process}}{\sum_i k_i}$.

The quantum yield of singlet oxygen formation, Φ_Δ, is directly proportional to the quantum yield of triplet state formation of the PS, Φ_T:

$$\Phi_\Delta = \Phi_T S_\Delta S_q \qquad \textbf{Equation 5}$$

Where S_Δ is the fraction of molecules in the triplet state that is de-exited by the molecular oxygen, while S_q is the fraction of oxygen dependent triplet deactivations whose denominator takes into account all the de-excitation pathways of the triplet state [35]:

$$S_q = k_q \frac{[O_2]}{k_q[O_2] + k_{decay}^T} \qquad \textbf{Equation 6}$$

The characteristics that a PS should have are [35], [36]:

- High molar extinction coefficient in the red / near infrared region, to achieve greater tissue penetration (this feature is important for *in vivo* anticancer applications, but not as pressing for treating bacterial infections and for sanitizing food or water).
- Suitable photophysical characteristics: high quantum yield of triplet state formation, high quantum yield of singlet oxygen formation, sufficiently high energy of the triplet state (E ≥ 94 kJ/mol).
- Low photobleaching: to prevent PS degradation so that it can continue producing singlet oxygen in multiple photoexcitation cycles.
- High chemical stability: single compounds, well characterized, known and with constant composition.
- Low dark cytotoxicity: a PS should not be harmful to the target until it is irradiated.
- Rapid elimination from the body after the treatment.
- Target recognition: PS should preferentially accumulate on target cells.
- Soluble in an aqueous environment, to allow an eventual intravenous administration and facilitate its disposal. Otherwise, a hydrophilic system is needed to bring the PS to the target.

PDT requires the use of light whose wavelength must be absorbed by the PS, but not by other molecules present in or around the treated site. For example, human tissues are able to absorb most wavelengths of UV, visible and NIR, but allow light to pass in the range of approximately 650 to 850 nm called the "phototherapeutic window" (**Figure 4**) [37]. The presence of endogenous chromophores (such as hemoglobin and melanin) and scattering phenomena prevent deep tissue penetration of the wavelengths below 650 nm. Using two-photon absorption, it is possible to excited PS molecules absorbing in the blue-green, using near infrared photons whose wavelength falls in the tissue transmission window.
Conversely, water molecules absorb wavelengths greater than 1300 nm and therefore, for these wavelengths, tissue penetration is reduced [37].

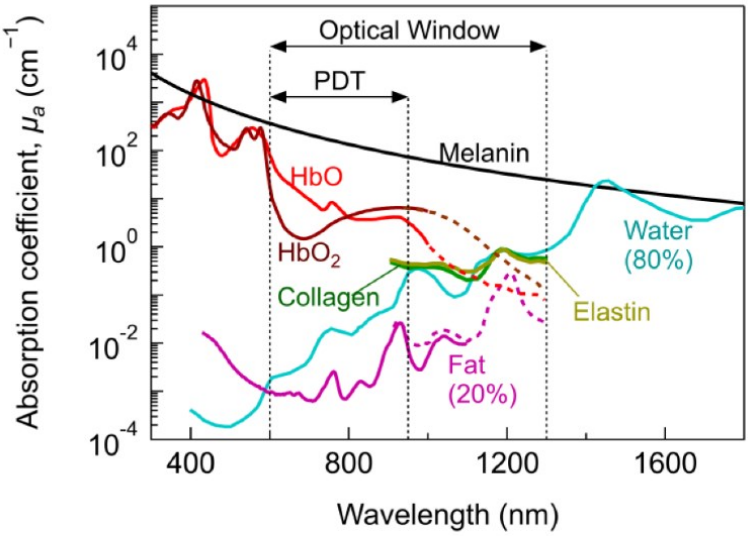

Figure 4. Phototherapeutic window. The spectral range between 650 and 850 nm is not absorbed by human tissues and allows a higher penetration into tissues. Reproduced from Algorri et al. [37].

3.2 Formation of reactive oxygen species

Like almost all organic molecules, in the ground state PS have pairs of electrons with opposite spin in the highest occupied molecular orbital (ground singlet state, S_0). The absorption of light with an appropriate wavelength excites a ground-state electron bringing it into a higher energy orbital without changing its spin. This state is called an excited singlet state and it has a short lifetime, on the order of, or below, a few nanoseconds. Higher energy states S_n relax non radiatively to S_1. The PS can lose the extra energy in S_1 and return to the ground state by emitting light (fluorescence) or heat [38].
Alternatively, the S_1 state can undergo intersystem crossing, a process in which the spin inversion of an excited electron occurs, transitioning to the excited triplet (T_1) state. This inversion of spin is the reason for the relatively long lifetime, on the order of microseconds, of T_1 [38]. From the T_1 state, PS can return to the ground state by emitting light (phosphorescence). These electronic steps can be represented in the Jablonski diagram (**Figure 3**).
As an alternative to phosphorescence, the T_1 state of PS can return to the ground state by transferring energy to another molecule. It can also lose energy through internal conversion or non-radiative transitions colliding with other molecules [38]. The longer the lifetime of a PS in the T_1 state, the greater the chances of a collision with another molecule occurring, producing chemically reactive species.

While in the T_1 state, the PS can be involved in two types of processes (**Figure 5**) [39].
In the type I process, PS at the T_1 state takes an electron from a reducing molecule in its vicinity (such as NADPH, nucleic acids, amino acids tryptophan and tyrosine), this creates a pair of radicals: a radical anion ($PS^{\cdot -}$) and a radical cation (biomolecule$^{\cdot +}$). In the presence of oxygen (aerobic environment) the radical anion transfers its extra electron to the molecular oxygen (O_2), in this way the superoxide radical anion ($O_2^{\cdot -}$) is produced and the PS is brought back to its ground state. The superoxide thus formed can perform both an oxidizing and a reducing action and can also react with other radicals leading to the formation of biologically toxic products (such as organic hydroperoxides and quinones).
In the type II process, the PS at the T_1 state transfers its energy directly to the molecular oxygen since in its ground state it is in the form of a triplet ($^3O_2$) and according to the selection rules this reaction is not spin-forbidden (there is no spin inversion so it can take place. This energy released by the PS excites one of the two electrons of the singlet oxygen triplet state in a higher energy orbital and reverses its spin, converting molecular oxygen from the triplet ground state to the excited singlet state ($^1O_2$).
The de-excitation of PS in the T_1 state by electron transfer competes with energy transfer and most PS generate both radicals and singlet oxygen [32]. Electron transfer (to form $O_2^{\cdot -}$ the reaction rate k is less than 10^7 $M^{-1}s^{-1}$) is slower than energy transfer ($k \sim 2x10^9$ $M^{-1}s^{-1}$), moreover the superoxide radical anion is less reactive than the singlet state, for these reasons singlet oxygen is considered the main cause of cell death caused by PDT [32].
Recently, has been proposed a type III process [4], in which free radicals of inorganic compounds are formed even in the absence of oxygen.

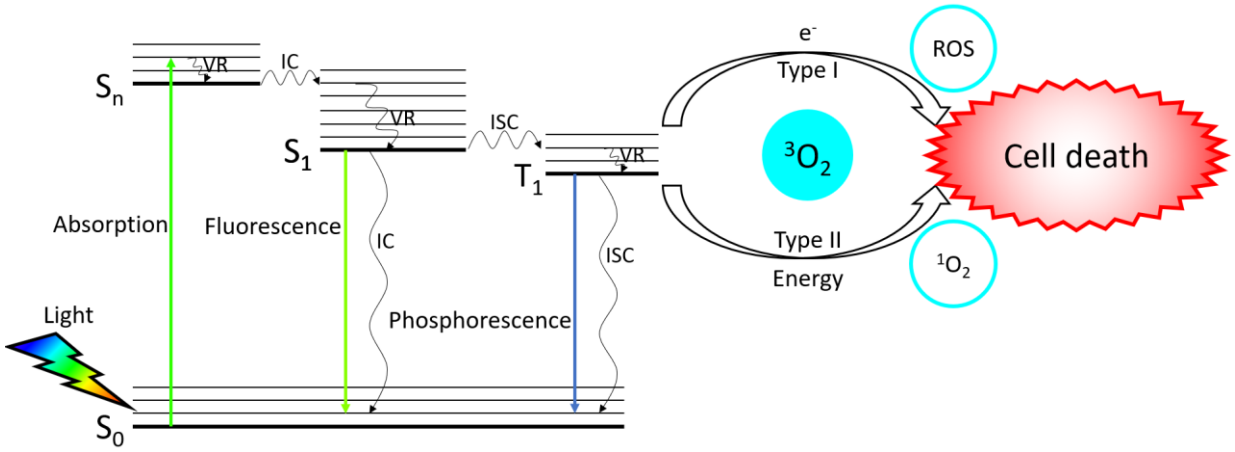

Figure 5. Jablonski diagram of PS and type I and type II processes. The PS can absorb the incident radiation, passing to the excited singlet state which can be converted into the triplet state. The triplet state of PS can interact with oxygen through the type I process (via electron transfer, with generation of $O2^{\cdot -}$, ·OH and H_2O_2) or the type II process (directly transfers energy to the oxygen in the ground state, leading to the formation of singlet oxygen). The PS thus returns to the ground state and can restart the process to lead to the generation of further ROS and singlet oxygen.

The electronic configuration of O_2 gives rise to three states termed $O_2(X^3\Sigma_g)$, $O_2(a^1\Delta_g)$, and $O_2(b^1\Sigma_g)$. According to Hund's rule, the lowest energy configuration is $O_2(X^3\Sigma_g)$, with two unpaired electrons of total spin S = 1 and a triplet multiplicity, as confirmed by the paramagnetic properties of molecular oxygen ground state. The states $O_2(b^1\Sigma_g)$ and $O_2(a^1\Delta_g)$ are located at 156.9 kJ/mol and 94.3 kJ/mol above the ground state $O_2(X^3\Sigma_g)$, respectively [32]. Having a lower energy, $^1\Delta_g$ is more stable than $^1\Sigma_g$ [40]. The lifetime of $^1\Delta_g$ is affected by two processes: physical quenching (energy transfer without product formation) and chemical quenching (chemical reaction that generates products).
The higher reactivity of singlet oxygen compared to the triplet state is based on the conservation of angular momentum if oxygen in the triplet state reacts with a molecule in the singlet state, to maintain the overall

angular momentum, a triplet adduct must be formed, which is spin-forbidden, hence slow; conversely, when oxygen is in the singlet state the reaction is faster because the angular momentum is conserved. Singlet oxygen can react with carbon-carbon double bonds and with neutral nucleophiles (e.g., sulphides, amines and anions) leading to the formation of peroxides [41]. These peroxides can therefore generate radicals which in turn trigger chemical reactions that lead to the formation of products that are harmful to cell survival [41].

As mentioned, singlet oxygen lifetime is affected by physical and chemical quenching. Due to physical quenching the lifetime of singlet oxygen in water is approximately 4 μs, and due to chemical quenching in the cells its lifetime is further shortened [42]. Without considering chemical quenching, the maximum distance that singlet oxygen can go through is about 150 nm [42] (as described in the next chapter) which, compared to the size of a cell (10-30 μm for a mammalian cell, around 1 μm for bacteria [43]), is extremely small.

Therefore, due to its short lifetime, the singlet oxygen produced by the photoexcitation of the PS must be in the vicinity of the target cell. So, the location of the PS is essential to determine which cellular components will be damaged by the PDT.

3.3 Diffusion of singlet oxygen

As mentioned, when the PS is in the triplet state it can interact with molecular oxygen and lead to the formation of singlet oxygen. For this molecule to affect biological substrates, it must diffuse to them and the distance d it can travel, according to diffusion theory, is:

$$d = \sqrt{6tD} \qquad \textbf{Equation 7}$$

Where D is the diffusion coefficient of singlet oxygen, t is the time interval during which the molecule can diffuse and depends on the lifetime of singlet oxygen τ_Δ.

This lifetime τ_Δ is defined as the time interval required for a given population of singlet oxygen to be reduced by a factor of 1/e,

$$c_{t=\tau_\Delta} = \frac{c_{t=0}}{e} \qquad \textbf{Equation 8}$$

It is reasonable to assume $t = 5\tau_\Delta$ for the singlet oxygen population to decay to zero [40].

To estimate the distance that singlet oxygen can travel inside a cell, it is necessary to know the diffusion coefficient D described by the Stokes-Einstein equation

$$D = \frac{k_B T}{6\pi\eta r} \qquad \textbf{Equation 9}$$

Where k_B is the Boltzmann constant, T the absolute temperature, η the viscosity of the fluid and r the radius of the diffusing molecule (approximated to a sphere).

The diffusion coefficient of oxygen is inversely proportional to the viscosity in which it is found, but a cell is an inhomogeneous environment and therefore the viscosity varies according to the area in which the oxygen is found. Inside a cell the diffusion coefficient of oxygen ($D \sim$ 2-4x10^{-6} cm^2/s) is lower than that in water ($D \sim$ 2x10^{-5} cm^2/s) [40].

The lifetime τ_Δ of singlet oxygen can be estimated to be about 2 μs, therefore the time interval t during which oxygen can diffuse is about 10 μs. Substituting these data and a diffusion coefficient D of approximately 4x10^{-6} cm^2/s in **Equation 7** it is possible to estimate that the singlet oxygen diffusion distance is 155 nm [40]. This distance represents the radius of the surrounding environment that singlet oxygen can reach and damage inside the cell.

For comparison, this diffusion distance is much shorter (about 100 times) than the average length of a eukaryotic cell (about 10-30 µm). Therefore, the phototoxic effects of singlet oxygen are limited to a small area of the cell where PS is present, but the distance that singlet oxygen can travel is sufficient to reach molecular targets whose damage then leads to cell death.
The short-range sphere of action of the PSs means that the compound must be brought in close vicinity of the molecular targets to exert a phototoxic action. This requires the introduction of targeting and selectivity properties in the photoactive molecular structure.

3.4 Molecular targets in antibacterial PDT

The cell wall of bacteria is their first defensive barrier against external agents and a potential site of molecular targets.
Bacteria are classified into Gram-positive and Gram-negative depending on their response to the Gram stain test, which reflects the different composition of their cell walls (**Figure 6**).
The cell wall of Gram-positive bacteria consists of a plasma membrane (a phospholipid bilayer) externally covered with a thick layer of peptidoglycan. At physiological pH, this outer layer is negatively charged, so Gram-positive, as well as Gram-negative, can be targeted using cationic PS [6].
The cell membrane of Gram-negative bacteria, on the other hand, is more complex. In fact, proceeding from the inside to the outside of the cell, it has a plasma membrane, a thin layer of peptidoglycan, an external membrane (a further phospholipid bilayer) and lipoproteins. This thick and compact structure of the Gram-negative cell membrane limits PS penetration [6] moreover, due to the presence of lipopolysaccharides, the outer membrane of Gram negative bacteria is negatively charged preventing access to neutral or anionic PS [14].
The different structure of the cell wall of the bacteria leads to a different susceptibility to aPDT; this is more effective against Gram-positive, whose single membrane allows a greater penetration of PS [44].

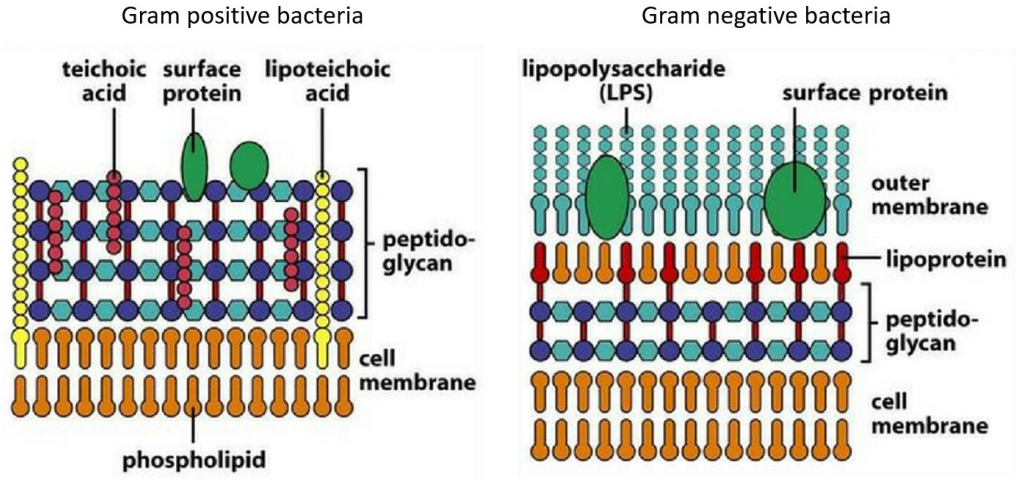

Figure 6. Cell membrane structure of Gram-positive and Gram-negative bacteria. The cell wall of Gram-positive consists of a bilayer of phospholipids and a layer of peptidoglycan, while that of Gram-negative has an additional bilayer of phospholipids and lipoproteins.

Inside a cell, photosensitized singlet oxygen and ROS can oxidize and damage various biomolecules. The probability that these biological substrates can be targeted depends on the distance between them and the excited oxygen, their concentration (both their biological availability and cellular oxygenation) and the rate constant of the reaction [32].

Given their abundance, proteins are the main target of PDT. Furthermore, their oxidation by singlet oxygen and ROS has relatively high rate constants (although highly variable according to the amino acid considered) [45]. These oxidations cause damage to the amino acid side chains and impair protein function.
Under physiological conditions, the main amino acids that interact with singlet oxygen ($k > 10^7$ $M^{-1}s^{-1}$) are: cysteine, methionine, tyrosine, histidine and tryptophan. The phototoxicity of HO· depends on the concentration of proteins and, for most of the amino acids, its reaction rate is diffusion limited [45].
The type of amino acids targeted is not the only parameter that affects the damages incurred by a protein, the position and the function of the amino acid within the protein being also important factors [45]. For this reason, different proteins have different susceptibility to PDT.
Obviously, the localization of the PS and consequently the environment that the excited oxygen can reach, also affects the damage suffered by the proteins.

Also, DNA can be subject to the oxidative action caused by PDT through singlet oxygen or radicals (especially $O_2\cdot^-$ and HO·) and by direct one-electron oxidation (PS in the triplet state takes an electron from the DNA).
The main target of singlet oxygen is guanine (k = 5x10^6 $M^{-1}s^{-1}$) [46]. Given its low ionization potential, guanine is also susceptible to direct oxidation [47].
Among ROS, the hydroxyl radical is the one that damages DNA the most since it can interact with all its various constituents. The main modification that HO· causes to the nucleotide bases is an addition to the double bonds [47].

Within cells, lipids are present to a lesser extent than proteins, but the high content of fatty acids within cell membranes makes them an excellent target for singlet oxygen and ROS. In fact, if the PS penetrates the cell membrane, or in an environment with a high concentration of oxygen, the probability that the PS in the triplet state can generate singlet oxygen increases by the interaction with unsaturated fatty acids [32]. The reaction rate between singlet oxygen and unsaturated fatty acids depends on the number of double bonds present in the lipids (k between 0.74 and 2.4x10^5 $M^{-1}s^{-1}$) [48]. While located in a bilayer membrane, the diffusion coefficient of singlet oxygen is two times lower than that in water [49].
Oxygen has a high solubility within lipids, so an excited PS that is in, or close to, a lipid environment has a high probability of being able to excite molecular oxygen and thus cause oxidation of fatty acids [48].
Singlet oxygen oxidizes unsaturated fatty acids leading to the formation of lipid peroxides, while ROS can induce lipid peroxidation [50] which alters membrane functions (e.g. in metabolism and signaling) leading to cell death. However, if the PS remains in the extracellular environment and not in the proximity to the membrane, or in an environment where the oxygen concentration is lower, the produced singlet oxygen will be more likely to return to the ground state before it can affect the components of the cell membrane [32].

3.5 Antimicrobial PDT and selective targeting

Many aPDT studies have been conducted against *S. aureus* and a number of PS molecules of different classes have been used, including, among others, porphyrins [23], hypericin [51], curcumin [52], porphycene [53], phenalenone [54], eosin [55] and methylene blue (MB) [56]. Some of the investigated PS molecules are under clinical trials, as detailed in the **Table** in ref. [57].
Of special interest to this work are eosin and methylene blue. For about a century, with the introduction of Levine EMB (eosin, methylene blue) agar [58], eosin is known to inhibit the growth of Gram-positive bacteria

(such as *S. aureus*). For example, by irradiating with 30 J/cm^2 it is possible to obtain a cell death of 8-logs of *S. aureus* and *E. coli* using 5 µM and 10 µM of EMB, respectively [59].
Some photoinactivation studies [60] showed that eosin reduces the cell viability of *S. aureus*, but this PS alone has a lower efficacy than other xanthenic dyes [61]. After being irradiated, eosin causes cell death of approximately 99.9% (at 1 µM and 60 J/cm^2) [62], while when the PS is bound to an antimicrobial peptide [(KLAKLAK)2] its phototoxic activity increases (99.999% at 1 µM and 236 J/cm^2) [63], [64]. It was also noted [61], [62] that after photoexcitation eosin causes morphological changes in *S. aureus*.
Furthermore, it has been shown that the use of eosin in aPDT against *S. aureus* does not lead to a significant increase in resistance to photodynamic action (after 10 cycles of aPDT under conditions of cell death by approximately 50%) [55].
MB has been studied for many years for its ability to photo-inactivate bacteria and there are hundreds of studies investigating its applications in this field.
Although effective against *S. aureus* and other bacterial strains, molecules such as eosin or methylene blue are devoid of targeting capability and selectivity. Moreover, as mentioned before, one of the problems of PSs is their low solubility in water solutions so, to enhance those factors these molecules have been conjugated to several molecular or supramolecular species, or nanoparticles [65], [66]. One of the most promising carriers are proteins, also because they can be easily modified to covalently bind a PS. To further improve the targeting, it is possible to use antibodies that recognize specific molecules present on the target cell, although this methodology is predominantly used in anti-tumor PDT [67]. Photo-immunotherapy (PIT) is based on the use of photo-immunoconjugates (PICs), i.e. complexes in which a PS is conjugated with a specific antibody capable of recognizing and binding the antigens present on a particular target cell [68], especially tumor cell. This strategy allows to combine the advantages of PDT with the targeting capacity and the high specificity of antibodies (their dissociation constant is of the order of nM).

Based on the moiety used, there are various strategies to conjugate a PS to a protein. The amines of the lysine side chains of the protein can react with the isothiocyanate or succinimidyl ester groups present on modified PSs [68], [69]. The thiol groups of cysteines present in the protein can interact with the maleimide or succinimidyl functional groups introduced in PSs [70]. Carboxyl groups present on a PS can be activated by carbodiimide compounds (such as EDC and DCC), so that the PS can react with amino groups present on a protein [67], [69], [71]. By modifying a protein and a PS it is possible, through a chain of reactions called a "click path" (CuAAC; copper(I)-catalyzed alkyne-azide cycloaddition), to bind them by reacting an azide and a terminal alkyne [68], [69], [71]–[73].
Conjugation of the PS with the protein may occur at positions that could interfere with its binding properties (e.g. an antigen-binding site if the protein is an antibody) and possibly compromise its ability to recognize the substrate (epitope). A possible measure to overcome this problem is the modification of reactive groups in the binding site of the antibody that would bind the PS. However, in this case it is necessary to verify that the changes made do not alter the immunoreactivity (targeting activity) of the antibody [68].

Some PIT studies have already been performed against some *S. aureus* strains. For example, the PS chlorine e6 was conjugated with IgG [74] or to the antibody CE6 [75] obtaining an effective and selective photoinactivation of bacterial cells.
ConA has already been used as targeting system for aPDT. In particular, in presence of this protein, the efficacy of dextran-coated gold nanoparticles labeled with MB against *Klebsiella pneumoniae* (16 µM of PS and 143 J/cm^2) increased by around 2 logs [76]; also the photokilling of RB against *E. coli* (5 µM of PS and 5 J/cm^2) increased by around 2 logs when the PS is directly bound to ConA [77].

Aside from directly conjugate a PS to a protein, it is possible to add a spacer to create a complex exploiting, for example, the high affinity between streptavidin and biotin. This approach was used only with antibodies, in particular it has been demonstrated [78] the phototoxic action of chlorine e6 indirectly linked to an antibody anti-*Aggregatibacter actinomycetemcomitans*.

To date there are no studies showing the phototoxic effect caused by a complex containing eosin and an antibody against a bacterium and in only one case MB and ConA have been used together [76].

4 Supramolecular constructs for targeted antimicrobial PDT

The aim of this research is to create modular complexes (**Figure 7**) for aPDT to address the limitations of PS molecules regarding selectivity and targeting ability towards bacterial targets.
The supramolecular architecture consists of a PS (which, depending on the experiment to be carried out, such as in fluorescence microscopy, can be replaced with a fluorophore), a junction system (consisting of the tetrameric protein streptavidin, able to bind the vitamin biotin with high affinity) and a targeting system towards bacterial constituents (by changing the targeting system is possible to target different molecular receptors or different cells).
To create a photoactive terminal, a PS (or a fluorophore) modified with a group reactive towards amines is covalently bound to streptavidin. The targeting system is biotinylated at multiple Lys residues. Taking advantage of the high affinity between streptavidin and biotin, the photoactive and the targeting units are brought together and form a stable supramolecular complex.

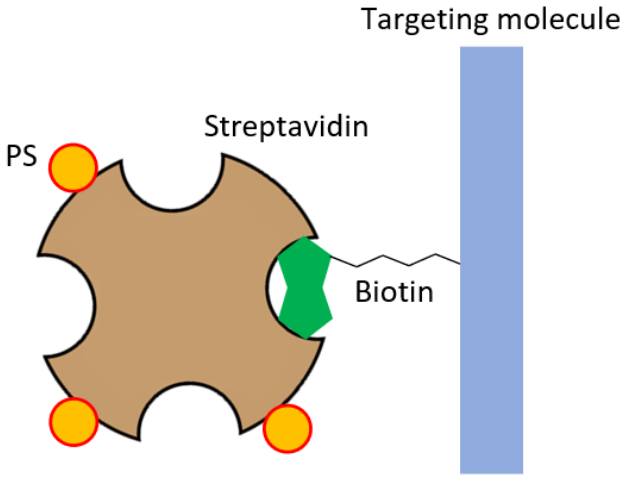

Figure 7. Scheme of the basic structure of the formed complexes. The complexes consist of three parts: a PS, a junction system (consisting of streptavidin and biotin) and a targeting protein.

4.1 Photosensitizers

4.1.1 Eosin 5-isothiocyanate

Tetrabromofluorescein (disodium salt), or eosin, is a red dye used in textiles and inks; its use is approved by the FDA for pharmaceutical and cosmetic applications [79]. In this work, we have used the 5-isothiocyanate derivative (EITC) of eosin. In EITC, the carbon atom in the isothiocyanate group (N=C=S) is electrophilic and therefore can react with nucleophiles such as amino, hydroxyl and thiol groups.
Proteins contain lysine residues which have a free amine in the side chain. These aliphatic amines are moderately basic, so they can interact (via acylation) with molecules containing an isothiocyanate group, but this reaction depends on the pH. In fact, the isoelectric point pI of lysine is 9.8, this means that at pH below 8 the concentration of deprotonated amines is very low and therefore the reaction kinetic is slow, while at higher pH it occurs in deprotonated form and therefore acts as a nucleophile (binding to the isothiocyanate group). For this reason, the labeling of proteins with isothiocyanate molecules is typically done at pH > 9 [80].

Unlike fluorescein, eosin has four bromine atoms which enhance the probability of transition to the triplet state by increasing the spin-orbit coupling.
The chemical formula of the EITC is $C_{21}H_7Br_4NO_5S$ (**Figure 8**) and has a molar absorbance coefficient at 525 nm of 95,000 $M^{-1}cm^{-1}$. Some photo-physical properties of eosin are reported in **Table 1**.

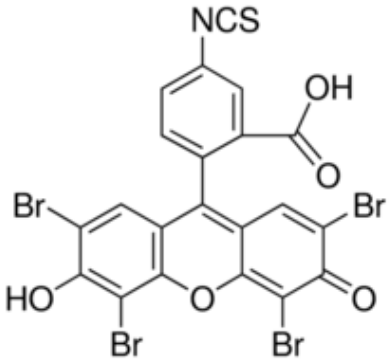

Figure 8. Chemical structure of the EITC.

	H_2O
Fluorescence lifetime (ns)	1.21 [81]
Quantum yield of fluorescence	0.2 [82] 0.24 [81]
Quantum yield of triplet state formation	0.64 [83] 0.71 [84] 0.8 [82]
Quantum yield of singlet oxygen formation	0.61 [83]

Table 1. Photophysical properties of eosin.

A limitation in the use of the EITC for aPDT is that, at neutral pH, it is a dianionic molecule and unless a specific carrier is used, the compound has little effect on Gram-positive or Gram-negative bacteria that are impermeable to neutral or anionic molecules [85].

4.1.2 Methylene blue

Methylene blue (MB, **Figure 9**) is an organic compound showing a strong absorption in the red, and is often used as a blue dye. Due to its positive charge, it is used in histology to stain negatively charged organelles and DNA.
FDA has approved the use of MB for the treatment of rare methemoglobinemia disease [86], caused by a high presence of methemoglobin (a protein in which the iron in heme is in the Fe^{3+} state and this prevents oxygen from being reversibly bound) in the blood.

MB has a molar absorbance coefficient at 664 nm of 85,000 $M^{-1}cm^{-1}$ [87].
The shape of the absorption spectrum of MB depends on its concentration, since there is an equilibrium between monomer (with an absorption peak at 664 nm) and dimer (peak at 604 nm) with an equilibrium constant of approximately 4×10^3 M^{-1} [88].

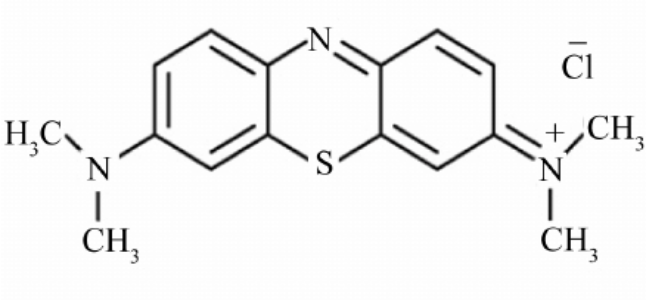

Figure 9.Chemical structure of the MB.

In **Table 2** are reported some photo-physical properties of MB.

	H_2O
Fluorescence lifetime (ps)	354 [89] (1 µM) 379 [90] (1 µM) 520 [91] (5 µM)
Quantum yield of fluorescence	0.03 [92] 0.04 [87]
Triplet state lifetime (µs)	65 [92] 77 [91]
Quantum yield of triplet state formation	0.52 [87]
Quantum yield of singlet oxygen formation	~0.5 [87]

Table 2. Photo-physical properties of MB.

Dimerization MB has effects on the photochemistry of the compound. Photoexcitation of the monomeric form mostly leads to singlet oxygen production, whereas for the dimeric form type I reactions are favored [93].

PDT with MB alone has demonstrated the phototoxic efficacy of this PS against various cellular targets: bacteria (both Gram-positive and Gram-negative and also some antibiotic-resistant strains), fungi (such as *Candida albicans*), tumors and viruses (e.g. HSV-1, HIV-1 and SARS-Co-2 [94]) [87].

4.2 Molecular partners in linking unit

4.2.1 Streptavidin

Streptavidin is a homo-tetrameric protein with a molecular weight of 52.8 kDa, produced by the bacterium *Streptomyces avidinii*.

Each streptavidin monomer consists of eight antiparallel β-sheets folded into a β-barrel.

One of the main characteristics of streptavidin is its extraordinary affinity for biotin: the dissociation constant k_d is about 10^{-15} M and this makes their binding one of the strongest non-covalent interactions known in nature [95]. The biotin binding site is at the interface between a β-barrel and the adjacent monomer subunit (**Figure 10**). The binding pocket consists of the residues of a β-barrel and the Trp120 residue of the adjacent barrel [96].

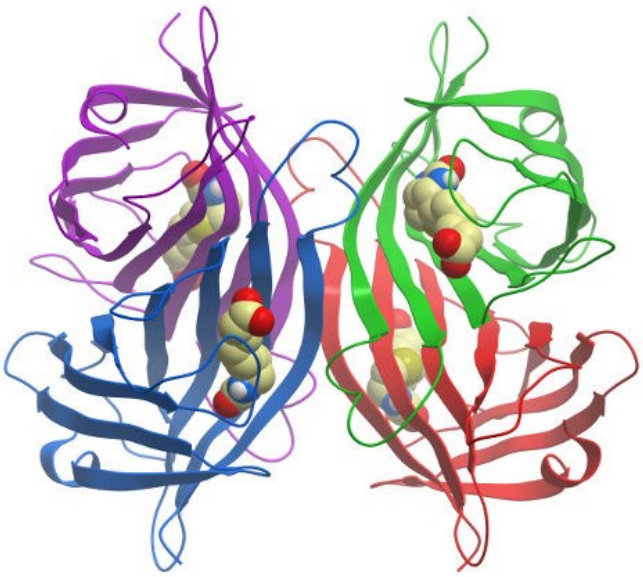

Figure 10. Tetrameric structure of streptavidin and relative position of biotin. Streptavidin (PDB: 1STP) is made up of four β-barrels (newcartoon) which two by two form a binding site for biotin (VDW).

The high affinity between streptavidin and biotin is given by the presence of multiple interactions.
The binding site has a complementary shape to biotin and when biotin is hosted in the hydrophobic pocket, numerous van der Waals and hydrophobic interactions are established [97].
Furthermore, when biotin is in its binding site it forms two so-called "shells" consisting of a network of hydrogen bonds. The first shell (**Figure 11**) consists of eight hydrogen bonds (established with the residues Asn23, Tyr43, Ser27, Ser45, Asn49, Ser88, Thr90 and Asp128), while the second shell involves further residues that interact with those of the first shell [97].
Finally, the streptavidin-biotin bond is stabilized by the L3/4 loop (from Ser45 to Ser54, between the β 3 and 4 strands) which, by folding on the biotin, acts as a closure preventing the dissociation of the biotin from the binding site [97].

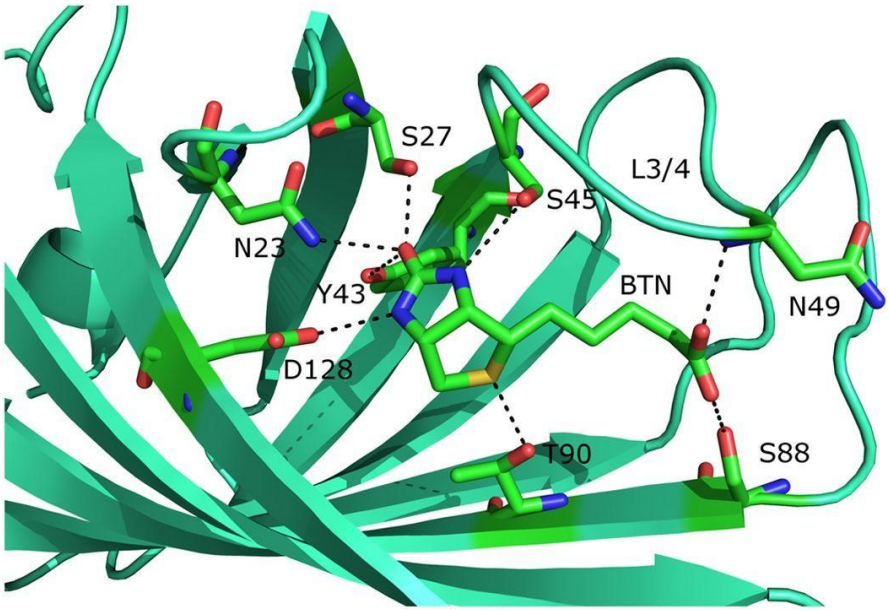

Figure 11. Main hydrogen bonds between streptavidin and biotin. When biotin is at its binding site, it forms hydrogen bonds (dotted lines) with streptavidin, the so called first shell, which prevent the biotin from dissociating. Reproduced from Liu et at. [97].

The molar absorbance coefficient at 280 nm of the streptavidin monomers is 41,326 $M^{-1}cm^{-1}$.
Streptavidin can be easily conjugated to fluorophores or PSs, as it is a "robust" protein that retains its functionality even in an alkaline reaction environment, conditions that are necessary for reactions with Lys residues of isothiocyanate bearing PSs.
The high affinity between streptavidin and biotin can be exploited for the assembly of complexes in which a biotinylated molecule is associated with a labeled streptavidin.

4.2.2 Biotin

Biotin is a vitamin, defined as vitamin H, B_7 or B_8, depending on the classification (**Figure 12**). This molecule shows absorption with a maximum in the far UV (around 210 nm).

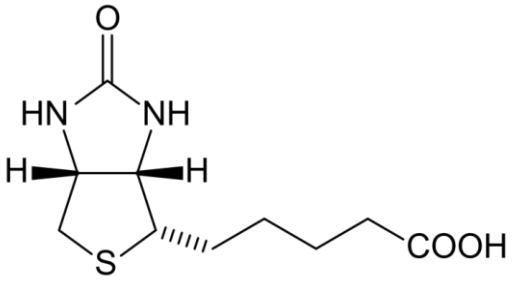

Figure 12. Chemical structure of biotin.

Using a biotin derivative reactive with Lys residues, such as an NHS ester, it is possible to covalently link biotin to a protein.
Biotin has two characteristics that make it an ideal candidate for protein labeling [98]:

- Biotin has a much smaller size than globular proteins and this allows more biotins to be conjugated to the same protein.
- On its side chain, biotin has a valeric acid ($CH_3(CH_2)_3COOH$) which can be used to introduce chemical modifications to biotin in order to make it reactive with specific amino acid side chains. Furthermore, this modification occurs on the site opposite to the streptavidin binding portion, and it is expected not to affect the affinity between the vitamin and the protein.

Chemically modified biotins, called biotinylation reagents, have a similar structure (**Figure 13**), with the biotin end connected to a reactive group through a chain, called a spacer.
The reactive moiety, located at one end of the modified biotin, serves to conjugate this molecule to a specific reactive group on the target molecule (for example a protein or a fluorophore) [96]. Biotin may interfere with the protein function, and affect its binding capability to its physiological targets. Therefore, it should be verified that labeling with biotin does not result in protein function impairment.
The length of the spacer can be adjusted to meet the experimental needs. For example, by increasing the length of the spacer, it is possible to move away a biotin-conjugated fluorophore from streptavidin, reducing the quenching effect due to the interactions of the molecule with the protein.

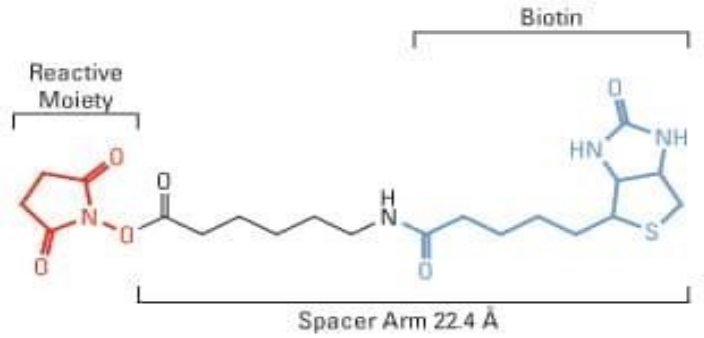

Figure 13. Main parts of a biotinylation reagent. In the reported biotin succinimidyl ester structure, biotin (blue) is connected through a spacer (black) to the reactive group (red).

4.3 Targeting systems

4.3.1 Immunoglobulin G

Immunoglobulins (Ig), a type of antibodies, are a class of serum glycoproteins (i.e. proteins whose polypeptide chain is linked to a chain of oligosaccharides) found in vertebrates.
During the immune response, the most abundant Ig are IgG which make up about 70-75% of the Ig present in the serum. The characteristic of IgG is that they act as opsonins (**Figure 14**), i.e. they are molecules that, by coating a microorganism or a foreign molecule, allow to increase the efficiency of phagocytosis (opsonization) thanks to the bond between a receptor present on the phagocyte and the Fc fragment present on the IgG [99].

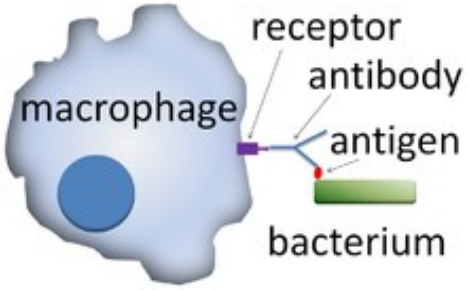

Figure 14. Opsonization system. Thanks to the presence of an antigen, the opsonin (IgG) binds a foreign microorganism while its Fc fragment is recognized by a phagocyte which then can target the microorganism.

The quaternary structure of Ig takes the form of a Y. At the ends of the arms of this structure there are binding sites that allow the Ig to recognize a substance foreign to the body, or potentially dangerous for it, called antigen.
Antibodies have an Y shape and are composed of a “stem” and two “arms”. The “stem” is formed by two crystallizable fragments (Fc) each of which consists of two heavy domains (H); each of the two “arms” is formed by two fragments that have the ability to bind the antigen and for this they are defined fragments antigen-binding (Fab), each of them is made up of a different type of domain (heavy H or light L). Finally, all domains (both H and L) are formed by two chains; both domains of Fc consist of constant chains (C_H), while domains of Fabs consist of a variable chain (V_L) and a constant (C_L) [100].
Both chains (constant and variable) of Ig have a sandwich structure, i.e. they are formed by two β-sheets (each composed of 3 β-strands (IgGV) or 5 β-strands (IgGC)) folded and whose ends are stabilized by a

disulfide bridge. The heavy domains of IgG are called type γ and, as mentioned, include a variable domain (V_H) and three constant domains (C_H1, C_H2, C_H3); there are four types of chains γ (γ1, γ2, γ3, γ4) which originate many IgG subfamilies (IgG1, IgG2, IgG3, IgG4) [100].
Figure 15 shows the structure of an IgG. Its molecular weight is approximately 150 kDa and at 280 nm it has a molar absorbance coefficient of 210,000 $M^{-1}cm^{-1}$.

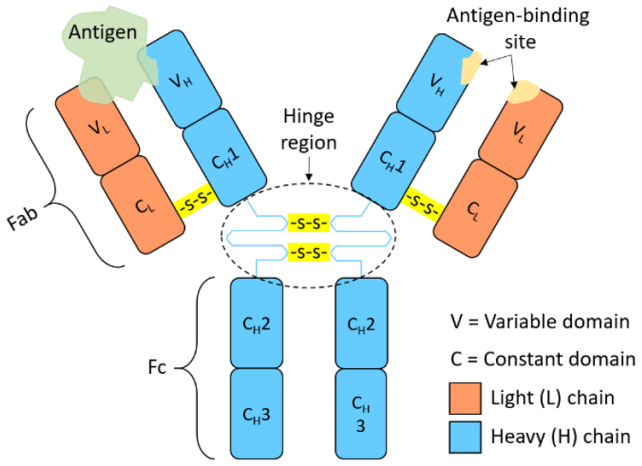

Figure 15. Schematic structure of an IgG. IgGs consist of four domains, two heavy (H) and two light (L), linked by disulfide bridges. H domains consist of a variable chain (V_H) and three constants (C_H1, C_H2, C_H3), while L domains consist of a variable (V_L) and a constant (C_L) chain.

IgG can recognize and bind protein A (SpA), a protein of about 42 kDa found on the outer surface of the cell wall of the bacterium *S. aureus*. The dissociation constant k_d between IgG and protein A is about 10 nM [101]. Protein A is made up of five domains, folded into 3 α-helices, which interact with the Fc of the IgG and, in the case of IgGC, with the Fab [102].
S. aureus has developed protein A as a virulence factor, in fact binding of this protein to IgG allows the bacterium to evade the host's immunosurveillance, as the Fc of the antibody cannot bind phagocytes and therefore the organism cannot activate opsonin mediated phagocytosis [24].
Protein A is anchored to the pentaglycine bridges (chains of five glycine residues) by the transpeptidase sortase A present on the peptidoglycan layer [103]. On its surface, *S. aureus* presents foci of secretion of protein A arranged in ring structures, this implies that the secretion of protein A occurs in a well-organized way and that its distribution is not homogeneous [104].

4.3.2 Concanavalin A

ConA has a molecular weight about 102 kDa (in the tetrameric form) and at 280 nm its molar absorbance coefficient is about 116,000 $M^{-1}cm^{-1}$ [105].
ConA is a protein belonging to the lectin family, i.e. proteins that have a high specificity for carbohydrates. In particular, ConA interacts with polysaccharides which contain α-glucose, mannose, glucosamine and α-N-acetylglucosamine [106]. ConA has a dissociation constant k_d of 0.25 μM for glycogen and 2.89 μM for mannan [107].
These carbohydrates, or their derivatives, are present in the outer membrane of bacterial cells (**Figure 16**).

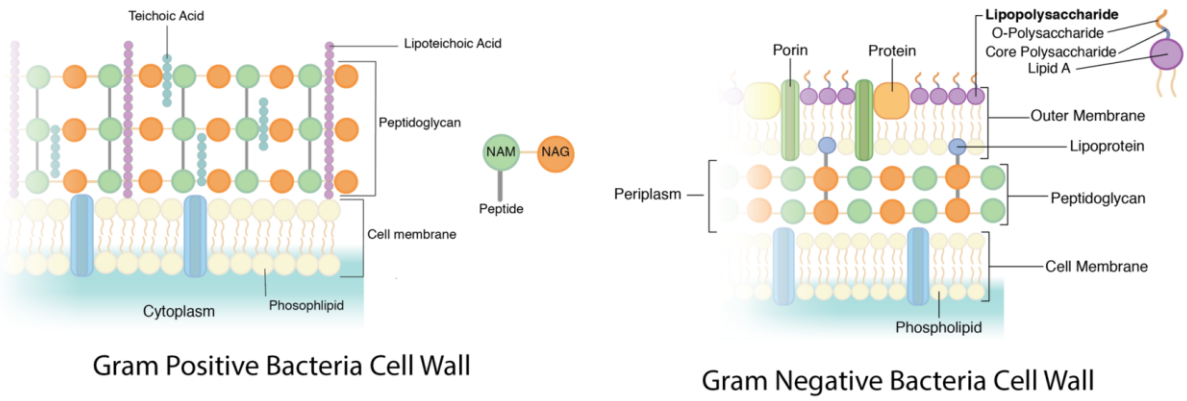

Figure 16. Representation of the bacterial cell wall. In Gram-positive bacteria (right) there is a thick layer of peptidoglycan (composed of NAG and NAM) inside which teichoic acids are inserted. In Gram-negative bacteria (left) there is an outer membrane coated with lipopolysaccharides.

The cell membrane of Gram-positive bacteria is externally covered with a thick layer of peptidoglycans, that comprises teichoic acids. Peptidoglycan is a polymer consisting of glucose derivatives such as N-acetylglucosamine acid (NAG) and N-acetylmuramic acid (NAM) [108]. Also, a typology of teichoic acids (disaccharides called lipoteichoic acids) consists of NAG.
The cell membrane of Gram-negative bacteria is covered by a thin layer of peptidoglycans and an outer membrane. The innermost layer of this outer membrane is made up of phospholipids while the outermost is made up of glycolipids, in particular lipopolysaccharides (LPS) [108]. The saccharide part (consisting of carbohydrates) of the LPS protrudes from the membrane and, by coating the bacterial cell, gives the cell antigenic properties.

In Gram-positive bacteria, ConA can therefore bind to teichoic acids since they are made up of α-glycosylates (e.g. in *S. epidermidis*) and α-N-acetylglucosamine (e.g. in *S. aureus*) [106]. Furthermore, ConA can be used to bind monocytes and thus stimulate the phagocytosis of *S. aureus* [109].
In Gram-negative bacteria, ConA can bind to the glucose and mannose residues contained in the LPS [77].

5 Materials and methods

5.1 Materials

EITC was from Sigma-Aldrich.
Streptavidin (salt-free lyophilized powder), from *Streptomyces avidinii*, was from Sigma-Aldrich.
A labeling kit (Biotin SE Protein Labeling Kit) from Biotium Inc. (Fremont, CA, USA) was used for the biotinylation of the IgG. A labeling kit (Water-soluble Long-arm Biotin Labeling Kit) from MyBioSource (San Diego, CA, USA) was used for the biotinylation of the ConA.
MB-labeled streptavidin (ATTO MB2 streptavidin) was from ATTO-TEC (Siegen, Germany).
Human IgG from human serum was from Sigma-Aldrich.
ConA from *Canavalia ensiformis* was from Sigma-Aldrich.
Biotinylated STAR635 and STAR635-streptavidin were from Abberior GmbH (Göttingen, Germany).
Chromeo488-labeled streptavidin was from Active Motif, Inc.
AlexaFluor647 NHS ester was from Invitrogen by Thermo Fisher Scientific (Waltham, Massachusetts, USA).
Sephadex G25, PD-10 column, used for the purification of the EITC-streptavidin complex, was from Cytiva (Marlborough, MA, USA).

5.2 General methods

Steady-state optical spectroscopy

Absorption spectra were collected using a Jasco V-650 spectrophotometer (Jasco Europe).

Steady-state fluorescence excitation, emission and anisotropy spectra were collected using an SF5 spectrofluorometer equipped with temperature control, and excitation and emission polarizers (Edinburgh Instruments Ltd., Livingston, UK).
The fluorescence quantum yield Φ_F of the sample was calculated from the emission spectra using a reference molecule:

$$\Phi_{F,sample} = \Phi_{F,reference} * \frac{n_{sample}}{n_{reference}} * \frac{Area_{sample}/\left(1-10^{-A_{Ex_{sample}}}\right)}{Area_{reference}/\left(1-10^{-A_{Ex_{reference}}}\right)} \quad \textbf{Equation 10}$$

Where n is the refractive index of the solvent, $Area$ is the area under the fluorescence emission curve and A_{ex} is the absorbance at the excitation wavelength.

Mass spectrometry was carried out using the mass spectrometer LTQ Orbitrap (Thermo Fisher Scientific). The protein samples were separated in a reverse-phase column Phenomenex Aeris™ PEPTIDE XB-C18 (3.6 µm), developed in a 200 µl/minute gradient with 0.1% formic acid/water - 0.1% formic acid/acetonitrile.
The area under the curves of the peaks were analyzed with the Xcalibur™ data analysis software.

Time resolved optical spectroscopy

The fluorescence decays were recorded by a TCSPC FLS920 system (Edinburgh Instruments Ltd., Livingston, UK) with pulsed LED excitation at 500 or 600 nm and a repetition rate of 5 MHz.

The signals were deconvolved from the IRF using the data analysis software FLS980.

FCS experiments were performed using a PicoQuant Microtime 200 system, based on an inverted confocal microscope (Olympus IX71) and equipped with two SPADs used in cross-correlation mode. As excitation, a 475 nm or 635 nm picosecond diode laser operating at 20 MHz was used. The fluorescence emission was collected through a band-pass filter (555/20 nm or 670/20 nm) and it was split between the two detection channels with a 50/50 splitter.
The autocorrelation curves $G(\tau)$, for a single diffusive species, were fitted with the function:

$$G(\tau) = \frac{1 - \Theta_T + \Theta_T e^{-\tau/\tau_T}}{1 - \Theta_T}\left[\frac{1}{\langle N\rangle}\left(1 + \frac{4D\tau}{w^2}\right)^{-1}\left(1 + \frac{4D\tau}{z^2}\right)^{-1/2}\right] \quad \textbf{Equation 11}$$

Where Θ_T is the characteristic time of the triplet state (non-emitting state), $\langle N\rangle$ is the mean number of particles in V_{eff}, D is the diffusion coefficient, w and z are the dimensions of the effective volume axes.

Triplet state formation and decay were monitored using a home built, previously described nanosecond laser flash photolysis setup [110]. The absorbance changes were observed at 500 nm (for EITC) or 582 nm (for MB) using a Xe lamp as the monitoring source. The transmitted photons were passed through a monochromator and then measured with a photomultiplier coupled to a digital oscilloscope. Photoexcitation was obtained with the second harmonic (532 nm) of a nanosecond Nd:YAG laser (Surelite I-10, Continuum, San Jose, CA, USA) with a repetition frequency of 1 Hz.
The time course of triplet decay was analyzed using an exponential decay. The quantum yield for triplet state formation Φ_T was calculated using a reference compound and the amplitude Amp of the exponential decay:

$$\Phi_{T,sample} = \Phi_{T,reference} * \frac{n_{sample}}{n_{reference}} * \frac{Amp_{sample}/\left(1 - 10^{-A_{Ex\,sample}}\right)}{Amp_{reference}/\left(1 - 10^{-A_{Ex\,reference}}\right)} \quad \textbf{Equation 12}$$

Where n is the refractive index of the solvent and A_{ex} is the absorbance at the excitation wavelength.

In the photoacoustic measurements, photoexcitation was obtained from the second harmonic (532 nm) of a nanosecond Nd:YAG laser (Surelite I-10, Continuum, San Jose, CA, USA), the beam was shaped with a 280 µm slit and the pressure wave was detected by a piezoelectric transducer (Panametrics V-103) and amplified before being sent to a digital oscilloscope (LeCroy 9370). The system used has been previously described [111].

The singlet oxygen time-resolved phosphorescence signals were detected using a modified PicoQuant Fluotime 200 system. A pulsed diode Nd:YAG laser (FTSS355-Q, Crystal Laser; Berlin, Germany) operating at a repetition rate of 1 kHz (emission at 532 nm, 1 µJ per pulse) was used for the excitation. A 1064 nm long-pass filter (Edmund Optics, York, UK) was placed before the sample to remove any residual components of the fundamental emission; to measure the emitted phosphorescence, a filter 1273±86 nm (Interferenzoptik Elektronik GmbH, Germany) was placed before the detector. The NIR luminescence of the sample was detected at 90°, using an H9170-45 photomultiplier (Hamamatsu Photonics, Japan) operating in photon counting mode and a NanoHarp 250 multichannel scaler (PicoQuant, Berlin, Germany).
The singlet oxygen signals S were analyzed with the PicoQuant FluoFit 4.0, using a biexponential decay:

$$S(t) = S(0)\frac{\tau_\Delta}{\tau_\Delta - \tau_T}\left(e^{-t/\tau_\Delta} - e^{-t/\tau_T}\right) + y_0 \quad \textbf{Equation 13}$$

Where $S(0)$ is the amplitude of the signal at time zero, τ_Δ is the lifetime of singlet oxygen, τ_T is the lifetime of the triplet state, y_0 is the background given by the dark counts.

The quantum yield for singlet oxygen formation, Φ_Δ, was determined using a comparative method with a reference photosensitizer. For each compound $S(0)$ was plotted as a function of $1\text{-}10^{-A}$ (where A is the absorbance at the excitation wavelength) and the slope was used to calculate the Φ_Δ:

$$\Phi_{\Delta,\text{sample}} = \Phi_{\Delta,\text{reference}} \frac{S(0)_{sample}}{S(0)_{reference}} \qquad \textbf{Equation 14}$$

Fluorescence microscopy

Microscopy experiments (confocal and STED) were conducted using a Leica TCS SP5 STED equipped with a CW laser for excitation (488 nm) and a depletion line at 592 nm. The detector was a HyD detector with higher sensitivity in the range 495-550 nm and an acquisition of 1400 Hz, a pinhole with an aperture of 0.4 au was used. The field of view was 512x512 and the photon average was 128. The filters used were a 488/561/633 and a 594-notch filter. A 100x (oil) immersion objective was used.

STORM experiments were conducted using a Nanoimager-S equipped with four CW lasers (405 nm, 488 nm, 561 nm, and 640 nm), a 100x, oil immersion, 1.45 NA Olympus objective. The camera was split in two channels (576-620 nm and 665-705 nm). The sample was kept at constant temperature using a temperature controller and was illuminated in TIRF mode.

6 Photoinactivation

A SORISA Photocare LED lamp that emitted green light (521±19 nm, used with the EITC complex) and a Red Light Man lamp that emitted red light (660±10 nm, used with the MB complex) were used for the bacterial photoinactivation tests.
The microbiology laboratory was equipped with a Telstar BV-100 hood (in which we have handled the bacteria), a Telstar AH-100 hood (to irradiate the bacteria), a Telstar Aelous V hood (where we prepared the Petri dishes), a JP Selecta incubator for bacteriology culture used to grow over-night the bacteria, a JP Selecta incubator chamber with a shaker at 100 rpm, a JP Selecta Presoclave III Plus autoclave.
As culture medium we used TSB, a liquid medium used for qualitative sterility testing procedures and for the enrichment and to culture aerobic microorganisms. For inoculation into Petri dishes, we used TSB with agar.
The experiments were conducted in a sterile environment: under a hood, on surfaces sterilized with alcohol, near a Bunsen; culture media (TSB and TSB with agar), PBS, pipette tips and Eppendorf tubes were autoclaved.

The day before the experiments we pre-inoculated the bacteria so they could be used the next day, we prepared the pre-inoculum diluting a previous inoculum (prepared from a colony taken from a Petri dish) in TSB.
By letting the bacteria grow overnight, in an incubator at 37 °C with a shaker (100 rpm), they reach the stationary phase and then re-incubating them for around one hour they return to the growth phase with the desired OD_{600}.
Then to remove the culture medium, we centrifuged the solution at 10,000 g for 10 minutes, removed the supernatant, resuspended with PBS and repeated this process 2 more times.

6.1 Photoinactivation tests

We prepared a 96-well plate (**Figure 17**), where each well represents a different experimental condition (sample, PS-labelled streptavidin concentration, and light conditions). We also prepared another 96-well plate which has not undergone irradiation (dark control).
Then we placed the former 96-well plate under the light source, irradiating them from the top.

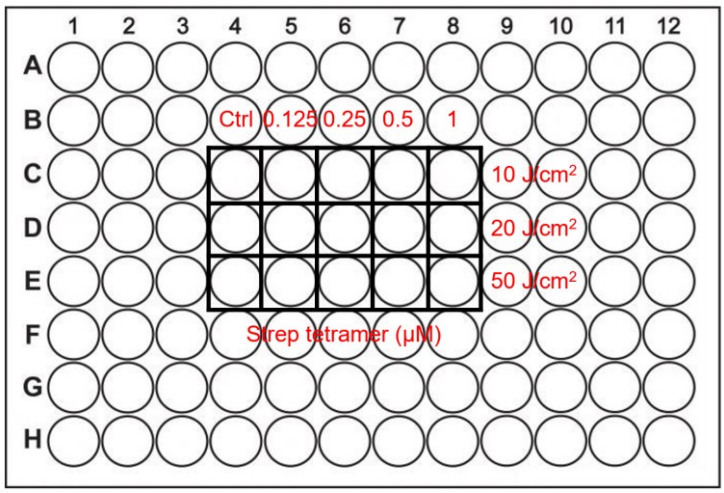

Figure 17. Schema of the irradiated 96-well plate. The reported concentration and light fluence values are those used with the EITC-Streptavidin-biotin-IgG complex.

We prepared a different 96-well plate (**Figure 18**) where we introduced the solution that was irradiated and the non-irradiated (dark) controls into the first well of each lane (column A), then diluted it into each subsequent well of the same row by, each time, a factor of 10. In this way, each row corresponds to a different experimental condition.

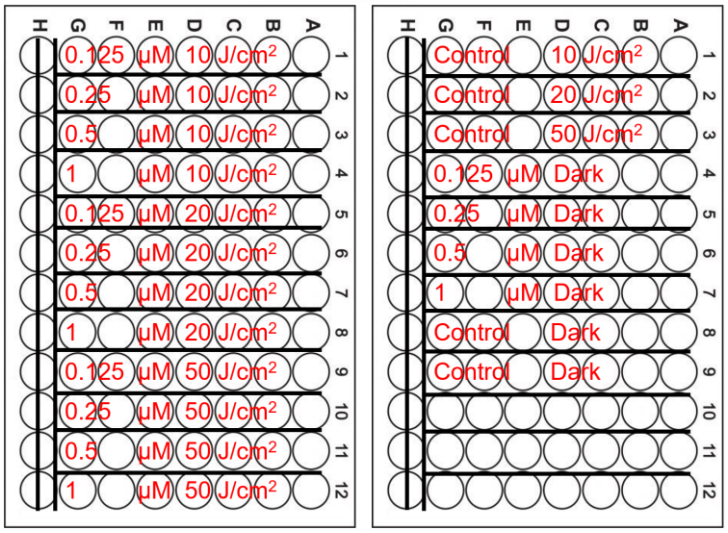

Figure 18. Scheme of the 96-well plate used to dilute the solution with bacteria. The reported concentration and light fluence values are those used with the EITC-Streptavidin-biotin-IgG complex.

Subsequently, we seeded each well of the same row (hence the sample with the same experimental condition, but different dilution factor) in a Petri dish.

We let the plates incubate overnight at 37 °C. We then counted the colonies that survived the photoinactivation.

7 Assembly of supramolecular complex between IgG and eosin labeled streptavidin

This chapter reports the results concerning the complex formed by EITC, streptavidin, biotin and IgG and directed against cells of *S. aureus* (**Figure 19**).

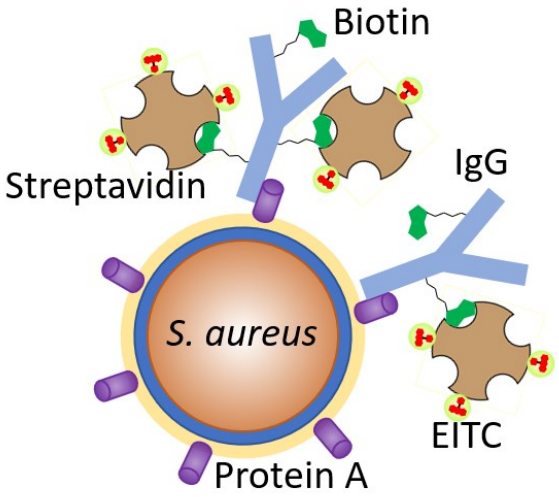

Figure 19. Cartoon representation of the interaction between the bacterial protein A and the supramolecular complex formed by the biotinylated IgG and eosin labeled streptavidin.

7.1 Chemical modification of molecular partners

In order to introduce photosensitizing properties on streptavidin, we labeled the protein with the amine reactive eosin 5-isothiocyanate (EITC). Streptavidin is a tetrameric protein with three potentially reactive Lys residues in each monomer. In principle, up to three EICT molecules could bind each streptavidin monomer, for a total of 12 eosins per protein. As described in "Appendix A – Labeling of streptavidin with EITC", after the reaction between streptavidin and EITC we purified the solution using a desalting column, in order to separate the unbound PSs from the protein-conjugated PSs.

To quantify the extent of labeling, we define a DOL of 1 when there is one PS molecule per monomer, or equivalently four EITCs per streptavidin tetramer:

$$DOL = \frac{[EITC]}{[Streptavidin]_{monomer}} \qquad \textbf{Equation 15}$$

While a higher DOL may be expected to increase the photosensitizing capability of the complex, we found that a higher binding efficiency negatively affects the overall photophysical properties of the complex.

It is well known that the reaction efficiency between the isothiocyanate group in EITC and the Lys residues improves as the pH of the reaction buffer is increased above neutrality [80]. We therefore used a carbonate-bicarbonate buffer at pH 9 to obtain an acceptable DOL.

In order to link IgG to streptavidin, we chemically modified IgG by linking it to an amine reactive modified biotin (NHS ester). In this case, the estimate of the DOL is prevented by the strong overlap of the absorption by biotin and the protein in the UV. Nevertheless, it is reasonable to assume that multiple biotins are present on IgG after labeling.

7.2 Photophysical properties of EITC labeled streptavidin

7.2.1 Absorption spectra

Eosin shows a prominent absorption band at 525 nm in PBS buffer with a molar absorption coefficient of 95,000 $M^{-1}cm^{-1}$, and smaller intensity bands extending to the UV.

From the absorption spectrum of EITC (**Figure 20**) it can be seen that the compound absorbs also at 280 nm, where aromatic amino acids absorb. In the case of streptavidin, its molar absorption coefficient at 280 nm is 41,326 $M^{-1}cm^{-1}$. The contribution of EITC absorption at 280 nm must be taken into account when estimating the protein concentration from the absorption spectrum. Using the EITC spectrum in PBS, it is possible to estimate that the absorption of EITC at 280 nm is 0.28 times the absorption at 525 nm. In the spectra of EITC-streptavidin, the absorption at 280 nm due to streptavidin only can be readily calculated as:

$$Abs_{Strep}(280\ nm) = Abs(280\ nm) - Abs_{EITC}(525\ nm) \times 0.28 \qquad \textbf{Equation 16}$$

Where $Abs(280\ nm)$ is the absorption measured at 280 nm and $Abs_{EITC}(525\ nm)$ is the absorbance at the peak in the visible range due to EITC bound to streptavidin.

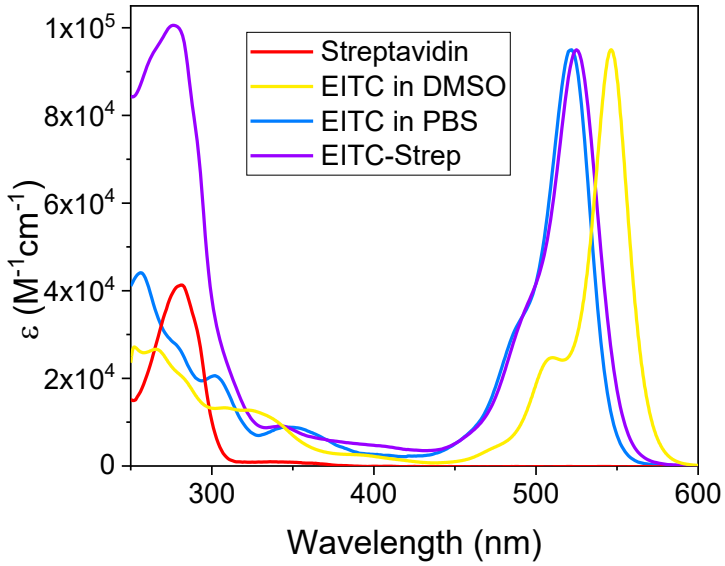

Figure 20. Molar absorption coefficient of EITC (in DMSO and PBS), EITC-streptavidin (in PBS), and streptavidin (in PBS) as a function of wavelength.

By varying the conditions in which the reaction between EITC and streptavidin takes place, different DOL can be obtained, ranging from one molecule of PS per tetramer (DOL = 0.25) to six EITC per tetramer of streptavidin (DOL = 1.5).

Figure 21 shows the absorption spectra of EITC-streptavidin complexes at different DOL, normalized for the protein absorption at 280 nm (i.e. corrected for the EITC contribution at 280 nm).

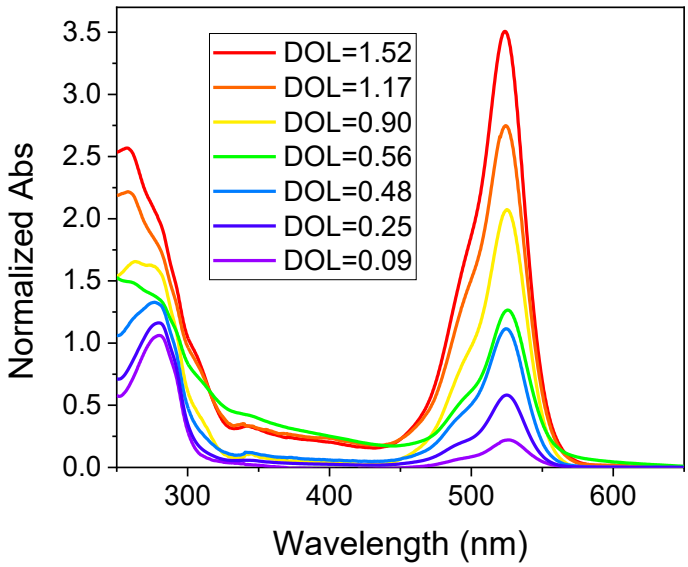

Figure 21. Absorption spectra of the EITC-streptavidin complex at different DOL. Spectra are normalized at 280 nm for the protein absorption. As the pH at which the reaction between streptavidin and EITC occurs increases, the DOL increases, the number of EITC bound to streptavidin increases.

The different DOL were obtained by changing the temperature and the pH at which the reaction between EITC and streptavidin takes place. We used a concentration of PS five times that of the protein. At more basic pH and at higher temperatures the reaction is favored, in particular:

- Using a PBS buffer at pH 7-7.4 we obtained a DOL between 0.09 (when the reaction occurs at 4 °C) and 0.4 (at room temperature).
- Using a more basic PBS (up to pH 8), when the reaction take place at 4 °C we obtained a DOL around 0.5, while at room temperature a DOL 0.9.
- Using a sodium bicarbonate buffer and incubating at 4 °C the DOL obtained was between 1.1 (for pH less than 9) and 1.6 (pH greater than 9).

pH values exceeding 10 were not explored as this leads to protein denaturation.
In principle, a higher DOL is expected to lead to a greater photosensitizing efficiency. As will be shown later, we found that the opposite occurs.

7.2.2 Fluorescence emission and excitation spectra

Fluorescence emission and excitation spectra of EITC in DMSO and of EITC-streptavidin in PBS buffer are reported in **Figure 22**. The excitation and emission peaks are almost identical for EITC and for EITC-streptavidin (520 nm/542 nm) in PBS. Due to the different environment of PS (solvatochromism), he peaks are red-shifted for EITC in DMSO (534 nm/552 nm).

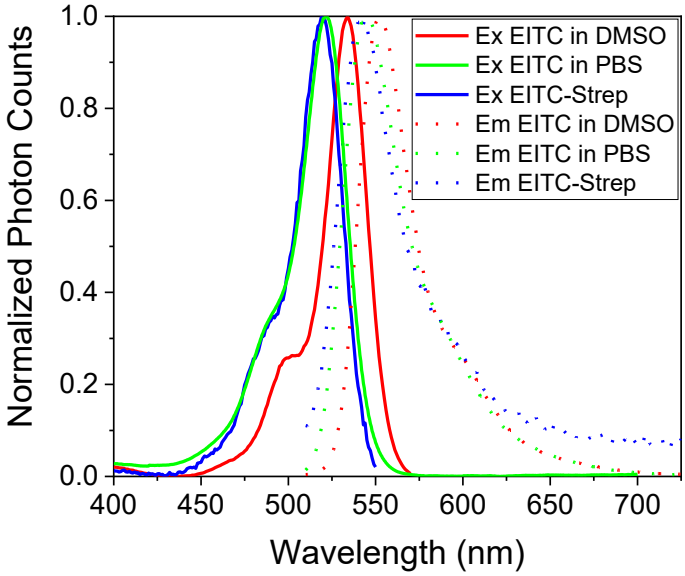

Figure 22. Normalized emission (dashed lines) and excitation (solid lines) spectra of EITC in DMSO (red), EITC in PBS (green),and EITC-streptavidin (DOL = 0.9) in PBS buffer (blue lines). For the emission spectra, excitation was set at 500 nm. For excitation spectra, the emission was collected at 580 nm.

7.2.3 Fluorescence anisotropy

The fluorescence anisotropy of EITC solutions is nearly zero (**Figure 23**), as expected for a small molecule with a high degree of rotational freedom. When EITC is conjugated to streptavidin, fluorescence anisotropy increases to nearly 0.2, indicating that the fluorophore has a reduced rotational freedom, due to the much larger size of the molecule. This information confirms binding of EITC to the protein.
The excitation wavelengths correspond to the range in which the PS absorption peak is maximum.

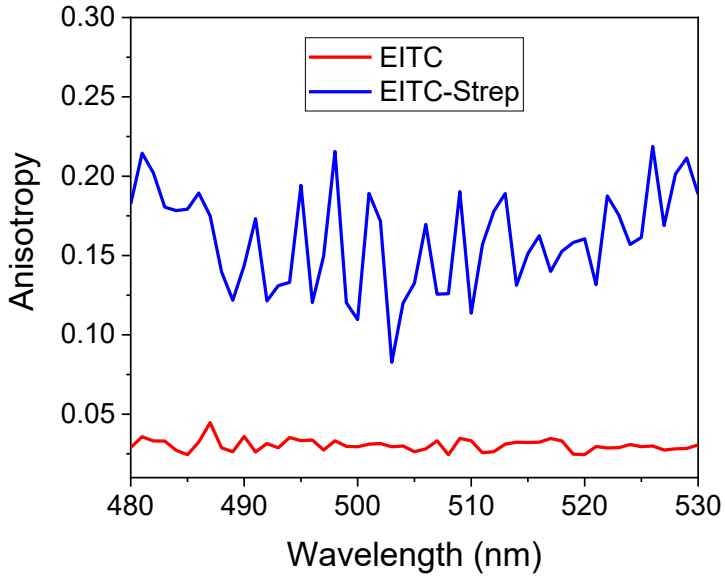

Figure 23. Fluorescence anisotropy of EITC in PBS (red) and EITC–streptavidin (blue) in PBS. Emission was collected at 560 nm.

7.2.4 Fluorescence correlation spectroscopy

Since the molecular weight of the EITC is much lower than that of streptavidin, the FCS measurements (**Figure 24**) allow to verify if the PS binds to the protein since in the latter case the observed diffusion coefficient should be that of the protein.
A wavelength of 475 nm was used for excitation, while the emission was collected through a 535-575 nm filter. The sample was air equilibrated.

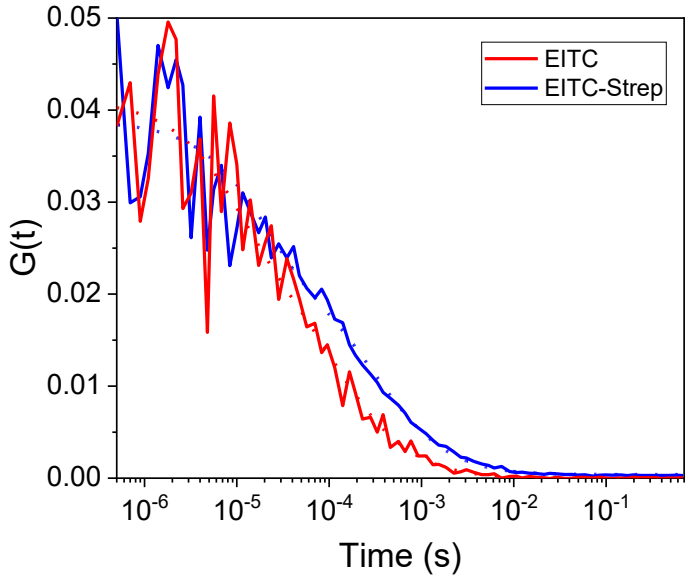

Figure 24. Cross-correlation function of the EITC (red) and EITC bound to streptavidin (blue). When PS is bound to the protein, the cross-correlation curve shifts to longer time-scales and the diffusion coefficient of the complex is that of the tetrameric protein.

The cross-correlation curves of the PS and the EITC labeled streptavidin show that, in presence of the protein, the diffusion of EITC becomes much slower indicating that the PS is bound to streptavidin.
The diffusion coefficient of the PS and the complex obtained from the reaction between EITC and streptavidin can be calculated from the analysis of the cross-correlation function. The curves are best described by a model comprising a short time triplet contribution and a single diffusing species. From the analysis we obtained a diffusion coefficient D of 240 μm^2/s for EITC and 49 μm^2/s for the EITC labeled streptavidin, which is in agreement with the one reported in the literature for the streptavidin tetramer [112]. The triplet state contribution is characterized by a lifetime τ_T = 10 μs.
Since the diffusion coefficient of the fluorescent species coincides with that of the protein, these data demonstrate that EITC is bound to streptavidin.

7.2.5 Mass spectrometry

As further confirmation that EITC is bound to streptavidin, we performed mass spectrometry experiments.

The major elution peak of streptavidin alone that we obtained was at 12.56 minutes. For EITC-labeled streptavidin (with a DOL lower than 1) we obtained two peaks in the mass spectrum: one at 12.83 minutes (corresponding to unlabeled streptavidin monomers) and one at 14.34 minutes (corresponding to monomers bound to EITC molecules).

Comparing the peak deconvolutions of the labeled streptavidin sample (**Figure 25**) a mass difference of 704.7 Da can be observed, consistent with the molecular weight of one molecule of EITC. This demonstrates that some streptavidin monomers (eluted at 12.83 minutes) are labeled with only one molecule of EITC (eluted at 14.34 minutes).

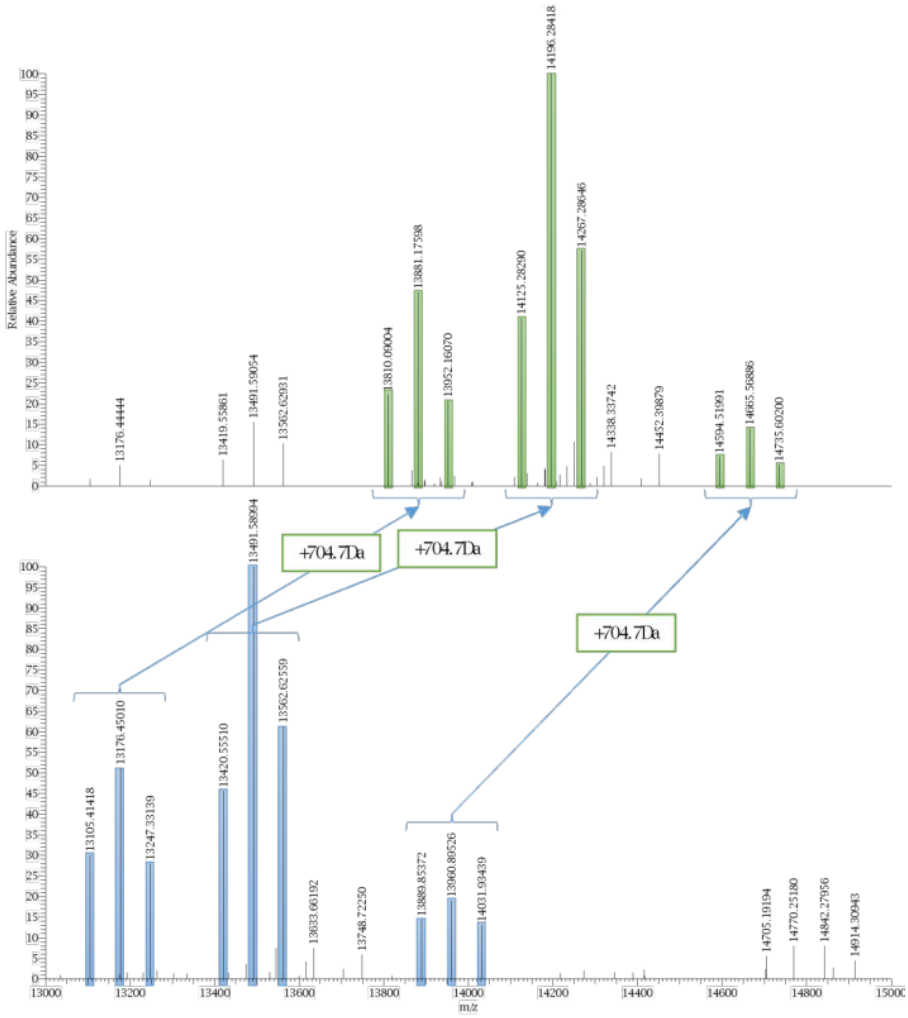

Figure 25. Deconvolution of mass spectrum. The mass difference between labeled streptavidin monomer eluted at 14.34 minutes (top) and native streptavidin monomers eluted at 12.83 minutes (bottom) is 704.7 Da consistent with an EITC molecule.

7.3 Fluorescence emission as a function of DOL

Having obtained EITC-streptavidin complexes with different DOL, we have measured fluorescence emission spectra to assess the effect of protein binding and DOL on fluorescence yield and lifetime.

7.3.1 Emission spectra

By comparing the fluorescence emission spectra (obtained by exciting at 500 nm) of streptavidin at different DOL (**Figure 26**) it can be seen that as the DOL increases, the fluorescence emission decreases.
The spectra were normalized for the absorbance at 500 nm to make the measurements comparable to each other. No changes in spectral shape is observed with DOL.

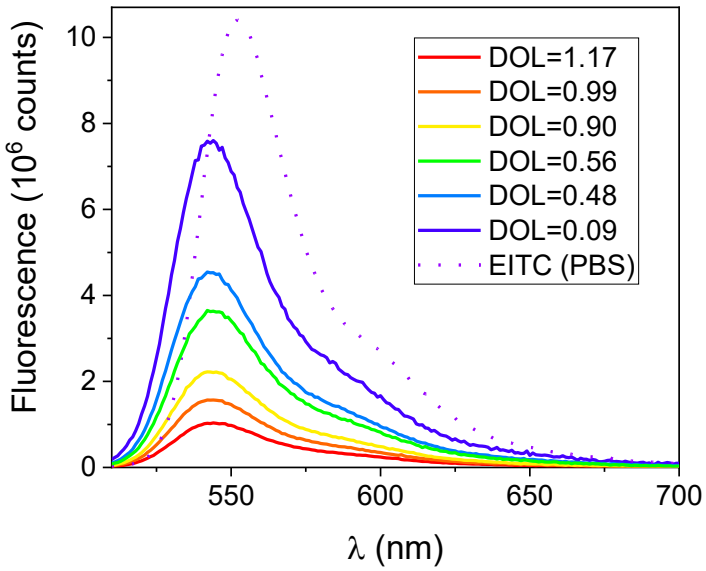

Figure 26. Fluorescence emission of EITC in PBS (dashed line) and of the EITC-streptavidin complex at different DOL (solid lines). Fluorescence spectra are normalized for the absorbance at 500 nm (excitation wavelength).

Using the emission spectra, and knowing the quantum yield of eosin (in PBS), it is possible to calculate the fluorescence quantum yield [113] of EITC and of the PS bound to streptavidin ((**Table 3**) and (**Figure 27**)):

$$\Phi_{F,EITC-strep} = \Phi_{F,eosinY} * \frac{F_{EITC-strep}/\left(1-10^{-A_{Ex_{EITC-strep}}}\right)}{F_{eosinY}/\left(1-10^{-A_{Ex_{eosinY}}}\right)} \qquad \textbf{Equation 17}$$

Where F is the area under the fluorescence emission spectra and A_{Ex} is the absorbance (of eosin and of the EITC-streptavidin complex) at 500 nm.

For EITC solubilized in DMSO instead of PBS, it is necessary to correct for the refractive index of the media (1.478 for DMSO [114] and 1.333 for PBS [115]):

$$\Phi_{F,EITC} = \Phi_{F,eosinY} * \frac{1.478}{1.333} * \frac{F_{EITC-strep}/\left(1-10^{-A_{Ex_{EITC-strep}}}\right)}{F_{eosinY}/\left(1-10^{-A_{Ex_{eosinY}}}\right)} \qquad \textbf{Equation 18}$$

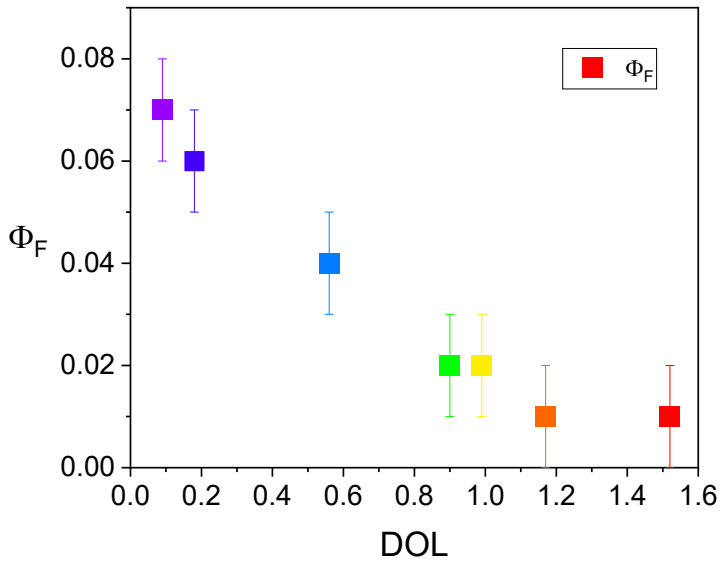

Figure 27. Fluorescence quantum yield of the EITC-streptavidin complex at different DOL.

As can be seen, as the DOL increases the fluorescence quantum yield decreases. When the PS binds the protein its fluorescence quantum yield decreases, and this could be due to an interaction between EITC and the amino acid residues surrounding the EITC binding site on streptavidin. The decrease in quantum yield with increasing DOL could be due to non-radiative deexcitation caused by the interaction between different EITC molecules bound to the same protein.

	Water	DMSO	PBS
Eosin	0.20 [82], [116]		0.24 [81]
EITC		0.58±0.06	0.18±0.02
EITC-Streptavidin			0.07±0.01 DOL=0.09 0.07±0.01 DOL=0.18 0.04±0.01 DOL=0.56 0.02±0.01 DOL=0.9 0.02±0.01 DOL=0.99 0.01±0.01 DOL=1.17 0.01±0.01 DOL=1.52

Table 3. Fluorescence quantum yield of EITC and EITC bound to streptavidin. When PS is bound to the protein, the fluorescence quantum yield decreases and the loading of more PSs on the protein causes a progressive decrease in the quantum yield.

7.3.2 Excited state lifetime

The time resolved fluorescence emission by eosin (in PBS) and EITC (in PBS and DMSO) are reported in **Figure 28**. The decays were analyzed performing convolution of the IRF with a single exponential decay function. A representative fit is reported in **Figure 29** (right). The fluorescence lifetimes are reported in **Table 4**.

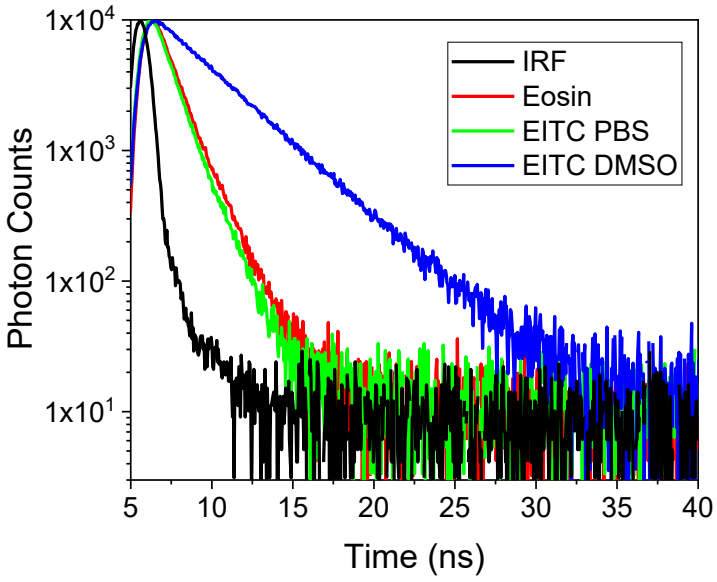

Figure 28. Fluorescence decays for eosin in PBS (red) and EITC in PBS (green) and DMSO (blue). Excitation was at 500 nm, emission at 550 nm.

Furthermore, since the fluorescence quantum yield of the EITC-streptavidin complex is influenced by the DOL, we tested whether the DOL also affects the decay lifetime (**Figure 29** (left)).

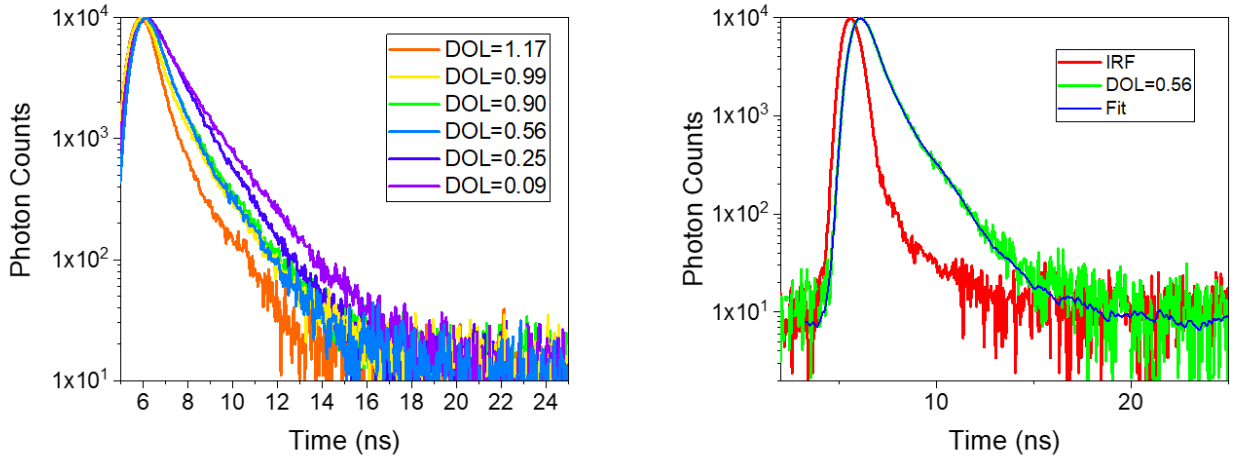

Figure 29. Fluorescence decays of the EITC-streptavidin complexes at different DOL (left), representative fit (blue) of a fluorescence decay (green) for EITC-streptavidin using deconvolution with the IRF (red) (right). Excitation was at 500 nm, emission was collected at 550 nm.

Observing the time course of the fluorescence emission for the EITC-streptavidin complex, it can be noted that as the DOL increases, the fluorescence decay becomes faster.

The fluorescence decays were described by a bi-exponential function (in **Table 4** are reported the mean lifetimes), in which the fastest lifetime is at the limit of the instrumental resolution (about 0.1 ns) and is independent of the DOL.

	τ (ns)
Eosin (PBS)	1.21 [81] 1.231±0.003
EITC (PBS)	1.117±0.003
EITC (DMSO)	3.107±0.004
EITC-Streptavidin (PBS)	1.16±0.05 DOL=0.09 1.05±0.05 DOL=0.25 0.67±0.05 DOL=0.56 0.59±0.05 DOL=0.9 0.55±0.05 DOL=0.99 0.36±0.05 DOL=1.17 0.34±0.05 DOL=1.52

Table 4. Fluorescence lifetimes of eosin and EITC alone and bound to streptavidin. The fluorescence lifetime decreases as the DOL increases.

The faster decay of the excited singlet state of EITC at increasing DOL, suggests that a dynamic quenching mechanism through non radiative decays is operative (e.g. interaction between multiple copies of EITC bound to the same streptavidin and/or different interaction between EITC molecule and protein residues).

7.4 Triplet state formation

The faster decay of the excited singlet state of EITC at increasing DOL suggests that quenching of the excited state due to interactions between EITC molecules on the same protein, may negatively affect also other deexcitation pathways, in particular intersystem crossing to the triplet state.

We then determined the quantum yield of triplet state formation of the EITC-streptavidin complexes at different DOL.

The extent of triplet state formation, and the time course of its decay, were followed by monitoring the bleaching of the ground state at 500 nm of air equilibrated samples (**Figure 30**). At this wavelength only the ground state should absorb, thus the change in absorbance only reflects relaxation of the PS to the ground state. After the excitation the ground state get depleted (the absorbance decreases) while the singlet excited state is formed; then this state undergoes transition to the triplet state which has a lifetime of the order of μs; finally, the triplet state relaxes to the singlet state repopulating the ground state (the absorbance increases).

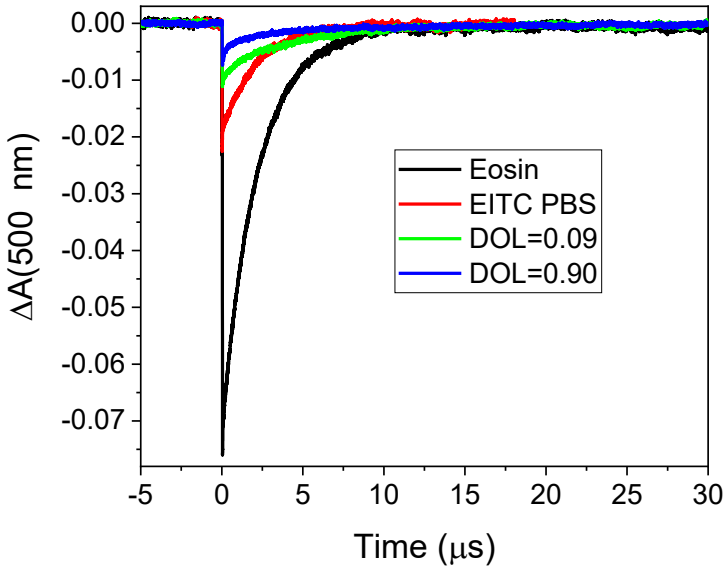

Figure 30. Transient absorption at 500 nm for eosin in PBS (black), EITC in PBS (red), EITC-streptavidin in PBS at DOL = 0.09 (green) and DOL = 0.9 (blue). Solutions were air equilibrated. Nanosecond excitation was at 532 nm.

The transient absorbance signal has a negative sign due to the bleaching of the ground state after photoexcitation at 532 nm. The time course shows the typical formation of the triplet state within the duration of the laser pulse, followed by recovery of the absorbance of the ground state. By analyzing the recovery portion of the signals through an exponential decay, we determined the lifetime of the triplet state (**Table 5**).

	τ_1 (μs)	Amp_1	τ_2 (μs)	Amp_2
Eosin (PBS)	2.0±0.1			
EITC (PBS)	2.1±0.1 1440±50 §			
EITC (DMSO)	2.5±0.1			
EITC-Streptavidin DOL=0.09	4.32±0.01			
EITC-Streptavidin DOL=0.9	1.71±0.01	68%	10.1±0.1	32%
EITC-Streptavidin DOL=1.58	2.09±0.02 1140±50 §	79%	12.9±0.5	21%

Table 5. Lifetimes of the triplet state of eosin and EITC alone and bound to streptavidin. § Nitrogen-saturated solution.

The lifetime of the EITC is in agreement with that of a triplet state quenched by molecular oxygen in an air equilibrated solution (with $[O_2] \sim 0.2$ mM), while when the EITC is bound to streptavidin at low DOL, the

lifetime increases because the protein protects the PS from molecular oxygen and the lifetime of the triplet is lengthened. For higher DOL, triplet decay of the EITC-streptavidin samples was best described by a double exponential decay, where amplitude and lifetimes depend on DOL. This could reflect interactions between different EITC molecules bound to the same protein, and/or the presence of different local environments sensed by the multiple copies of EITC bound to the protein.
By flushing nitrogen in the samples, in order to remove oxygen, we observed (not reported) that the lifetime increases, and this confirms that the measured lifetime was that of the triplet state.
The absorbance change at the end of the laser pulse, proportional to the extent of triplet formation, was used to calculate the triplet yield. By analyzing the curves it is also possible to determine the amplitude (Amp_fit) of the lifetimes through which it is possible to calculate the quantum yield of triplet state formation (**Table 6**):

$$\Phi_{T,EITC-Strep} = \Phi_{T,EITC} * \frac{Amp\_fit_{EITC-Strep}/\left(1-10^{-Abs\_532nm_{EITC-Strep}}\right)}{Amp\_fit_{EITC}/(1-10^{-Abs\_532nm_{EITC}})} \quad \textbf{Equation 19}$$

Where Abs_532nm is the absorbance (of EITC and EITC-streptavidin complex) at 532 nm. For the EITC solubilized in DMSO instead of PBS, it is necessary to correct for the refractive index of the medium (1.478 for DMSO [114] and 1.333 for PBS [115]).

	Water	DMSO	PBS
Eosin	0.64 [83] 0.71 [84] 0.8 [82]		
EITC		0.06±0.01	0.49±0.05
EITC-Streptavidin			0.10±0.01 DOL=0.09 0.09±0.01 DOL=0.56 0.07±0.01 DOL=0.9 0.04±0.01 DOL=1.58

Table 6. Quantum yield of triplet states formation of EITC and EITC bound to streptavidin. When the PS is bound to the protein, the quantum yield decreases and binding more PS to the protein causes a decrease in the quantum yield.

As it can be noticed, as the DOL increases, the quantum yield of the triplet state formation decreases. This could negatively affect the performance of the complex, since if the probability of the PS to form the triplet state decreases, the probability to form ROS and singlet oxygen also decreases, resulting in a lower phototoxicity effect.

7.4.1 Time resolved photoacoustics

To independently confirm that the quantum yield of the triplet state formation decreases as the DOL increases, we performed time-resolved photoacoustics measurements.
As a calorimetric reference we used brilliant black (BBN, a water-soluble synthetic dye). We performed the measurement in the 5-30 °C range.

Figure 31 shows the photoacoustic signals of an EITC-streptavidin complex. As it can be seen, as the temperature decreases the amplitude of the signal decreases and shifts to longer time scales (as the pressure wave speed decreases).

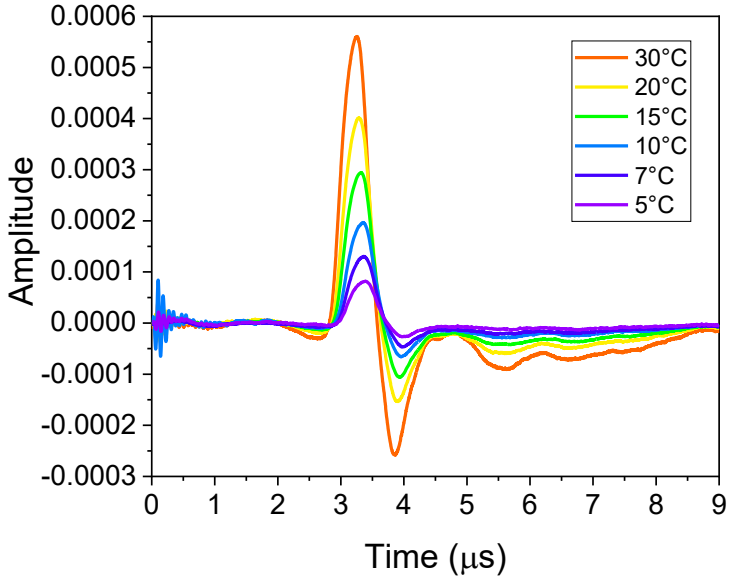

Figure 31. Photoacoustic signals of the EITC-streptavidin complex as a function of temperature. Excitation at 532 nm.

By analyzing the signals of the sample and of the BBN at different temperatures and using the convolution program Sound Analysis, we concluded that the analysis was optimal when two transient species were used (**Figure 32**).

The decay with faster lifetime (less than the experimental resolution) is associated with ground-state relaxation and its amplitude (φ_1) represents the heat released by under-resolution fast relaxations (such as internal conversion, ground-state relaxation and intersystem crossing). The longer lifetime describes the heat released by the decays of the triplet state and singlet oxygen; the values of these two transients were not separable (due to their very similar lifetimes, around 2 μs) and therefore we had to set an intermediate lifetime, whose amplitude (φ_2) describes the energy of both decays considered.

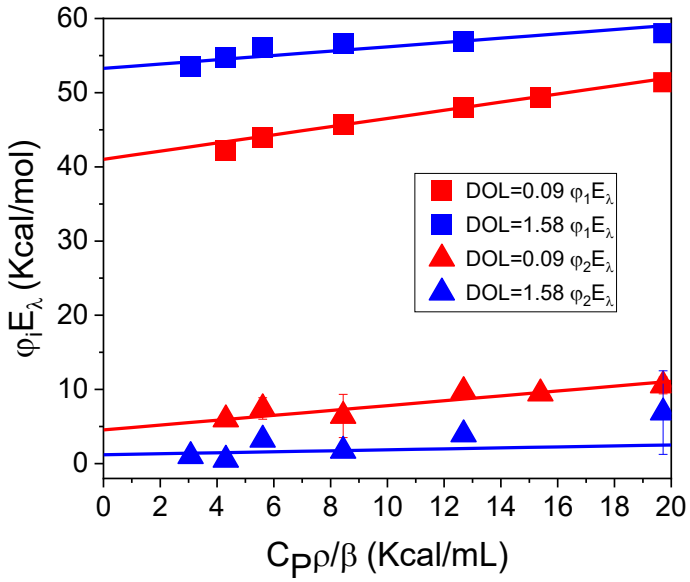

Figure 32. Transient species as a function of thermoelastic factor for EITC-streptavidin samples. Decay 1 is characterized by a lifetime below resolution (<20ns), while the decay 2 contains contributions from relaxation of the triplet state and singlet oxygen.

The amplitude contains both enthalpic and volumetric contributions that can be separated using the following equation

$$\varphi_i = \alpha_i + \frac{\Delta V_{e,i}}{E_\lambda}\frac{c_p \rho}{\beta} \qquad \textbf{Equation 20}$$

Where α is the fraction of the absorbed energy released in form of heat, ΔV the variation in structural volume, E_λ the energy of the excitation wavelength, $c_p\rho/\beta$ the thermoelastic factor (with c_p the specific heat, ρ the density and β the thermal expansion coefficient) [117].

It can be noted that in the first transient (φ_1) there is a release of heat (the intercept of the fitting) and that this increases as the DOL increases, suggesting that fast non radiative decays of the excited singlet state become more efficient.

The second transient is due to the relaxation of triplet state and singlet oxygen, so its intercept is linked to the quantum yield of the triplet state formation. Assuming the amplitude reflects the overall energy released after formation of the triplet state we can derive the triplet yield as:

$$\Phi_T = Q_2 * \frac{\lambda_T}{2.86x10^4} \qquad \textbf{Equation 21}$$

with $Q = \alpha E_\lambda$ (heat released) the intercept at T = 0 °C obtained from the fitting and λ_T the phosphorescence emission wavelength of the triplet state (we used the value of 680 nm for eosin [118]).
For each DOL it is therefore possible to calculate the quantum yield of the triplet state formation obtained by photoacoustic measurements and to compare them with those obtained by LFP (**Figure 33**).

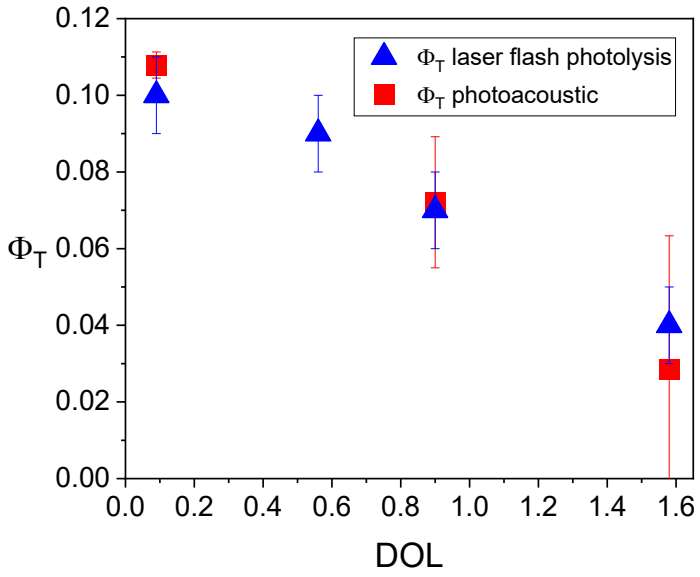

Figure 33. Comparison between the values of $\boldsymbol{\Phi_T}$ by Laser Flash Photolysis (blue triangles) and time resolved photoacoustics (red squares). The values obtained with the two techniques are comparable.

It can be noted that the quantum yields of triplet state formation determined with the two different techniques are comparable. The error bars related to photoacoustic measurements are greater and this is due to the fact that the analyzed system is complex: there are two unresolved transients (relaxation of the triplet and singlet oxygen) and the photophysics of the EITC is influenced by the different interaction with the streptavidin residues.

7.5 Singlet oxygen formation

The quantum yield of EITC-streptavidin triplet state formation decreases as the DOL increases, and this is expected to negatively affect singlet oxygen formation.
In order to verify this effect, we measured the singlet oxygen formation using near-infrared time-resolved phosphorescence emission.

By comparing the phosphorescence signals obtained for EITC bound to streptavidin with that for reference molecules, it is possible to calculate the quantum yield of singlet oxygen formation for EITC bound to the streptavidin as a function of DOL.

From time-resolved phosphorescence measurements of air-equilibrated samples, it is possible to derive signals (**Figure 34**) corresponding to formation and decay of singlet oxygen, sensitized by the PS triplet state.

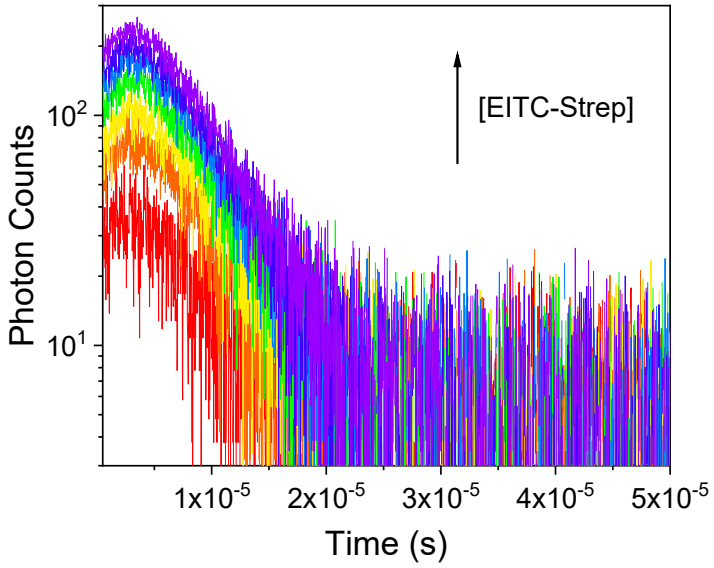

Figure 34. Time-resolved phosphorescence of EITC labeled streptavidin at different concentrations. As the concentration of EITC-streptavidin increases, there is a greater production of singlet oxygen and therefore the signal increases. In these signals, the rise before the peak corresponds to decay of singlet oxygen, while the subsequent decay tracks PS triplet state decay. Excitation at 532 nm, singlet oxygen phosphorescence emission collected at 1275 nm.

By analyzing the signals with a bi-exponential decay (to describe both the formation of the triplet state and the decay of singlet oxygen) it is possible to estimate the lifetimes and the relative amplitudes (that should match) of the two processes. From these parameters it is therefore possible to calculate $S(0)$ for each concentration.
By plotting $S(0)$ as a function of the absorbed energy (**Figure 35**) and fitting it with a linear function, it is possible to determine a representative slope for the emission intensity.
Performing similar experiments with reference molecules of know singlet oxygen quantum yield, affords reference slopes. It is possible to calculate the quantum yield of singlet oxygen formation of the sample (**Table 7**). As reference molecule we used: rose bengal (RB) (Φ_{Δ} = 0.75 [119]), tetra(4-N-methylpyridyl)porphine (TMPyP) (Φ_{Δ} = 0.74 [119]) and tetraphenylporphine tetrasulfonic acid (TPPS) (Φ_{Δ} = 0.62 [120]).

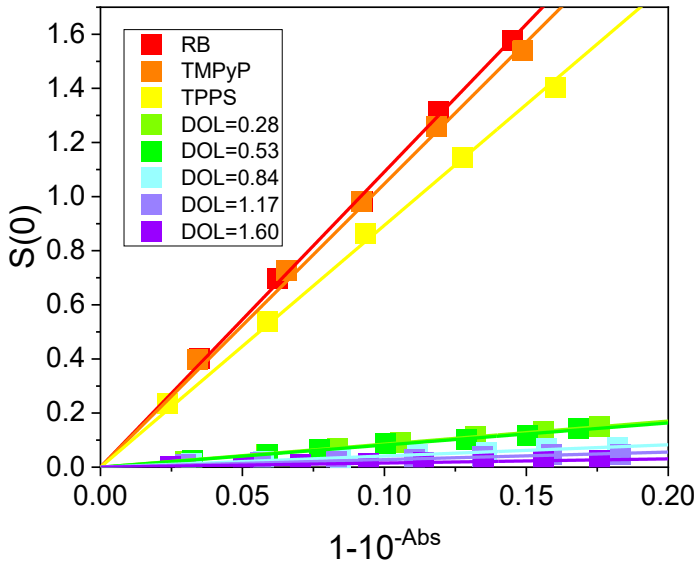

Figure 35. $S(0)$ for reference molecules and EITC-streptavidin samples at different DOL as a function of absorbance. By comparing the slopes of the different samples, it is possible to calculate the quantum yield of singlet oxygen formation of the EITC bound to streptavidin.

	Φ_Δ
EITC-Streptavidin DOL=0.28	0.06±0.02
EITC-Streptavidin DOL=0.53	0.06±0.02
EITC-Streptavidin DOL=0.84	0.03±0.01
EITC-Streptavidin DOL=1.17	0.02±0.01
EITC-Streptavidin DOL=1.6	0.01±0.01

Table 7. Quantum yield of singlet oxygen formation of EITC bound to streptavidin.

From the results obtained, it can be deduced that the quantum yield of singlet oxygen formation decreases as the number of PSs present on the same protein increases. Moreover, Φ_Δ is systematically lower than Φ_T, (**Figure 36**, left), a possible indication that the protein environment also decreases the energy transfer efficiency from the triplet state to molecular oxygen, also because the oxygen trapping efficiency is 99.3%. Thus, it may be concluded that at increasing DOL, the phototoxic effect of the complex decreases.

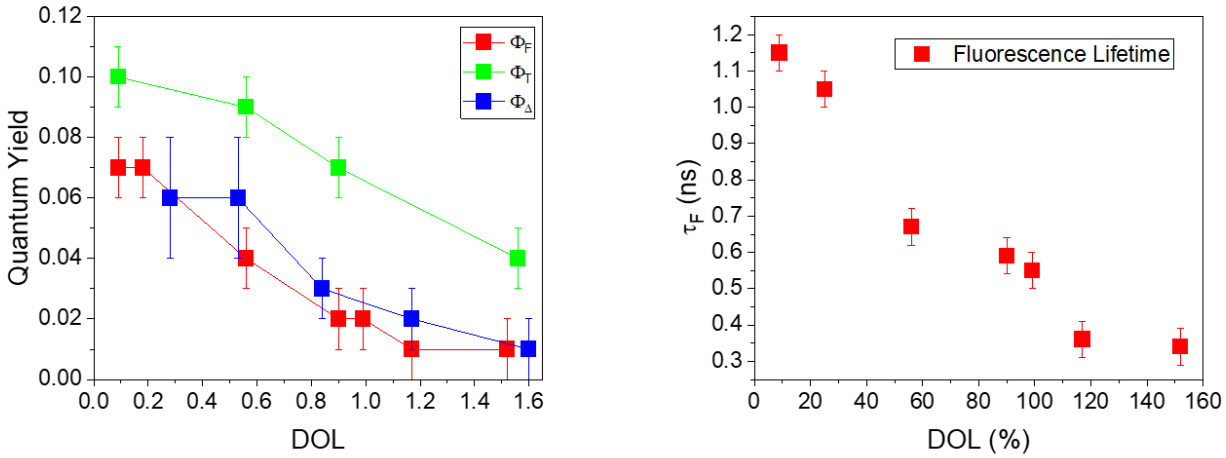

Figure 36. Comparison between Φ_F (triangles), Φ_T (squares), and Φ_Δ (circles) on the left and fluorescence lifetime on the right, as a function of DOL.

As observed with photoacoustics, the fast transient φ_1 (associated with ground-state relaxation) increase as DOL increases, indicating that the singlet excited state is quenched more efficiently. This non-radiative dynamic quenching also affects the fluorescence lifetimes (**Figure 36**, right) which decrease as DOL increases. Furthermore, the probability that the PS can pass to the triplet state and, subsequently, generate singlet oxygen also decreases (**Figure 36** , left).

7.6 EITC bound to streptavidin does not affect biotin binding sites

Labeling of streptavidin with EITC may interfere with the capability of the protein to bind biotin, a fact that would be detrimental to the development of the supramolecular construct. We have thus checked the ability of EITC-streptavidin to bind biotin using a biotinylated fluorophore (STAR635) and monitoring the concomitant changes in fluorescence emission intensity and fluorescence anisotropy.

We decided to use a biotinylated STAR635 because we had preliminary indications that, upon binding to streptavidin, its fluorescence emission decreases (of about 90%) and the anisotropy concomitantly increases. Furthermore, given their spectral properties, no FRET is observed between EITC and STAR635.

To verify that biotin binding sites are all available, we have titrated STAR635 with increasing concentration of streptavidin. Since the affinity of biotin-STAR635 for streptavidin is extremely high, biding is quantitative. Upon binding to streptavidin, fluorescence emission of STAR635 is quenched (**Figure 37**), and the quenching increases with the concentration of streptavidin, until a saturation is reached when all dye molecules are bound to streptavidin. This is expected to occur when the streptavidin tetramer concentration is one quarter the concentration of STAR635. Equivalently, saturation is observed when the concentration of streptavidin monomers equals that of STAR635.

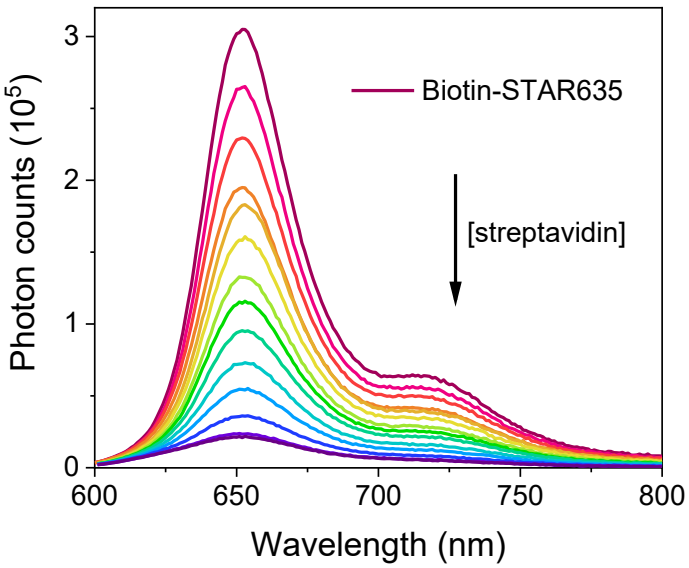

Figure 37. Emission spectra of STAR635 as a function of EITC-streptavidin concentration.

Using the formula

$$Quenching_i = \frac{Area\_emission_{MAX} - Area\_emission_i}{Area\_emission_{MAX}} * 100 \qquad \textbf{Equation 22}$$

It is possible to calculate, from the emission spectra of STAR635, the percentage quenching of the fluorescence as a function of the concentration of streptavidin (**Figure 38**).

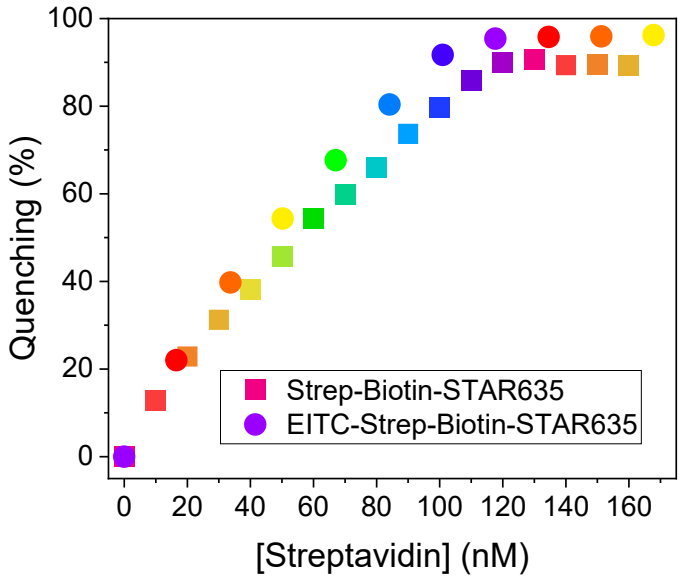

Figure 38. Quenching of biotinylated-STAR635 emission as a function of streptavidin (squares) and EITC-streptavidin (circles) concentration. Using a concentration of STAR635 of 100 nM, a concentration (in monomers) of streptavidin of around 100 nM is required to achieve saturation. The same result was obtained for both streptavidin alone and EITC-labeled streptavidin.

The linear trend in **Figure 38** (squares) indicates that the biotinylated fluorophore binds stoichiometrically to the protein. The concentration of streptavidin at which the trend changes from linear to plateau (saturation) provides an estimate of the number of available biotin-binding sites.
Having used a concentration of biotinylated STAR635 of 100 nM and since saturation is achieved with a concentration of about 100 nM of streptavidin monomers, all biotin-binding sites present on streptavidin are available and therefore the EITC does not block the bound between biotin and streptavidin.
A similar experiment conducted with EITC-streptavidin afforded the same result (**Figure 38**, circles), indicating that labeling with EITC does not impair binding.

We have verified binding by monitoring changes in fluorescence anisotropy along the titration. Fluorescence anisotropy is plotted in **Figure 39** as a function of streptavidin concentration, showing a transition from a very small value, when all or most fluorophores are unbound, to nearly 0.11, when all biotin-STAR635 molecules are bound to streptavidin.

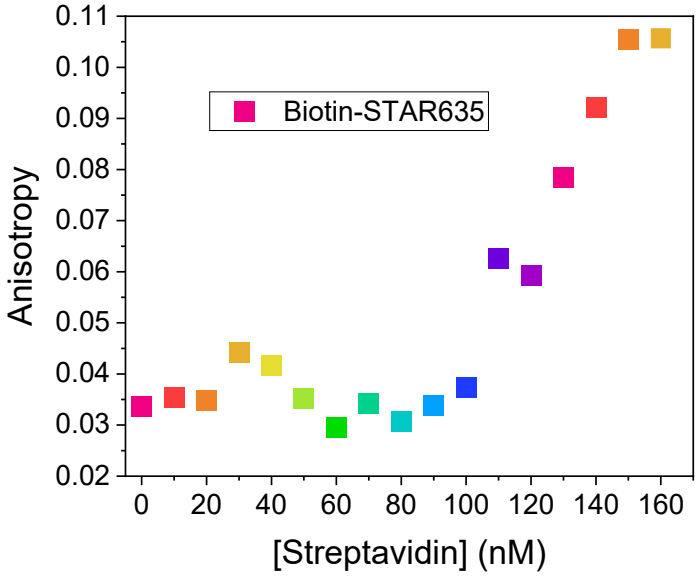

Figure 39. STAR635 fluorescence anisotropy as a function of EITC-labeled streptavidin concentration.

Initially, when the streptavidin concentration is low (less than 100 nM, in monomers), not all the biotinylated STAR635 binds to the protein and because the bound fluorophores have lower fluorescence emission (they undergo quenching) than the free fluorophores, the measured anisotropy is dominated by the fluorescence of the free STAR635 and therefore the resulting anisotropy is low.
After reaching the saturation concentration (about 100 nM of streptavidin monomers) all the fluorophores are bound, so that in the measured anisotropy the contribution of the fluorophores bound to the protein prevails.

In addition, we performed fluorescence emission measurements by varying the streptavidin concentration (as in the previous case) but using a different fluorophore: a biotinylated STAR488.
Also in this case we observed a quenching (of 85%) caused by the interaction between streptavidin and the fluorophore. Furthermore, using a biotin with a spacer (peg1000) we observed that the quenching decreases (of about 45%). This result suggests that a greater spatial separation, and therefore a lower interaction, between the fluorophore and protein enhances fluorescence emission.
Given that the increase in fluorescence could lead to an increase in the quantum yield of triplet state and singlet oxygen formation, the possibility of using PSs not directly bound to streptavidin but having a linker that distances them from the protein, could be explored.

7.7 Biotinylated IgG binds EITC-streptavidin

The binding between EITC-streptavidin and biotinylated IgG produces no observable changes in the measured spectra and fluorescence anisotropy (data not shown), but it is possible to verify the formation of this bond by FCS measurements, monitoring fluorescence emission by EITC-streptavidin.
IgG has a mass greater than streptavidin (150 kDa vs 55 kDa) thus, upon binding to IgG, the observed diffusion time τ_D increases, i.e. the autocorrelation function $G(\tau)$ is shifted towards longer time scales.
For these FCS measurements, a wavelength of 475 nm was used for excitation, while the emission was collected through a 535-575 nm filter.

For these samples, the autocorrelation function (**Figure 40**) is best described by a diffusion term multiplied by a triplet state term in the short time scale.

By keeping the concentration of EITC-streptavidin constant (60 nM of protein in tetramers), it can be seen that as the IgG concentration increases, the intercept increases (i.e. the number of diffusive molecules decreases) and that the autocorrelation function shifts to longer time scale (i.e. larger size species are present).

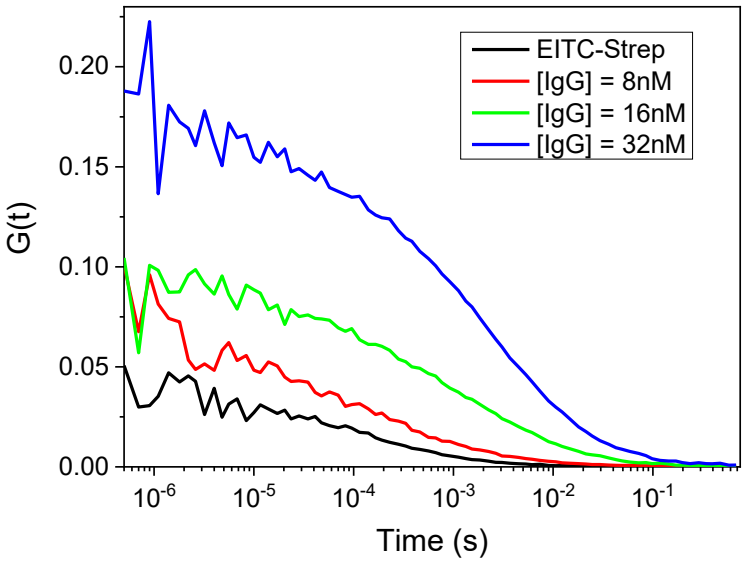

Figure 40. FCS traces of EITC-streptavidin and EITC-streptavidin + biotin-IgG complexes. As the concentration of the biotinylated IgG increases, streptavidin first binds to the antibody, then larger complexes are formed.

Figure 41 compares the normalized diffusive part of the autocorrelation curves to emphasize changes in the diffusional part upon binding of EITC-streptavidin to IgG.

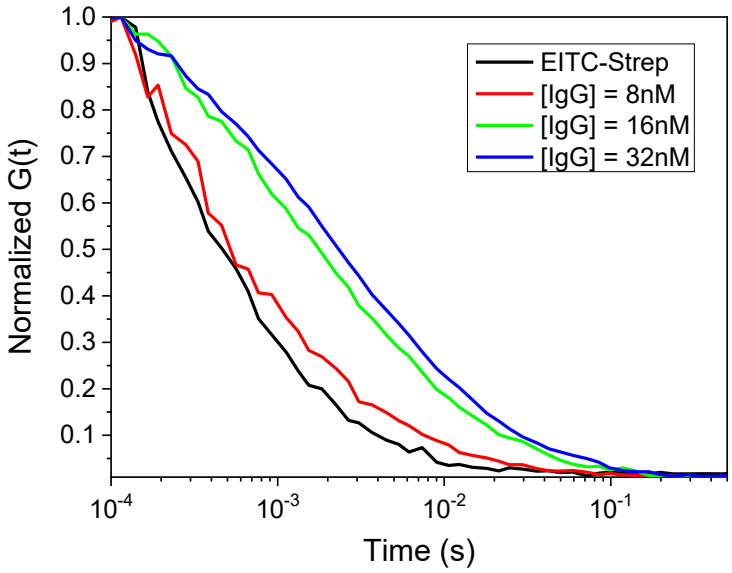

Figure 41. Comparison of the diffusive part of the autocorrelation functions. The EITC labeled streptavidin shifts to the left when it is bound to the biotinylated IgG, since its dimensions increases so it diffuses more slowly.

In the absence of IgG, the curve is described by a single diffusive species with $D \sim 50$ μm^2/s representing the EITC bound to a streptavidin tetramer, in accordance with what is reported in the literature [112], and by a triplet with a lifetime of about 10 μs.
As the antibody concentration increases, another diffusive species appears with $D \sim 40$ μm^2/s, which corresponds to a complex consisting of an EITC-labeled streptavidin tetramer and a biotinylated IgG. If the IgG concentration increases further, larger complexes with $D \sim 4$ μm^2/s are formed; indeed the presence of multiple biotin molecules on the same IgG and to the four binding sites for biotin on streptavidin leads to the formation of clusters consisting of multiple IgG that bind to multiple streptavidin.

From the inverse of the intercept $G(\tau = 0)$ it is possible to determine the number of diffusive particles present in the confocal volume. From **Figure 42** it can be seen that by increasing the concentration of IgG, the number of diffusive molecules decreases. This is a confirmation of the formation of larger complexes as the concentration of biotinylated IgG increases.

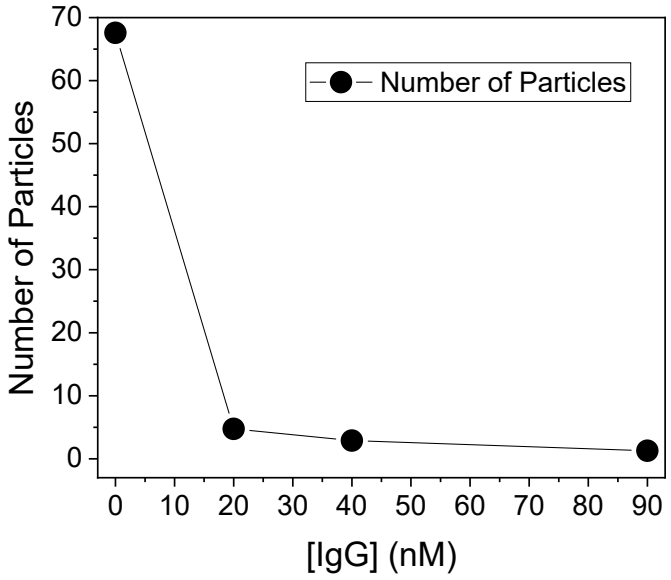

Figure 42. Number of molecules as a function of the IgG concentration. As the concentration of biotinylated IgG increases, the number of molecules present in the effective volume decreases.

In **Figure 43** the relative weight of the complexes with different diffusion coefficients is reported. As can be seen, as the concentration of biotinylated IgG increases, the free labeled streptavidin fraction (not bound to the antibody) decreases while the bound complex fraction increases and, at higher concentrations, the fraction relating to clusters prevails.

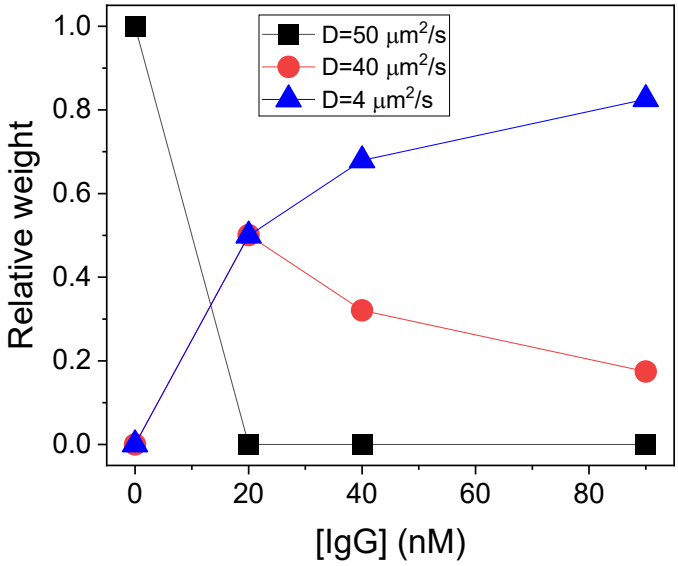

Figure 43. Relative weight of complexes with different diffusion coefficient. The relative weight of the EITC-streptavidin complex decreases as the concentration of biotinylated IgG increases, while the relative weight of the cluster increases.

To avoid formation of excessively large complexes, we decided to first incubate bacteria with biotinylated IgG and then add EITC-streptavidin; in this way the formation of clusters should be reduced and therefore a more uniform distribution of the complexes on the bacteria is expected.

7.8 Interaction between EITC-streptavidin-biotin-IgG and *S. aureus*

Having demonstrated the self-assembly between EITC-streptavidin and biotinylated IgG using FCS, it remains to be shown that the supramolecular complex can bind the target *S. aureus* cells. In principle, this can be accomplished using FCS, since the diffusion coefficient of the fluorescent supramolecular complex is expected to decrease dramatically upon binding to protein A on *S. aureus*.
Unfortunately, a preliminary control experiment showed that when a *S. aureus* suspension in PBS is illuminated with the same excitation laser used for EITC, a strong fluorescence emission was observed (**Figure 44**, **Figure 45**). This is observed even after three cycles of washing in PBS.

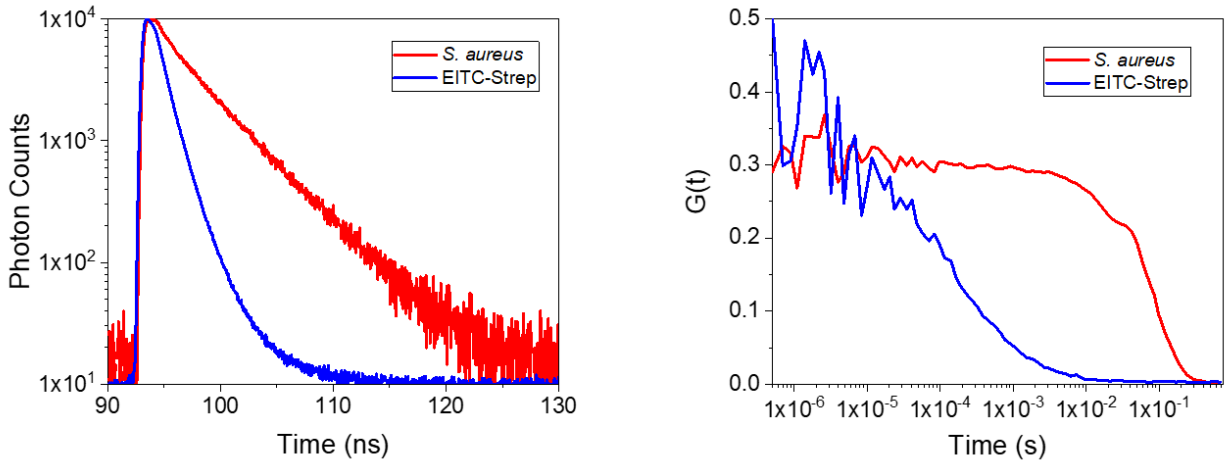

Figure 44. Comparison of the time resolved fluorescence emission (left) and the autocorrelation function (right) for an *S. aureus* suspension in PBS (red) and EITC-streptavidin (blue). Excitation was at 475 nm emission was collected at 535-575. While lifetimes are quite different, both samples are fluorescent and, for each of them an autocorrelation function can be measured. From these curves, it can be noted that the diffusion coefficient of bacteria is much higher than that of the EITC-streptavidin.

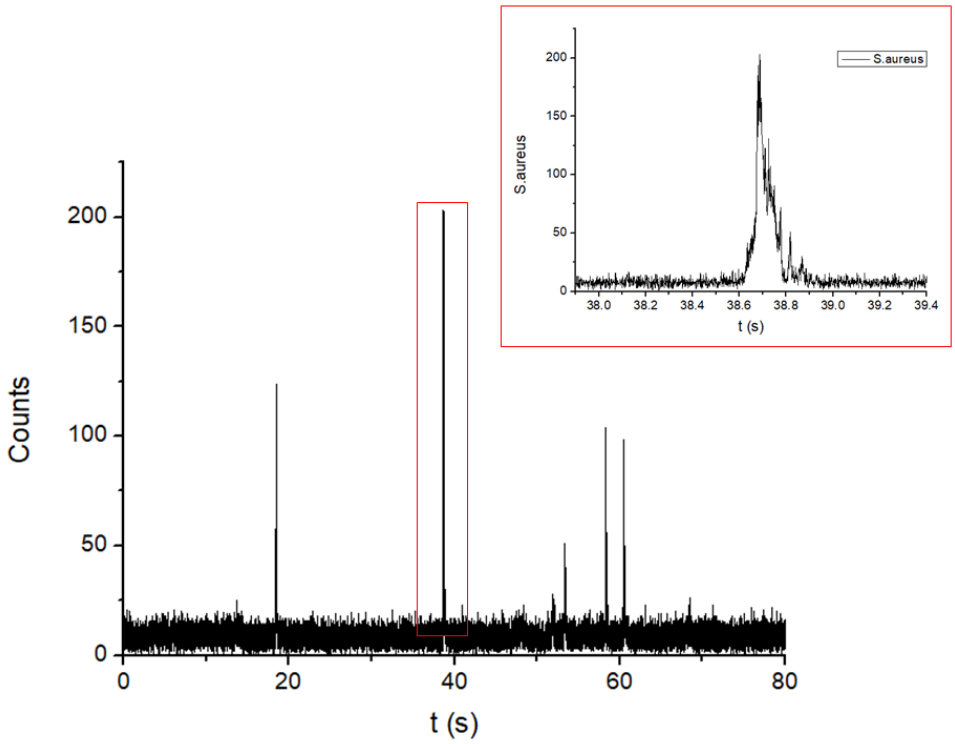

Figure 45. Portion of the MCS trace observed with the FCS setup for a *S. aureus* suspension in PBS. When a bacterium enters the effective volume, a fluorescence peak occurs.

We also checked whether the liquid media used to grow *S. aureus* (Luria Bertani (LB) and enriched LB) were fluorescent.

As can be seen from the fluorescence decays (**Figure 46**) and fluorescence lifetimes (**Table 8**), the growth media have a fluorescence comparable to that of a colony of *S. aureus* taken from a Petri dish and suspended in PBS.

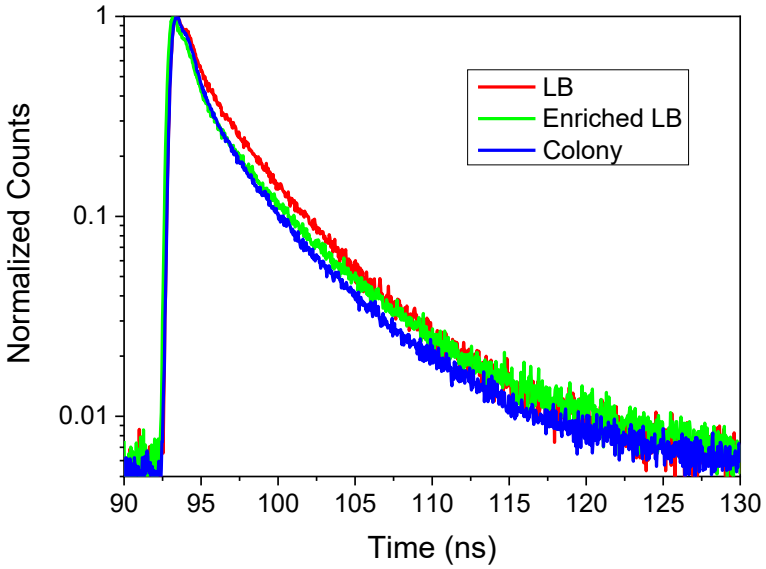

Figure 46. Fluorescence decays of LB, enriched LB media and of a colony of *S. aureus* suspended in PBS and measured using the FCS setup. Both liquid media have a fluorescence decay similar to that of a *S. aureus* colony.

	τ_1 (ns)	Amp_1	τ_2 (ns)	Amp_2	τ_3 (ns)	Amp_3
LB	7.5	17.4%	3.5	56.1%	0.7	26.5%
LB enriched	8.6	15.0%	3.4	45.3%	0.7	39.7%
***S. aureus* colony**	6.4	22.3%	2.6	41.5%	0.6	36.2%

Table 8. Fluorescence lifetimes of LB and enriched LB media and of a colony of *S. aureus* suspended in PBS. All the samples are best described by a tri-exponential function, the fastest of which may contain a substantial scattering contribution.

Since bacteria were fluorescent in the blue, to monitor binding of the supramolecular complex formed by EITC-streptavidin and biotinylated IgG and *S. aureus*, we labeled streptavidin with the fluorescent dye STAR635 instead of EITC. We were thus able to excite the sample with a 635 nm laser, where no autofluorescence is observed for bacteria.

We first washed *S. aureus* and resuspended the bacteria in PBS.
To verify binding, we incubated bacteria (OD_{600} ~ 0.4) with 0.5 µM of biotinylated IgG for 30 minutes at room temperature on a shaker; then we centrifuged (at 10,000 g for 10 minutes), removed the supernatant and resuspended the pellet. Bacteria were further incubated (for 30 minutes at room temperature on a shaker) with 1 µM (of tetramers) streptavidin labeled with STAR635. Finally, the suspension was centrifuged (at 10,000 g for 10 minutes), the supernatant was removed and the pellet was resuspended.
The resuspended pellet showed the typical STAR635 fluorescence emission (red curve in **Figure 47**), indicating binding of the supramolecular complex to *S. aureus*.
To verify that the IgG confers specificity to the complex, we also performed a control experiment by incubating *S. aureus* with STAR635-labeled streptavidin, centrifuging, removing the supernatant and resuspending the pellet.
In this case it is noted (**Figure 47**) that the signal of *S. aureus* only originates from light scattering, showing that no binding of STAR635-streptavidin occurred.

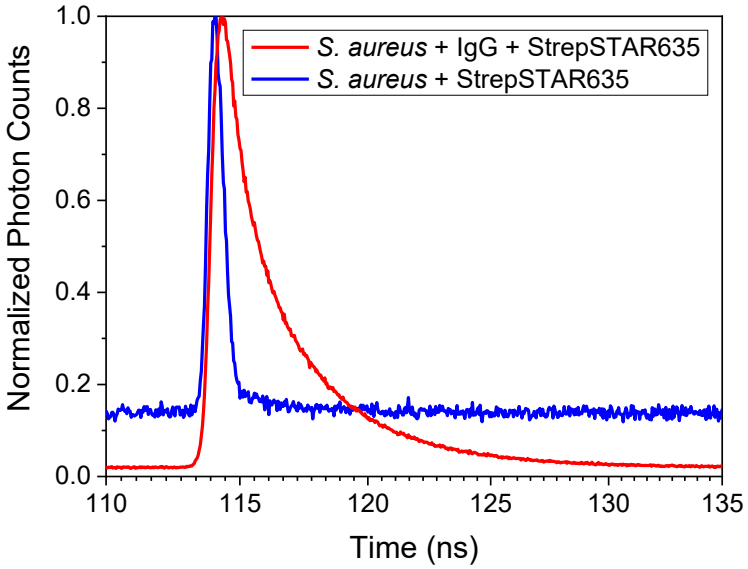

Figure 47. Fluorescence decays of *S. aureus* suspensions incubated with STAR635-streptavidin and biotinylated IgG (red) and *S. aureus* suspensions incubated with STAR635-streptavidin after centrifugation and resuspension of the pellet. While in the presence of biotinylated IgG, the typical fluorescence by STAR635-streptavidin is observed, in the absence of biotinylated IgG, only a scattering contribution is detected, showing the absence of binding. Excitation was at 635 nm, detection at 650-690 nm.

In agreement with the above findings, the autocorrelation function for a *S. aureus* suspension, incubated with the biotinylated IgG and STAR635-streptavidin (red curve in **Figure 48**), shows a much longer diffusion time (i.e. a much lower diffusion coefficient) than a STAR635-streptavidin solution (blue curve in **Figure 48**). For the latter case, the curve is described by a diffusive species with D ~ 45 $\mu m^2/s$ and a triplet of about 30 µs.

The above results demonstrate interaction of the full supramolecular compound with *S. aureus* and rule out appreciable non-specific interactions between labelled streptavidin and bacteria.

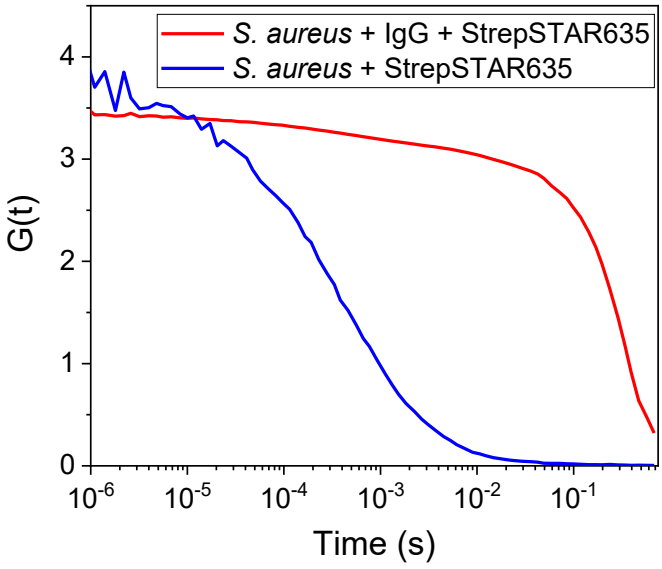

Figure 48. Autocorrelation functions of a STAR635-streptavidin solution (blue) and a *S. aureus* suspension incubated with biotinylated IgG and STAR635-streptavidin (red). Excitation was at 635 nm, detection at 650-690 nm.

7.8.1 Time-correlated single photon counting

The fluorescence emission can be monitored at a wavelength close to the excitation wavelength (500 nm) or at a longer wavelength. In the former case, the decay will be dominated by scattering; while in the latter, the contribution of scattering decreases and that of fluorescence increases. (**Figure 49**). However, by further increasing the wavelength, the fluorescence will not be sufficient to compensate for the dispersion.
We therefore decided to collect the emission at 600 nm.

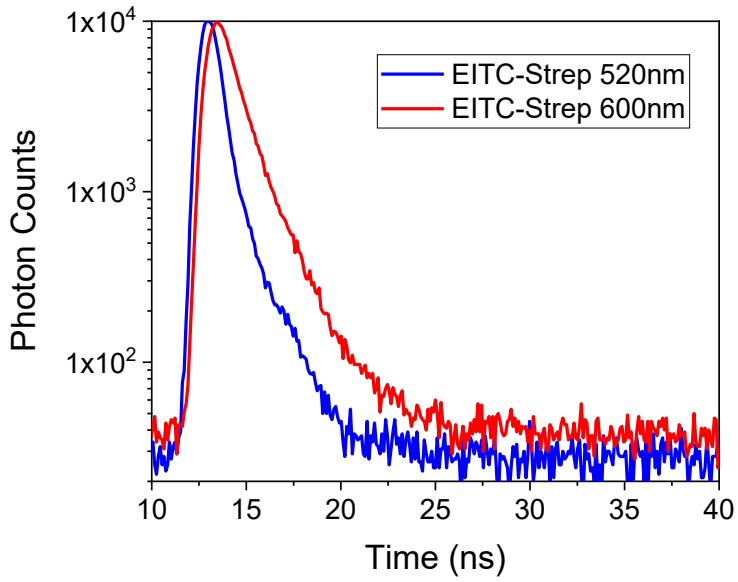

Figure 49. Fluorescence decays of the EITC bound to streptavidin collected at different wavelengths.

We analyzed the following samples:

- *S. aureus* (we removed the culture medium and resuspended the bacteria in PBS to obtain an OD_{600} of about 0.4)
- EITC-streptavidin (80 µM of protein tetramers and a DOL around 0.8)
- EITC-streptavidin-biotin-IgG (37 nM of IgG, we incubated in the dark and at room temperature for 3 minutes on a shaker)
- EITC-streptavidin-biotin-IgG-*S. aureus* (we incubated in the dark and at room temperature for 3 minutes on a shaker)
- Supernatant (we centrifuged the previous sample for 10 minutes at 7 400 g)
- Pellet (we resuspended the pellet obtained from the previous centrifugation in PBS)
- Additional supernatant (we re-centrifuged the previous sample)

Figure 50 shows the fluorescence decay spectra of the various samples.

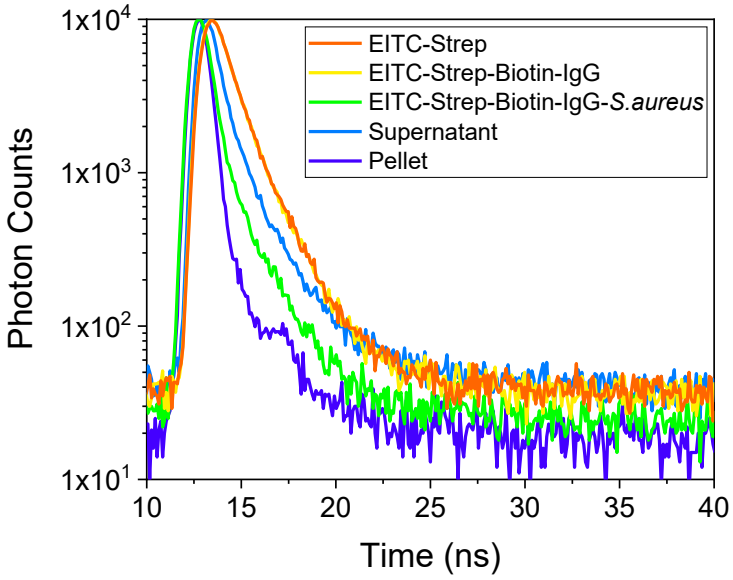

Figure 50. Fluorescence decay spectra obtained by TCSPC.

In **Table 9** are reported the parameters obtained from the analysis of the fluorescence decays.

	τ_1 (ns)	τ_2 (ns)
EITC-Streptavidin	1.45±0.02	
EITC-Streptavidin-Biotin-IgG	1.48±0.02	
EITC-Streptavidin-Biotin-IgG-*S.aureus*	1.10±0.04	2.9±0.3
Supernatant	1.20±0.04	
Pellet		2.57±0.08

Table 9. Fit parameters of fluorescence decays. When the complex binds to bacteria, the surrounding environment of EITC changes and the lifetime of the fluorescence (τ_1) increases.

All samples have a fast lifetime (<1 ns, not reported) which can be attributed to scattering.
The decay spectrum of bacteria alone (not reported) is indistinguishable from IRF, so it shows only scattering.
The fluorescence lifetimes of EITC bound to streptavidin and in the presence of biotinylated IgG are comparable. Therefore, binding to the antibody does not affect the fluorescence lifetime of the PS.
When the complex is in solution with *S. aureus*, it is necessary to introduce another lifetime to better describe the curve, this τ_2 represents the EITC bound to *S. aureus* through the complex. In this case, the first lifetime decreases probably due to the different environment in which the free EITC (labeled to the streptavidin but not bounded to the bacteria) is found.
The new lifetime introduced represents effectively the EITC bound to bacteria, in fact it is absent in the supernatant and is the only fluorescence lifetime present in the pellet. Therefore, after washing, the complexes not bound to the bacteria were removed and only those bound to *S. aureus* remained.
The supernatant shows some fluorescence because the EITC is present there, so not all complexes are bound to the bacteria. This could be due to the formation of clusters (as seen in the chapter on the bound between EITC-streptavidin and biotin-IgG) which reduced the affinity of IgG for *S. aureus*.
Centrifuging again and analyzing the new supernatant there is no fluorescence (not reported), so the free complexes were removed in the previous centrifugation.

7.8.2 Fluorescence emission

The samples analyzed were obtained as those described in the previous chapter (and therefore used for TCSPC measurements to show the binding between the complex and *S. aureus*).

The fluorescence spectra were obtained by exciting at 500 nm and monitoring the fluorescence emission at 600 nm; at this wavelength there is no fluorescence from the bacteria.

Figure 51 shows the emission spectra of the different samples.

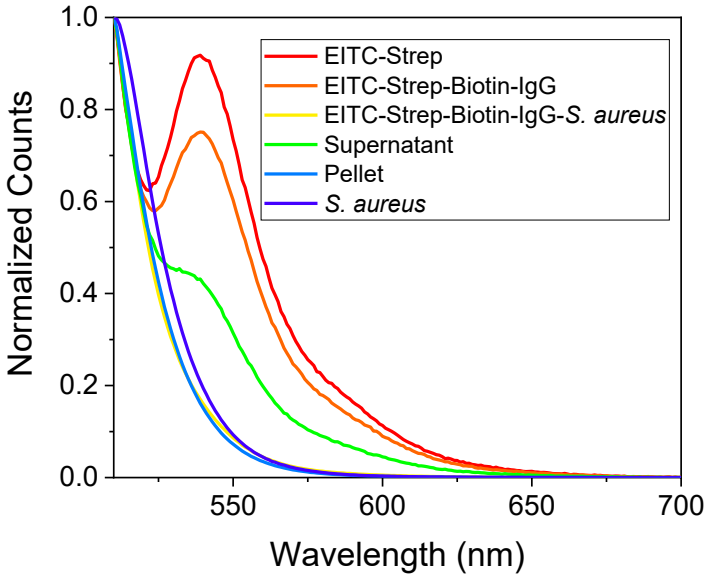

Figure 51. Fluorescence emission spectra. When the complex is not bound to bacteria there is a peak of fluorescence emission at 540 nm.

The solution containing only the bacteria shows no fluorescence peaks, only scattering.
The emission spectra of the EITC-streptavidin and EITC-streptavidin-biotin-IgG samples show the EITC fluorescence peak, around 540 nm.
When *S. aureus* is added to the complex, the emission peak is no longer present because the EITC fluorescence is suppressed by the scattering due to *S. aureus*. **Figure 51** reports the normalized counts, so this effect cannot be appreciated, but from not-normalized spectra (not reported) it can be observed that at 540 nm the EITC emission peak is about five times less than the counts in presence of *S. aureus*.
In the spectrum of the supernatant there is a shoulder representing the EITC fluorescence and this confirms the presence of complexes that have not remained bound to *S. aureus*.
The emission spectrum of the pellet is similar to that of *S. aureus* alone and in the presence of the complex.
After a new centrifugation, the supernatant shows no fluorescence (not reported), so the free complexes were removed in the previous centrifugation.

7.9 Imaging interactions between the supramolecular complex and *S. aureus* by confocal fluorescence microscopy and STED nanoscopy

Binding of the supramolecular complex to *S. aureus* can be further demonstrated by fluorescence imaging using high-resolution microscopy. In order to achieve sub-diffraction spatial resolution, streptavidin was labelled with a fluorophore suitable for the available setup.
Streptavidin was thus labeled with chromeo488, whose spectral properties better match the setup used (excitation at 488 nm, detection at 495-550 nm and, for STED microscopy 592 nm depletion beam).

For these experiments, the culture medium in which the bacteria were grown, was removed by washing the bacterial suspension with PBS.
Then, 500 µL of bacteria (with OD_{600} ~ 0.4) were incubated with 0.5 µM of biotinylated IgG for 30 minutes at room temperature (shaking every 10 minutes); then centrifuged (at 4,000 rpm for 10 minutes), removed the supernatant and resuspended the pellet; then incubated (for 30 minutes at room temperature and shaking every 10 minutes) with 1 µM (of tetramers) of streptavidin labeled with chromeo488; finally centrifuged (at 4,000 rpm for 10 minutes), removed the supernatant and resuspended the pellet.

To make the bacteria (negatively charged) adhere to the coverslip, 100 µl of 0.1 mg/mL poly-L-lysine (positively charged) were first added to the slide and then let incubate for 10 minutes; to eliminate the excess poly-L-lysine, the coverslip was washed by immersing it in PBS.
Finally, in the culture chamber for live cell imaging was placed the slide on which were also placed 270 µl of PBS and 30 µl of solution with the bacteria.

From measurements with confocal and STED microscopy (**Figure 52**) it can be seen that the supramolecular complexes concentrate on the cell wall of *S. aureus*. Furthermore, since STED allows to obtain a higher resolution, it can be seen that the complexes are grouped in some areas of the wall (the brightest spots) which, presumably, correspond to protein A foci since the distribution of this protein is not uniform on the cell wall of *S. aureus* but is concentrated near some deposition sites [104].
From these measurements it is also possible to obtain the size of the bacteria (about 1.2 µm) which is in agreement with what is reported in the literature [121].

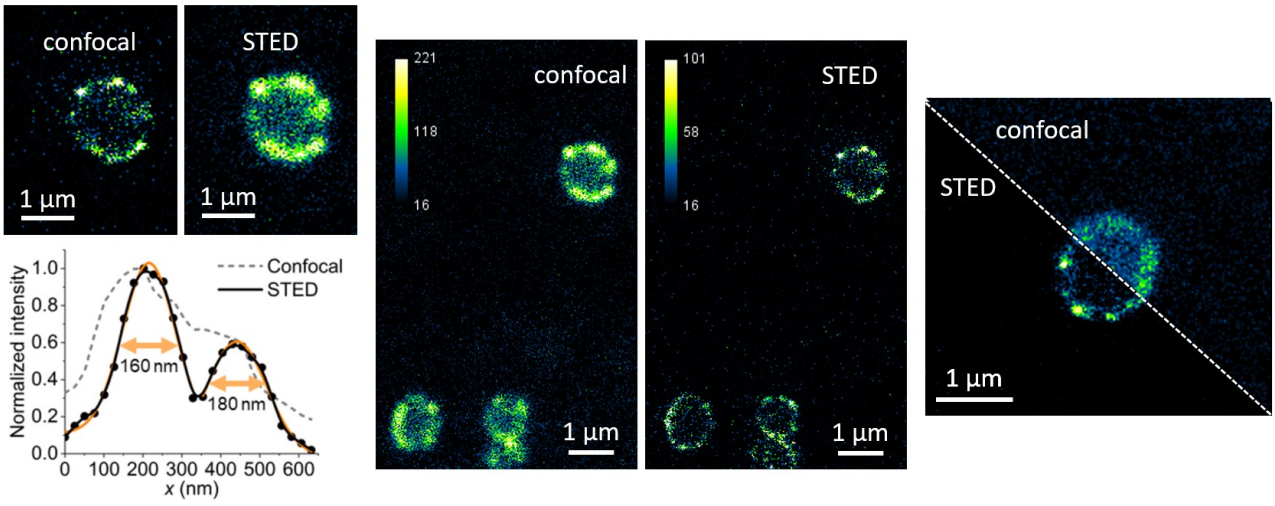

Figure 52. Confocal and STED microscopy comparison of *S. aureus* incubated with the complex. The IgG-streptavidin complex (labeled with chromeo488) is localized on the cell wall where protein A is present.

To verify the specificity of the complex (given by the interaction between IgG and protein A), a bacterium that does not express protein A, for example *Escherichia coli*, can be used. Thus, transmitted light and

confocal microscopy measurements (**Figure 53**), of the complex in solution with a mixed culture of *E. coli* and *S. aureus*, were performed.
Through confocal microscopy it can be seen that only *S. aureus* shows the fluorescence of the complex (found on the cell wall of the bacterium) while *E. coli* does not (since it does not express the protein A to which the complex binds). Using transmitted light it is anyway possible to confirm the presence of *E. coli*.

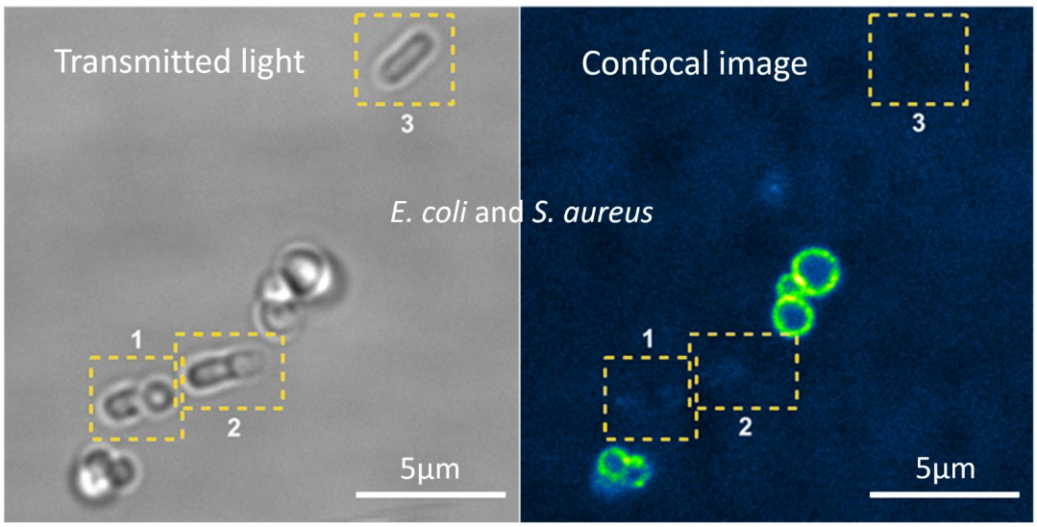

Figure 53. Selectivity of chromeo488-streptavidin-IgG for bacteria expressing protein A. Both *E. coli* (In the dashed boxes) and *S. aureus* can be seen in transmitted light (left). In confocal microscopy (right) only *S. aureus* shows the fluorescence emitted by the complex (labeled with chromeo488).

These microscopy measurements confirm that the formed complex (EITC-streptavidin-biotin-IgG) specifically targets the protein A on the cell wall of *S. aureus*.
As the complex does not bind to *E. coli*, we did not perform photoinactivation tests against this bacterium as we did not expect any phototoxic effects.

7.10 Photoinactivation

To evaluate the efficacy of the EITC-streptavidin-biotin-IgG complex against planktonic *S. aureus*, we conducted *in vitro* photoinactivation experiments.

In order to obtain a better control of stoichiometry, we conducted the experiments following the same sequence adopted previously, i.e. we first incubated the biotinylated IgG with *S. aureus* and then we added the EITC-labeled streptavidin.
In different Eppendorf tubes, one for each different concentration of EITC and one for the control, we introduced 300 µL of the bacterial suspension (diluted up to an OD_{600} of 0.2) for each light fluence used (from 10 to 50 J/cm^2) and for the control in the dark.
We then introduced in the bacterial suspension a volume of biotinylated IgG such as to obtain an IgG concentration of 100 nM, then we let it incubate at 37 °C on a shaker (100 rpm) for 30 minutes. We then added a volume of EITC-streptavidin in order to obtain the desired concentration (from 125 nM to 1 µM of streptavidin in the tetramers, DOL about 1), then we incubated it at 37 °C and shake (100 rpm) for 30 minutes in dark condition.

Based on the power of the lamp used (27.5 mW/cm^2) we calculated the time for which the samples must be irradiated to obtain a certain light fluence.
The light fluence received from each sample was calculated using the equation: $E = Pt$, where E is the fluence in J/cm^2, P is the irradiance (power density) in W/cm^2 and t the time in seconds.
We then placed the 96-well plate under the LED lamp with maximum emission at 521±19 nm.

For the photoinactivation tests we used the following conditions: 0.125, 0.25, 0.5 and 1 µM in EITC-streptavidin tetramers (DOL around 1); 0.1 µM of IgG; dark (no irradiation), 10, 20 and 50 J/cm^2.
For these conditions we performed the photoinactivation of *S. aureus* (ATCC 29213) (**Figure 54**, left). By carrying out photoinactivation in absence of biotinylated IgG (**Figure 54**, right), we verified whether EITC-labeled streptavidin has effects on bacteria and if the antibody increases the specificity of the complex for the bacteria.

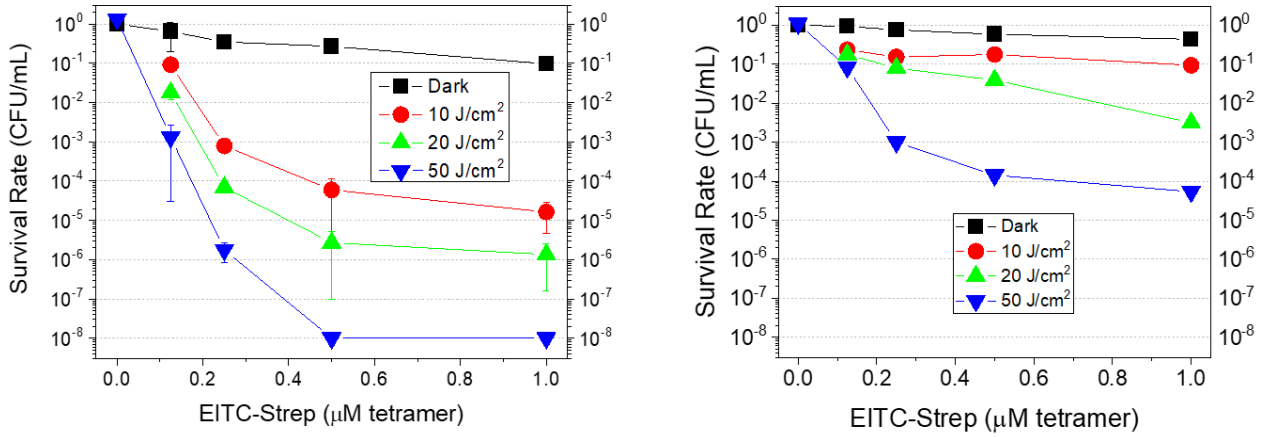

Figure 54. Photoinactivation of *S. aureus* ATCC 29213 (left) and in absence of biotinylated IgG (right). The bacteria were first incubated 30 minutes with biotinylated IgG (100 nM) (performed only in presence of the whole complex, left), then for 30 minutes with EITC-streptavidin (0.125-0.25-0.5-1 µM in tetramers), finally they were illuminated (with a light fluence of 0 (dark)-10-20-50 J/cm^2) using a green LED lamp (521±19 nm).

Due to the used concentration of bacteria, the total absence of bacterial growth in the Petri plates indicated a cell death of 8 logs.
From these dose-response curves it can be seen that as the concentration of PS and light fluence increases, a greater cell death is obtained.
In presence of IgG we obtained a cell death of 4 logs using 0.25 µM of EITC-streptavidin and a light fluence of 20 J/cm^2, we also obtained a complete inactivation (8 logs) with 0.5 µM of EITC-streptavidin and 50 J/cm^2.

Controls at maximum light fluence do not show photoinactivation by light, i.e. the survival rate is similar to that of the untreated control (not illuminated and in absence of EITC-streptavidin). This indicates that there is no toxicity caused by the light and heat caused by the lamp.

When IgG (i.e., the molecule that allows the recognition of the target cell) is absent, the cellular inactivation is less (2-4 logs), this indicates that this molecule confers a high specificity to the supramolecular complex.
The phototoxic effect of the EITC labeled streptavidin could be due to the presence of biotin molecules on the cell wall of bacteria: studies show that in some microorganisms biotin is found in form of biotinylated proteins [122]. To test this hypothesis, the biotin binding sites of streptavidin could be saturated so that the protein cannot subsequently bind to bacteria.

A different cause of this phototoxicity could be given by the interaction between streptavidin and the receptors present on the bacterial cell wall. Indeed, in streptavidin there is a RYD (Arg-Tyr-Asp) motif that mimics the RGD (Arg-Gly-Asp) motif which is a recognizing motif for different adhesion receptors (such as fibronectin, vitronectin, fibrinogen) [123].

8 The supramolecular complex between methylene blue-labelled streptavidin and concanavalin A

In this chapter we describe the assembly of the supramolecular construct between a methylene blue-labelled streptavidin (MB-streptavidin) and concanavalin A (ConA). The photosensitizing unit MB-streptavidin is linked to a biotinylated ConA, that warrants targeting towards *S. aureus* and *E. coli* (**Figure 55**). We used a commercial methylene blue-labeled streptavidin (at Lys residues) with a predefined DOL.

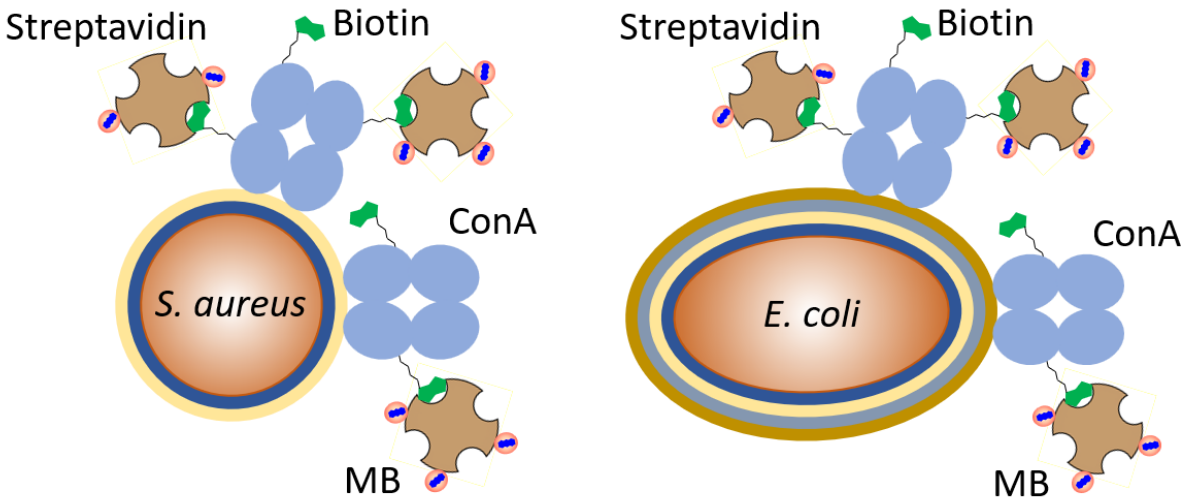

Figure 55. Cartoon representation of the interaction between the supramolecular complex between MB-streptavidin and ConA and *S. aureus* (left) or *E. coli* (right).

As shown in previous chapters, when the EITC is bound to streptavidin and the number of PSs present on the same protein increases, there is a decrease in the quantum yield of singlet oxygen formation and this could negatively effects the phototoxic efficiency of the complex formed using EITC.
For this reason, we have decided to use a different PS for the formation of the second complex.

8.1 Photophysical characterization of MB-Streptavidin

The DOL of streptavidin can be estimated from the absorption spectra of the compound. MB absorption at 280 nm must be taken into account when estimating the protein concentration.
The MB-labeled commercial streptavidin is characterized by a molar absorbance coefficient of 100,000 $M^{-1}cm^{-1}$ [124] at 664 nm. The molar absorbance coefficient at 280 nm of the dye can be estimated multiplying the value at 664 nm by the correction factor CF_{280} = 0.24 [124]. The MB-labeled streptavidin used in these experiments has the characteristic spectrum of a dimerized MB [125], i.e. the absorption peak at 610 nm is greater than the one at 664 nm (**Figure 56**). This leads to further uncertainty in the estimate of the DOL (ranging between 1.5 and 2.1).

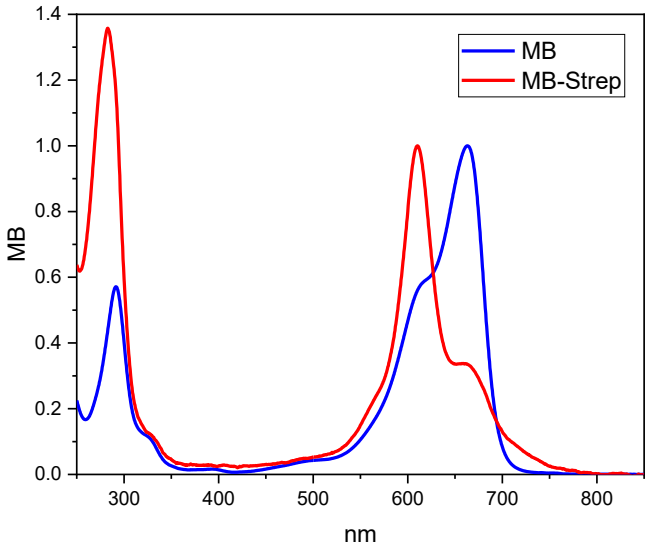

Figure 56. Normalized absorption spectra of MB and MB-streptavidin in PBS buffer.

Dimerization of the isolated MB dye is reported to occur in the concentrations range between 10 and 100 µM, where the dissociation constant of the dimer falls [125]. To verify if the observed shape of the spectrum reflects dimerization of MB we have measured the absorption spectra as a function of MB-streptavidin concentration through progressive dilutions down to the nanomolar range.

It can be noticed (**Figure 57**) that the spectrum maintains the same shape, therefore MB driven dimerization can be excluded as the reason for the observed absorption spectrum. The effect on MB spectra may arise from specific interactions between MB and amino acid residues on streptavidin. It can be hypothesized that a π-π interaction between MB and aromatic amino acids on the surface of the protein (there are six Trp per streptavidin monomer) may be at the basis of the observed effect. Furthermore, dimerization of MB molecules bound to the same streptavidin tetramer is unlikely.

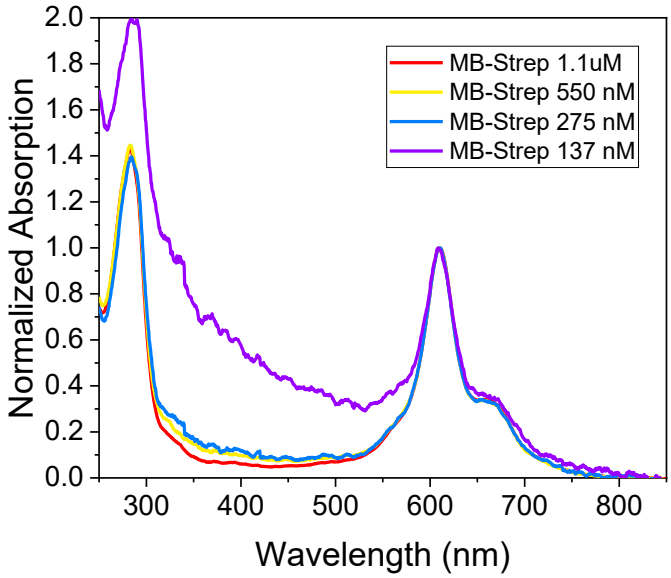

Figure 57. MB-labeled streptavidin at different concentrations. Spectra maintain the same shape even at concentrations much lower than those reported for the MB dimerization therefore these spectra may be due to a π-π interaction between MB and aromatic amino acids of streptavidin.

Although weak, fluorescence emission by MB can be exploited to gain information on the complex. Given the change in absorption when bound to streptavidin, fluorescence emission experiments were conducted using an excitation wavelength of 655 nm for MB and 610 nm for the MB-streptavidin. While emission of the excitation spectra was collected at 710 nm for the MB and at 690 nm for the MB labeled streptavidin.

From the excitation and emission spectra (**Figure 58**) is possible to notice that there is almost no shift between the peaks of the MB alone or bound to streptavidin.

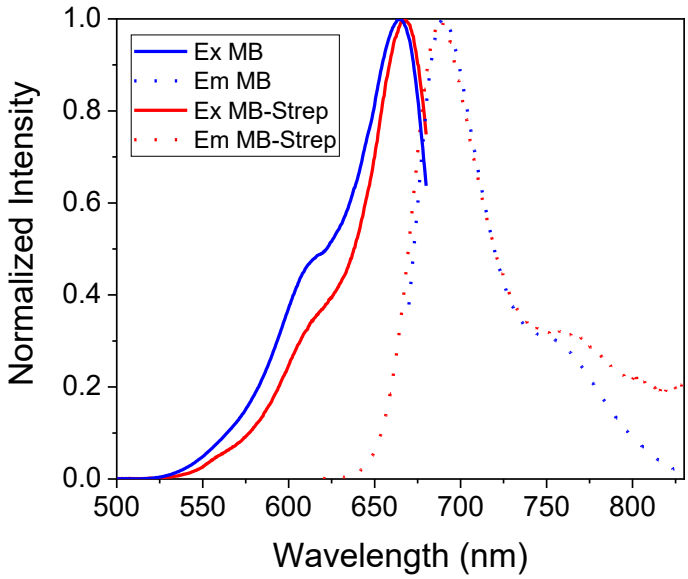

Figure 58. Normalized fluorescence excitation (solid lines) and emission (dashed lines) spectra of MB (blue) and MB-streptavidin (red). Fluorescence emission was excited at 655 nm (MB), or at 610 nm (MB-streptavidin). Fluorescence emission was collected at 710 nm for MB, and at 690 nm for MB-streptavidin.

From the emission spectra, and knowing the fluorescence quantum yield of STAR635, we calculate the fluorescence quantum yield of MB, Φ_F = 0.043±0.004, which is in agreement with the literature value [87] For MB-streptavidin the emission is quenched, Φ_F = 0.006±0.003.
So, as observed with the EITC, when MB binds streptavidin its fluorescence quantum yield decreases, due to interactions between the PS and the protein.

Binding of MB to streptavidin can be verified by measuring fluorescence anisotropy (**Figure 59**). Upon binding to the protein, the fluorescence excitation anisotropy of MB (less than 0.1) increases to around 0.25, in keeping with a hindered rotational averaging of the fluorophore.

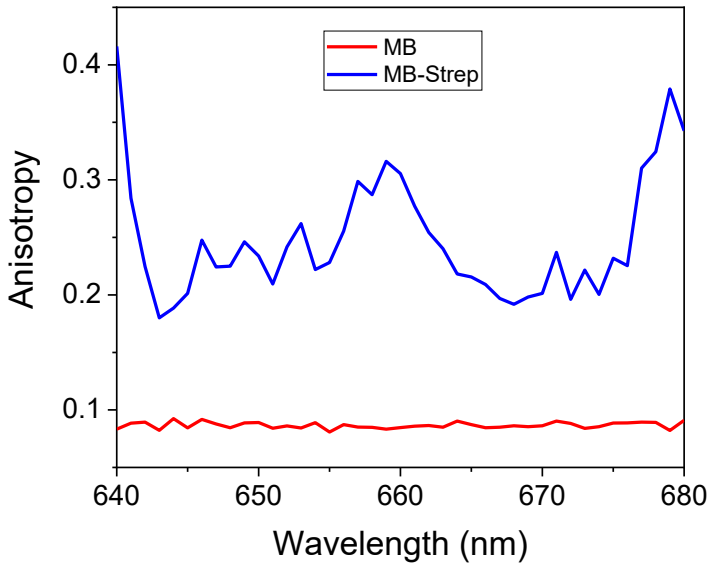

Figure 59. Fluorescence excitation anisotropy of MB and of MB-streptavidin. Emission was collected at 685 nm.

An additional check on the integrity of the MB-streptavidin complex was obtained using FCS. Although MB (and MB-streptavidin) have very low fluorescence yield, FCS experiments of the air equilibrated samples can be performed on the compounds using very long (30 mins) acquisition times. **Figure 60** compares the cross-correlation curves for MB and MB-streptavidin showing that, when bound to streptavidin, the diffusion of the MB fluorophore becomes much slower.

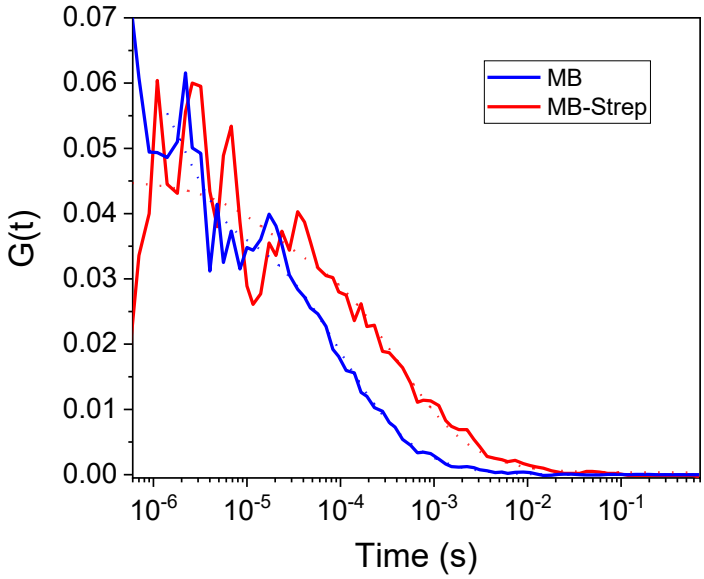

Figure 60. Cross-correlation curves of MB (blue) and MB-streptavidin (red). When bound to streptavidin, the correlation curve for MB fluorescence shifts to longer time-scales indicating that PS is bound to a bulky molecule (the protein). Excitation was at 635 nm, emission was collected using a 650-690 nm filter.

This measurement confirms what we observed using the fluorescence anisotropy, i.e. that MB is bound to streptavidin.

Although the curves are noisy, it is possible to estimate the diffusion coefficient of the species, also introducing the contribution of the triplet state τ_T of around 13 µs. MB alone has a D of about 350 µm^2/s

(compatible with that of a free dye in solution) while for the MB-labeled streptavidin D is around 90 μm^2/s (compatible with that of a tetrameric streptavidin, although a bit on the high side).

From the photon trace collected with the FCS setup, we were also able to collect fluorescence emission decays for MB and MB-streptavidin (**Figure 61**).

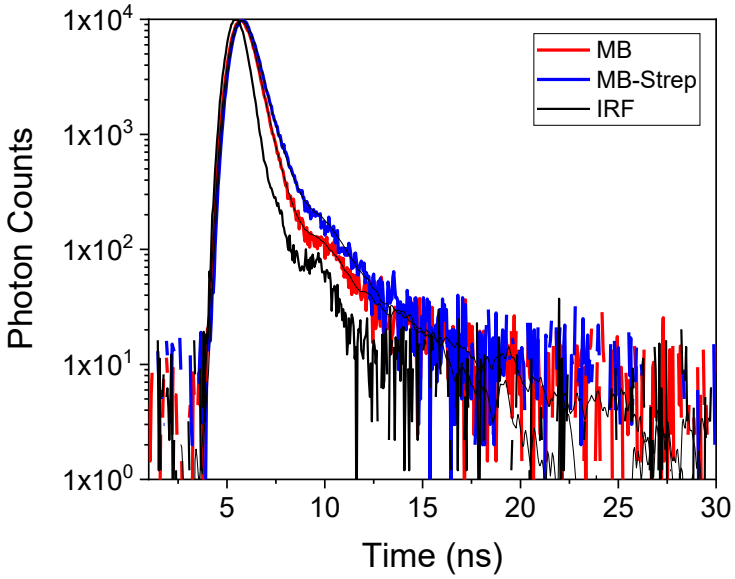

Figure 61. Fluorescence decay spectra obtained by FCS. When MB is bound to streptavidin, the fluorescence lifetime decreases.

In this way, we were able to estimate the fluorescence lifetime of the dye. For both (MB and MB- streptavidin) we obtained decays described by a bi-exponential function, with a very short lifetime of 0.38±0.01 ns for the PS and 0.41±0.01 for the labeled streptavidin) and a longer one of 6.1±0.6 ns (relative weight 2.8%) for the MB and 2.2±0.2 ns (1.4%) for the MB-streptavidin. MB has a mean lifetime of 0.54±0.04, while that of MB-streptavidin is 0.44±0.04; the decrease in lifetime confirms that a quenching mechanism exists when MB is bound to the protein.

The observed fluorescence quenching suggests that the interaction between MB and the protein results in quenching of the excited singlet state. Besides fluorescence emission, quenching of the excited singlet state is expected to reduce also intersystem crossing to the triplet state. To verify this, we monitored triplet state formation and decay using nanosecond laser flash photolysis on air equilibrated samples. **Figure 62** compares the triplet state formation and decay monitored at 633 nm, where bleaching of the ground state is detectable.

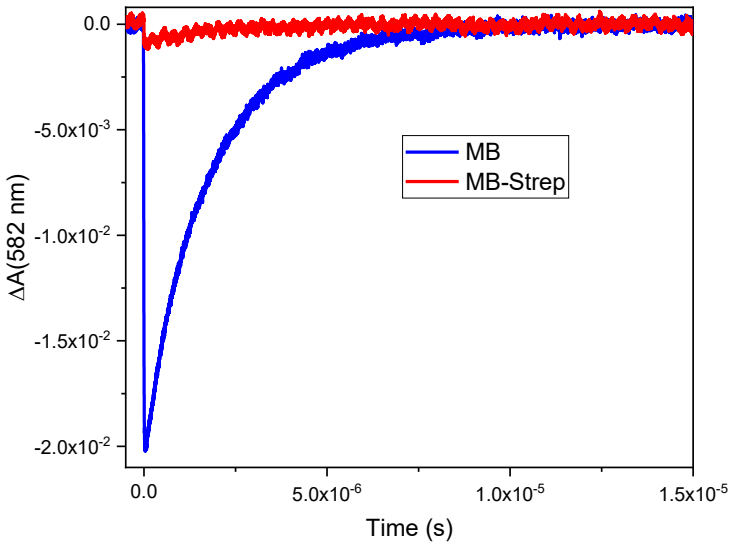

Figure 62. Triplet state formation and decay monitored at 633 nm, where bleaching of the ground state is observed. Excitation was with a nanosecond laser pulse at 582 nm. Blue curve is for MB, red is for MB-streptavidin.

By analyzing the signals using an exponential decay, we observed that the MB curve is best described by a bi-exponential function (τ_1 = 0.65 µs and τ_2 = 1.95 µs, with a relative weight of 17% and 83%, respectively) while the MB-streptavidin one can be fitted with a mono-exponential decay (τ = 4.6 µs).
The faster lifetime of MB alone that we obtained is in agreement with the lifetime reported [92]. Moreover, the lifetime of MB increases when it is bound to the streptavidin indicating that the protein protects the PS from molecular oxygen (so the lifetime of the triplet increases).

From the preexponential factor, and using the quantum yield of triplet state formation of MB (0.52 [87]) we calculated the quantum yield of MB bound to streptavidin: 0.03±0.02. As expected, the triplet yield for MB is lower when bound to the protein.

Using time-resolved phosphorescence we then measured the kinetics of singlet oxygen formation and decay for air-equilibrated samples. Signals were described by a bi-exponential function (one for the decay of the PS triplet state and one for the decay of the singlet oxygen). From the fitting parameters we calculated $S(0)$ and plotted them as a function of the fraction of absorbed energy (**Figure 63**).
In order to determine the singlet oxygen quantum yield, signals for MB and for MB-streptavidin were compared to those of some reference molecules of known Φ_Δ (RB, Φ_Δ = 0.75 [119]; TMPyP, Φ_Δ = 0.74 [119]; TPPS, Φ_Δ = 0.62 [120]). From the slope of the linear fits, we calculated the quantum yield of singlet oxygen formation of MB and MB-streptavidin.

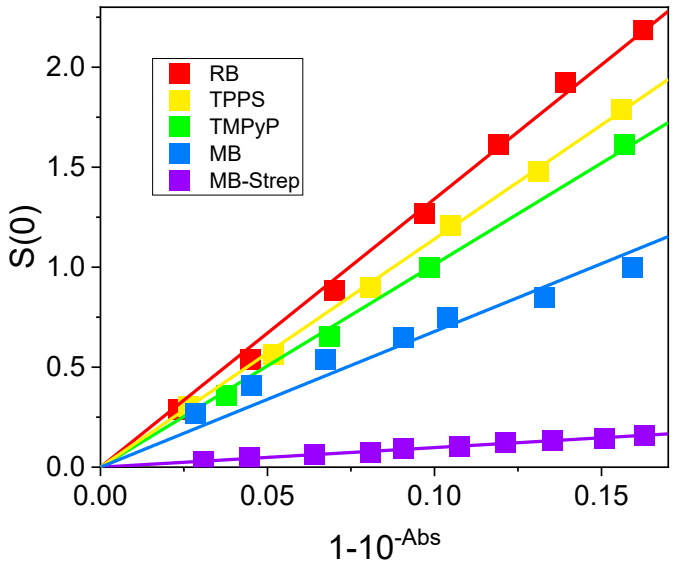

Figure 63. $S(0)$ retrieved for reference molecules (red, RB; yellow TSPP; green TMPyP), MB (blue) and MB-streptavidin (purple). By comparing the slopes of the different samples, it is possible to calculate the quantum yield of singlet oxygen formation of the MB bound to streptavidin. Excitation was at 532 nm, detection of phosphorescence was at 1275 nm.

As quantum yield of singlet oxygen formation of MB alone we obtained Φ_Δ = 0.55±0.02, which is in agreement with the literature data [87]. For the MB bound to streptavidin we obtained Φ_Δ = 0.056±0.003. So, as we observed with the EITC, when the PS is bound to streptavidin its quantum yield of singlet oxygen formation decreases negatively affecting the photodynamic properties of the PS.

8.2 ConA is able to drive the supramolecular complex to target bacteria

For these experiments we performed FCS measurements using an excitation wavelength of 635 nm and collecting the emission using a 650-690 nm filter.

Before verifying that ConA binds to bacteria, we checked the aggregation state of the protein. In fact, ConA assumes a dimeric conformation at a pH lower than 5.6, is tetrameric for a pH between 5.6 and 7 and it aggregates at higher pH [126].
We conjugated ConA with a fluorophore (STAR635) in order to perform FCS measurements. Then, we changed the buffer of the labeled protein with solutions at different pH (**Figure 64**). In this way, a shift in the cross-correlation curve would have indicated a change in the diffusion coefficient and this would have given us information on the form of ConA (tetrameric or aggregate).

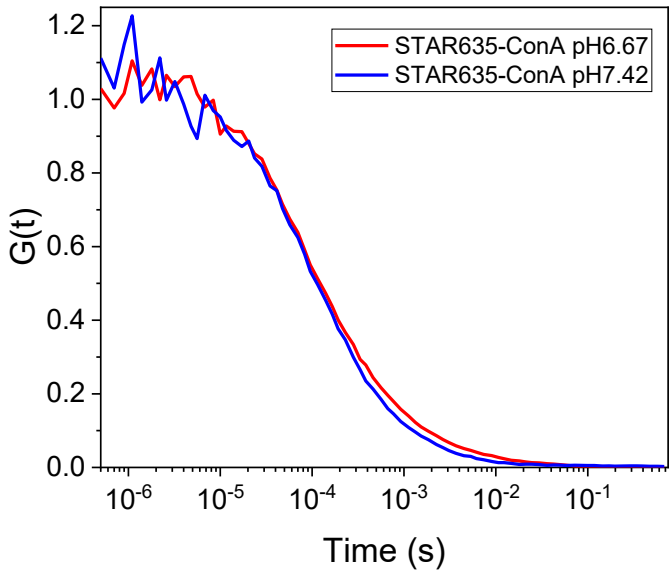

Figure 64. Cross-correlation curves of a labeled ConA at different pH. Although ConA should aggregate at pH above 7, no shift was observed in the cross-correlation curve.

However, we did not detect any changes and as the pH changed the diffusion coefficient of the protein was always around 70 $\mu m^2/s$.
This value is too high for a protein of about 100 kDa (for which D should be about 40 $\mu m^2/s$), but it could be due to a fraction of free fluorophore (diffusion coefficient around 300 $\mu m^2/s$) that cannot be discriminated during the analysis and, having a very high D, therefore increases the diffusion coefficient estimated. Furthermore, the lifetime of the triplet state (0.087 ms, with a relative weight around 15%), obtained from the analysis, could overlap with that of the free fluorophore, further confounding the analyses.
We decided to use ConA in solutions with pH 7.4-7.5.

S. aureus and *E. coli* suspensions were first washed with PBS to remove the culture medium from the solution (we centrifuged at 10,000 g for 10 minutes, removed the supernatant, resuspended with PBS and repeated this process two more times). Subsequently we incubated the bacteria ($OD_{600} \sim 0.2$) with 10 µM of the STAR635 labeled ConA for one hour at room temperature on a shaker.
From the analysis of the FCS cross-correlation curves (**Figure 65**) we obtained three lifetimes: the shortest one τ_1 of about 0.09 ms relative to a triplet state or a free fluorophore, the intermediate one represents the free ConA ($D_2 \sim 70$ $\mu m^2/s$) and the longest τ_3 corresponding to labeled bacteria. The lifetimes and their relative weight are reported in **Table 10**.

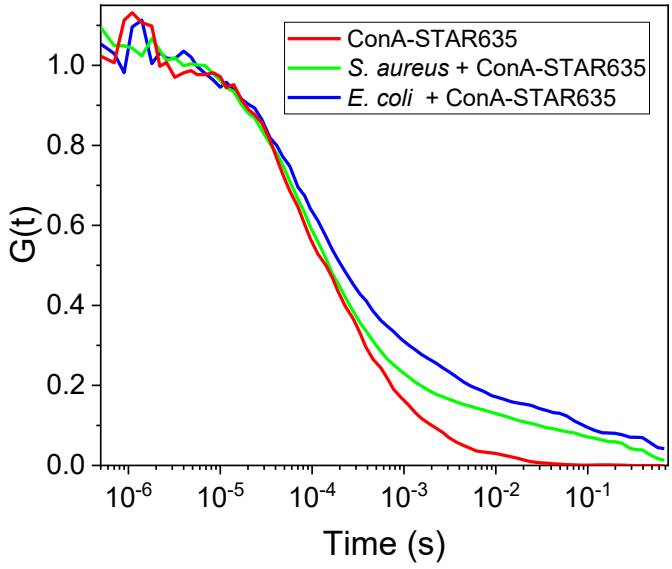

Figure 65. Cross-correlation curves of STAR635 labeled ConA in presence of *S. aureus* and *E. coli*. In presence of bacteria there is a secondo component (at longer time scale) indicating that the protein binds to the bacteria.

	τ_1 (ms)	Amp$_1$	τ_2 (ms)	D_2 (µm^2/s)	Amp$_2$	τ_3 (ms)	D_3 (µm^2/s)	Amp$_3$
S. aureus	0.09	33%	0.34	~ 70	30%	52	~ 0.59	37%
E. coli	0.09	13%	0.34	~ 70	70%	189	~ 0.16	17%

Table 10. Lifetimes and relative weights obtained from the analysis of the FCS cross-correlation curves of a STAR635 labeled ConA in presence of *S. aureus* and *E. coli*. The first component represents the triplet state or free fluorophore, the second corresponds to unbound ConA, and the third one the ConA bound to bacteria.

This result confirms that ConA binds *S. aureus* and *E. coli*.
ConA can target glucose and mannose residues in the lipopolysaccharides; this recognition was used, for example, to functionalize ConA with the PS Rose Bengal in order to photoinactivate *E. coli* more efficiently than using the PS alone [77].

8.3 Imaging interactions between the ConA, *S. aureus* and *E. coli* by STORM nanoscopy

Binding of the ConA to bacteria (*S. aureus* and *E. coli*) can be further demonstrated by fluorescence imaging. In order to achieve sub-diffraction spatial-resolution, streptavidin was labelled with Alexa647, a fluorophore with a higher fluorescence quantum yield than MB and with spectral properties which better match the setup used (excitation at 640 nm, detection at 665-705 nm, in the second channel). Importantly, Alexa647 is amenable to STORM microscopy.

100 µl of 0.1 mg/mL poly-L-lysine (positively charged) were first added to the slide, to make the bacteria adhere to the coverslip, and then let incubate for 20 minutes; to eliminate the excess poly-L-lysine, the coverslip drained and dried with nitrogen flow.
We attached the coverslip to a glass slide, obtaining an incubation chamber.

For these experiments, the bacterial suspension was washed with PBS to remove the culture medium.

500 µL of bacterial suspension (with OD_{600} ~ 1) were incubated with 50 nM of Syto13 (a nucleic acid dye) for 30 minutes at room temperature on a shaker (100 rpm) then centrifuged (10,000 g for 5 minutes) and resuspended in PBS. The bacterial suspension was transferred in the chamber and incubated with 1 µM of biotinylated ConA for 30 minutes at room temperature on a shaker (100 rpm) and washed with 200 µL of PBS. Subsequently, it was incubated (for 30 minutes at room temperature on a shaker at 100 rpm) with 0.2 µM (of tetramers) of Alexa674 labeled streptavidin; then washed with 200 µL of STORM buffer (160 µL of PBS, 20 µL of MEA, 20 µL of glucose 5% and 2 µL of GLOX). Finally, the chamber was sealed.

As can be seen from **Figure 66**, ConA localizes externally in both the bacteria (red spots around the green labeled DNA), suggesting that the protein interacts with saccharides present on the cell wall.
As previously observed using FCS, labeled ConA binds to a small fraction of the bacteria. Protein clusters (red aggregates not bound to bacteria) are also present.

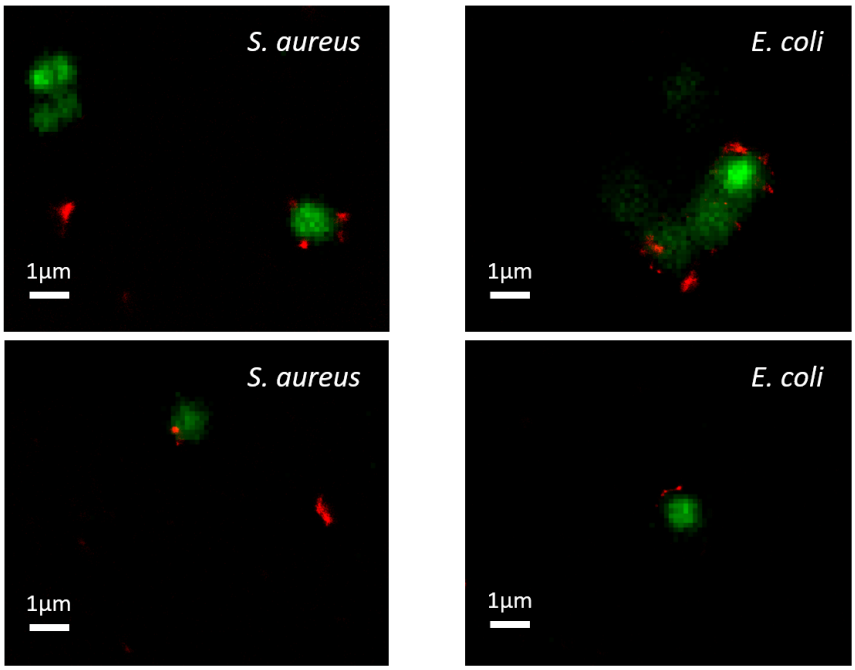

Figure 66. STORM microscopy of *S. aureus* (left) and *E. coli* (right) incubated with Alexa647 labeled ConA (red channel). The STORM image is overlayed to a low resolution image of DNA stained with Syto13 (green channel). The labeled protein is localized on the cell wall of the bacteria.

8.4 Photoinactivation

To evaluate the efficacy of the MB-streptavidin-biotin-ConA complex against *S. aureus* and *E. coli*, we performed *in vitro* planktonic photoinactivation tests.
As before, as culture medium we used TSB and TSB with agar for the Petri dishes and we performed the experiments in a sterile environment.
We let the bacteria grow and then we removed the growth medium in the same way as described in the previous chapter on photoinactivation.
We performed the experiments in the “after-assembly” conditions, i.e. we first incubated the biotinylated ConA with the bacteria and then we added the MB-labeled streptavidin. For these experiments we used the same procedure described previously, but with different conditions.

In the 300 µL of bacterial suspension, the microorganisms were diluted up to an OD_{600} of 0.1. The bacteria were incubated with 5 µM of biotinylated ConA for one hour at 37 °C with a shaker (100 rpm) and then they were incubated with 5 µM of MB-labeled streptavidin (the concentration is that of the PS) for 30 minutes at 37 °C and shake (100 rpm) in the dark. The lamp used, with a maximum at 660±10 nm, had a power of 48.3 mW/cm^2, so we irradiated the samples for the time needed to obtain a light fluence of 100 and 200 J/cm^2. We also performed the photoinactivation in the absence of biotinylated ConA and using the MB alone. As bacteria strains, we used *S. aureus* ATCC 6538 (**Figure 67**, left) and *E. coli* ATCC 25922 (**Figure 67**, right).

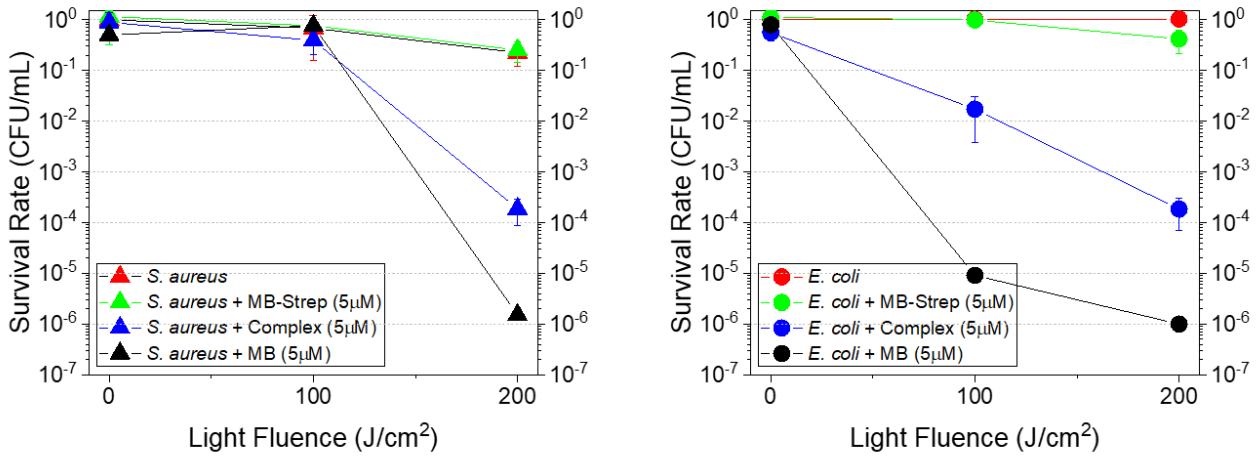

Figure 67. Photoinactivation of *S. aureus* ATCC 6538 in after-assembly condition (left), photoinactivation of *E. coli* ATCC 25922 in after-assembly condition (right). The bacteria were first incubated one hour with biotinylated ConA (5 µM), then for 30 minutes with MB-labeled streptavidin (5 µM of PS), finally they were illuminated (with a light fluence of 100 and 200 J/cm^2) using a red lamp (660±10 nm).

Due to the used concentration of bacteria, the total absence of bacterial growth in the Petri plates indicated cell death of 6 logs.

It can be noticed that for both the bacteria at 200 J/cm^2 there is a 4-logs decrease in survival while, interestingly, at 100 J/cm^2 the cell death is higher for *E. coli*, suggesting a higher selectivity for the Gram-negative bacteria.

For *E. coli* the control (only bacteria) at maximum light fluence shows no photoinactivation by light, while for *S. aureus* there is some cell death (less than 1 log) indicating that there could be some light- and heat-induced toxicity caused by the lamp.

Both bacteria, when treated with MB-labeled streptavidin and irradiated, show some cell death (less than 1 log). In the absence of ConA the photoinactivation effect is orders of magnitude (3 logs) lower than in presence of the protein, so ConA is necessary for the complex to effectively target the bacteria.

As expected, MB alone exerts phototoxicity on both bacteria. In keeping with literature, application of MB in the absence of a carrier leads to a higher cell death [87][127]. Nevertheless, under these conditions no specificity is granted, which means that (for example) in an infected wound, MB would not distinguish between host and bacterial cells, while the complex we made could in principle selectively target bacteria.

9 Conclusions

By exploiting the high affinity between streptavidin and biotin, we assembled two fully functional, versatile supramolecular complexes for aPDT, endowed with photosensitizing and targeting capability (**Figure 68**). Each complex comprises a photoactive unit, i.e. a streptavidin functionalized with a PS, and a targeting unit, i.e. a protein with high affinity for a bacterial molecular component.
Although the system streptavidin-biotin is often used to bind molecules together, its use in PDT is extremely limited: in two works it was used to treat cancer cells [128], [129], while for aPDT there is only one study [78].

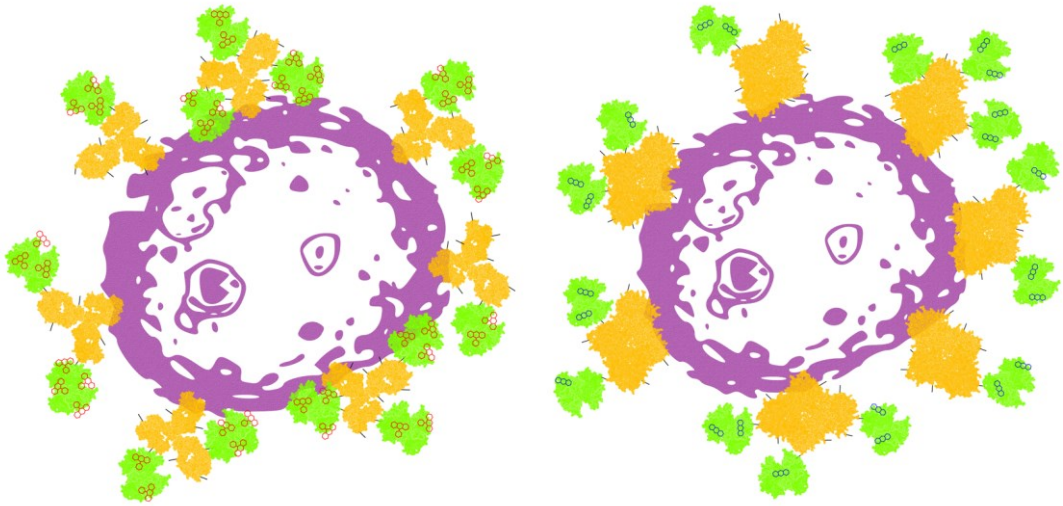

Figure 68. Representation of the complexes we made, bound to *S. aureus*. Right) Multiple copies of the first complex consisting of EITC (red), streptavidin (green), biotin (black) and IgG (ochre) bind to *S. aureus* (purple). Left) Multiple replicates of the second complex consisting of MB (blue), streptavidin (green), biotin (black) and ConA (ochre) bind to *S. aureus* (purple).

The photosensitizing unit was functionalized with amine reactive derivatives of two different PS, eosin and methylene blue.
A systematic study on the photophysical properties of streptavidin labeled with eosin-5-isothiocyanate (EITC) with an array of optical spectroscopic methods, demonstrated that upon binding streptavidin, the fluorescence, triplet and singlet oxygen yields of the PS decrease, due to non-radiative deexcitation. Quantum yields progressively decreases when multiple copies of eosin are present on the same streptavidin tetramer.
A second complex was assembled starting from a methylene blue-labelled streptavidin as a photosensitizing unit. Similarly to what observed for eosin, steady-state and time resolved optical spectroscopies showed that binding to the protein results in lower fluorescence and triplet state quantum yields.

Taking advantage of the versatility of the approach, streptavidin was labeled with amine reactive fluorescent probes (Alexa647 for STORM or Chromeo 488 for confocal microscopy and STED nanoscopy) that replaced the PS in microscopy studies.
As shown in this study, the quantum yield of fluorescence decreases when a molecule is bound to streptavidin. Furthermore, PSs generally do not excel in their fluorescent properties and therefore are little used for theranostics. The versatility of the approach we have used could allow to overcome this problem by conjugating, through reactive groups that interact with different residues, a PS and a fluorophore to the same streptavidin.

As observed, while the photophysics of the PS is negatively affected by the interaction with the protein, the presence of the PS does not hamper the biotin binding capability of the four binding sites on the streptavidin tetramer.

In the first complex, the antibody Immunoglobulin G (IgG) was exploited to selectively target protein A on Gram-positive *S. aureus*. IgG was labeled with an amine reactive biotin derivative. This provided IgG with streptavidin binding capability that was exploited to drive self-assembly of the photosensitizing (EITC-streptavidin) and the targeting (biotin-IgG) units into the supramolecular system, as demonstrated by FCS.
Using confocal or sub-diffraction resolution fluorescence microscopy, we were able to show binding of the complex between EITC-streptavidin and biotin-IgG to the external part of the bacterial wall of *S. aureus*, where binding occurs at discrete positions, presumably where protein A clusters. The complex does not bind appreciably to *E. coli*.
This complex has an excellent photoinactivating capability, allowing an 8-logs decrease in CFU/mL with only 500 nM of the compound, after irradiation with a 50 J/cm^2 green light fluence.
The photoinactivation results we obtained are consistent with those of other studies which used eosin for the treatment of *S. aureus*: a 2-logs cell death was achieved using 498 nM of PS and an irradiation of 9.98 J/cm^2 [130], 5-logs with 1 μM of eosin and 9 J/cm^2 [55], 6-logs with 5 μM of PS and 38.2 J/cm^2 [62]. Unlike those studies, however, we used a targeting molecule (IgG) which, as shown, increases the specificity of the complex and therefore should increase its efficiency compared to the PS alone. However, this advantage is partly compensated by the decrease of the phototoxic properties of the PS when bound to streptavidin. In view of the higher complexity of the supramolecular constructs, a different approach may be selected depending on the application. For surface disinfection, high specificity is not needed and therefore PS alone could be used directly, but for the treatment of infected wounds selectivity is crucial and therefore the use of a complex with a targeting system should be preferred.
Our complex causes more cell death than others which used eosin or IgG. For example, 1 μM of eosin bound to the antimicrobial peptide $(KLAKLAK)_2$ and a fluence of 60 J/cm^2 lead to a decrease of 5-logs [63], while 10 μM of the PS SnCe6 bound to IgG and irradiated with 21 J/cm^2 leads to a 5-logs cell death [131].
Interestingly, this is the first work in which eosin is used in a complex together with IgG for PDT.

In the second complex, concanavalin A (ConA) was adopted to target a molecular component that is found both in Gram-positive and Gram-negative bacteria. *S. aureus* and *E. coli* were taken as representative strains for the two classes. ConA belongs to lectins, a protein family known to have high affinity for α-glucose containing polysaccharides. We functionalized ConA with an amine reactive biotin derivative, so that, in the presence of MB-streptavidin, a supramolecular complex between biotin-ConA and MB-streptavidin self assembles.
STORM microscopy demonstrates binding of the complex to bacteria, where the interaction occurs at the external side of the wall, in keeping with the expected interaction with saccharides.
The complex between biotin-ConA and MB-streptavidin has good phototoxic effect on *E. coli* and *S. aureus*, where a 4-logs decrease in CFU/mL with 5 μM of MB-streptavidin was observed when exposed to light fluence of 200 J/cm^2 at 660 nm. While the phototoxicity is clearly lower for this second compound, it is able to exert its action also against Gram-negative bacteria.
Several works have demonstrated the efficacy of MB as PS for aPDT, also against *S. aureus* [132]. The results we obtained using MB alone led to comparable cell death of *S. aureus* compared other studies, for example in [127] a 5-logs decrease was obtained with 5 μM of MB and a fluence of 30 J/cm^2.
Furthermore, as already noted, the targeting system used for this complex (ConA) does not have a high affinity and therefore it is necessary to use a higher PS concentration than in cases in which MB is conjugated

to more selective molecules. For example, in [56] a 6-logs reduction in cell viability was achieved using 1 µM of PS bound to two different antibiotics (mupirocin and inezolid) and irradiating with 18 J/cm^2.
In one study [77] RB-labelled ConA was used to photoinactivate *E. coli*, achieving a 5-logs reduction using 5 µM of PS and a fluence of 5 J/cm^2. This result suggests a better photoinactivation efficiency than the one we obtained. It should be noted that the PSs and the bacteria strains used are different and therefore a direct comparison should be taken with caution. However, in both cases the use of ConA allows to increase cell death by about 2-logs.
Only one other study conjugated MB to ConA [76], obtaining a cell viability reduction of 4-logs in *Klebsiella pneumoniae*, using 4.8 µM of PS conjugated to dextran-coated gold nanoparticles and irradiating with 143 J/cm^2.

As targeting systems, we have chosen to use proteins as these are biocompatible and therefore excellent candidates for eventual *in vivo* applications.
Obviously, the use of targeting systems with very high affinity (such as antibodies) allows to create extremely specific complexes and therefore, virtually, to obtain high phototoxic capacities. However, the choice of targeting systems should not be limited to these molecules, since the use of less specific proteins (but which, nevertheless, allow to discriminate between the targeted cells and those that need to be preserved) allows a wider choice of targets. On the other hand, as observed in this work, the use of lower affinity proteins makes necessary to use a higher concentration and a higher light fluence to obtain a significant cell death.

The photoinactivation results we obtained not only show that the complexes made are effective, but also that they are excellent candidates for aPDT. In fact, on their cell wall, bacteria have few molecular targets that can be exploited to target them.
Furthermore, while to date there is no evidence that aPDT causes resistance, the history of antibiotics should make us cautious. However, protein A is a virulence factor that *S. aureus* has specifically developed to evade the host immunosurveillance and therefore it is extremely unlikely (and counterproductive for the bacterium) that it undergoes mutations which cause it to not bind IgG. Finally, ConA targets sugars which, in addition to being indispensable for the bacterium, are also molecules less subject to possible mutations.

The modular approach based on the junction system streptavidin-biotin we used has two main disadvantages. Streptavidin interacts with the molecules directly bound to it, negatively influencing their photophysical characteristics (the fluorescence of fluorophores and the singlet oxygen production of PSs decrease). Furthermore, it is hard to control the number of biotins present on the targeting system and this leads to the formation of clusters (in which multiple copies of the biotinylated targeting system may be present for each labeled streptavidin, or vice versa) which negatively affect the binding of the complex.
Despite these disadvantages, this modular system is a promising candidate, usable not only for antibacterial PDT, but for PDT against any type of cell.

Appendix A: labeling protocols

Preparation of streptavidin

When we had the protein already in a buffer (other than the one in which the reaction will occurs), we replaced this buffer through dialysis.

- Equilibration of the filter with the buffer. In an eppendorf tube with a filter (cut-off 10 kDa) we introduced an appropriate volume of carbonate-bicarbonate buffer and we centrifuged at 7,400 g for 10 minutes. We add some of the buffer inside the filter (to reach the same final volume) and centrifuged again. Then, we discarded the solution left inside the filter and the filtered one.
- Removal of the old buffer from the solution with the protein. We added an appropriate volume of the sample in the filter and centrifuge at 7,400 g for 10 minutes. We discarded the filtered solution (the old buffer) and add more sample inside the filter (to reach the same final volume). We did this until we filtered out all the old sample.
- Addition of the new buffer (carbonate-bicarbonate). We added the carbonate-bicarbonate buffer to the protein inside the filter (to reach the same final volume), we have centrifuged at 7,400 g for 10 minutes and then discarded the filtered solution (the new buffer). We repeated this four times and then, instead of centrifuging, we collected the solution inside the filter (the protein in the new buffer), repeating this last step once more in order to take out all the protein from the filter.

Finally, we determined the concentration of the protein via an absorption spectrum.

When a streptavidin solution was not available but the lyophilized one was available, we first solubilized it. For example, in a vial with 5 mg of lyophilized streptavidin we added 1 mL of buffer so that the final concentration of streptavidin in the monomers was 360 µM (4 * 5 mg / (1 mL * 55,000 Da)).

Labeling of streptavidin with EITC

To label the protein with PS we used the following protocol.

1. We prepared a concentrated solution of EITC in DMSO.
   We dissolved a small amount of EITC powder in DMSO. From the absorption spectrum we determined the concentration of the stock (in the order of a few mM) and then we calculated the next dilution to use.
2. In the protein solution add a small volume of the PS in DMSO in small aliquots.
   During the reaction, we added at most one eleventh (in volume) of EITC, so that streptavidin was in solution with (at most) 9% DMSO. This concentration of DMSO could desaturates the protein, but from absorption and circular dichroism spectra (not shown) performed after the reaction, we did not observe any differences with respect to streptavidin in the absence of DMSO.
   In the final volume, we added a concentration of PS 7 times that of the protein monomers, in order to have an excess of PS.
   We added the EITC dissolved in DMSO in 5 µL aliquots in order to avoid local aggregations.
3. After adding all the PS solution, to allow the PS to bind to the protein, we incubated the sample overnight in the dark using a shaker at 4 °C.

4. To separate the unbound PSs from the protein-conjugated PSs we filtered the sample using a desalting column (PD MiniTrapTM G-25). Furthermore, this step allows to remove the DMSO present in solution, since we use PBS as buffer to elute the EITC-labeled streptavidin.
   Due to their different size protein-bound PS and unbound PS elute at different times, the larger molecules eluting first.
5. We determined the ratio between the PS and the protein by measuring the absorbance, respectively, at 280 nm and 525 nm.
   EITC absorbs at 280 nm, in particular at this wavelength it absorbs 0.28 times of the peak at 525 nm. So, when calculating the protein concentration at 280 nm, the contribution of the EITC must be subtracted.
   The DOL was calculated with $DOL = \frac{[EITC]}{[Streptavidin]_{monomer}}$.
   In this way a DOL of 1 corresponds to one PS molecule per monomer or, equivalently, to four EITCs per streptavidin tetramer.

By changing the pH of the buffer (carbonate-bicarbonate for pH>8, PBS for pH lower than 8) in which the reaction between streptavidin and EITC occurs, we obtained different DOL (**Table 11**).

Degree of labeling	pH
~0.09	7.5
~0.3	8
~0.6	8.5
~0.9	9
~1.3	9.5
~1.5	10

Table 11. The DOL varies as the pH of the reaction buffer changes. The reactions were carried out with a 7-fold excess of EITC, at 4 °C and overnight. As the pH increases the DOL increases, because the more the pH is basic the more the reaction between the isothiocyanate group of the PS and the lysine of the protein is favored.

Labeling of IgG with biotin

Using the "CF® Dye & Biotin SE Protein Labeling Kit" we bound biotin to IgG. The following volumes, centrifugation parameters and incubation time are those reported in the kit.

1. Possible amines present in the lyophilized IgG should be removed.
   We applied the following steps can to 1 mg of IgG in 900 µL of PBS or a pre-existing IgG solution.
   - Concentrate the IgG. We introduced an appropriate volume of sample into the filter (cut-off 10 kDa) of the ultrafiltration vial and centrifuged at 14,000 g for 5 minutes. We removed the filtrate, added another aliquot of sample and homogenize.
   - Washing of the IgG. We added an appropriate volume of PBS, homogenized the solution and centrifuged at 14,000 g for 8 minutes; we removed the filtered solution. We repeated this process three times.
   - IgG preparation. We introduced an appropriate volume of PBS into the unfiltered solution (IgG), homogenized and withdrawn the solution. We repeated this operation once more.
   - We added 100 µL of sodium bicarbonate pH 8.3 to the solution and an appropriate volume of PBS to reach 1 mL.
2. Biotin preparation. We added 25 µL of DMSO to the biotin vial. Homogenized and centrifuged at 14,000 g for 1 minute.

3. Incubation. We introduced 25 µL of the DMSO biotin solution into the 1 mL IgG in PBS solution. We incubated for 1 hour in the dark using a shaker at room temperature.
4. Equilibrate the filter. We introduced an appropriate volume of PBS into the filter of the ultrafiltration vial and centrifuged at 14,000 g for 10 minutes. We discarded the filtrate.
5. Purification of IgG. We introduced an appropriate volume of IgG and biotin solution into the filter, centrifuged at 14,000 g for 10 minutes. We discarded the filtrate. We repeated until all the solution obtained in the previous step is centrifuged.
6. Washing of IgG. We introduced an appropriate volume of PBS into the filter and centrifuged at 14,000 g for 10 minutes, discarded the filtrate. We repeated this step three times.
7. We introduced an appropriate volume of PBS into the filter, homogenized the solution and collected it. We repeated this step once more.
8. We determined the IgG concentration by measuring its absorbance at 280 nm.

Labeling of ConA with biotin

Using a "Water-soluble Long-arm Biotin Labeling Kit" we bound biotin to ConA. The following volumes, centrifugation parameters and incubation time are those reported in the kit.
We applied the following steps to 1 mg of a lyophilized protein powder.

1. Biotin preparation. We added 30 µL of ultrapure water to the biotin vial, homogenized and let it stand for 10 minutes (the final concentration is 10 mM).
2. Protein preparation. we added 1 mg of ConA and 500 µL of Labeling Buffer to a filtration tube, then centrifuged at 12,000 g for 10 minutes. We discarded the filtrate.
3. Incubation. We introduced 13.3 µL of the ultrapure wand biotin solution into the 1 mg ConA in Labeling Buffer solution. We added Labeling Buffer to reach 500 µL, homogenize then incubate for 30 minutes in the dark at 37 °C.
4. Purify the ConA. We centrifuged the ConA and biotin solution at 12,000 g for 10 minutes. We discarded the filtrate, added an appropriate volume of Labeling Buffer to the filtration tube. We repeated this step once again.
5. We introduced a an appropriate volume of Labeling Buffer into the filter, homogenized the solution and collected it. We repeated this step once more.
6. We determined the ConA concentration by measuring its absorbance at 280 nm.

Appendix B: main methods

Fluorescence correlation spectroscopy

FCS consists in the analysis of the fluorescence intensity variations as a function of time, due to the diffusion of molecules in a volume illuminated by a laser beam.
A laser beam illuminates an elliptical volume V_{eff} of solution in which fluorophores diffuse and in which are excited and subsequently return to the ground state emitting fluorescence. The detected signal shows fluctuations due to the diffusion of the fluorophores in solution; these fluctuations can be caused by various factors, such as diffusive movements, binding between a ligand and a macromolecule, transition to dark state, for instance to a triplet state through intersystem crossing, the dynamics within the macromolecules.

At the same temperature and solvent used, the smaller the size of the fluorophore the greater its diffusion rate, so it takes less time to pass through the V_{eff} and its exposure time to the photons of the laser beam is shorter. Conversely, the greater the mass of a molecule, the slower its diffusion, therefore it is exposed for a longer time to the excitation beam. For a spherical particle, the diffusion coefficient D is given by the Einstein-Stokes equation:

$$D = \frac{k_B T}{6\pi\eta r} \qquad \textbf{Equation 23}$$

where k_B is the Boltzmann constant, T the temperature, η the viscosity of the fluid in which the particle is found and r the radius of the analyzed particle.
The diffusion coefficient D describes the average displacement of a particle due to its diffusive movement; D is inversely proportional to the radius of the particle (spherical and ideal) that approximates the analyzed molecule.

The diffusive motion of the molecule in solution is described by a random walk: while the fluorophore moves in the solvent, the molecules of the fluid collide with the fluorophore, which in turn makes small shifts in random directions.
The root mean square displacement of the diffusing molecule can be obtained from the following relation:

$$\langle r^2 \rangle = 6D\tau \qquad \textbf{Equation 24}$$

where τ is the diffusion time (s) and D the diffusion coefficient (μm^2/s).

Fluctuations observed with the FCS technique are described by the Poisson statistics [133]

$$P(n, N) = \frac{N^n}{n!} e^{-N} \qquad \textbf{Equation 25}$$

Where $P(n, N)$ expresses the probability that n fluorophores are present in V_{eff} when N molecules are present on average in solution. The variance is equal to the mean, $\sigma_N^2 = N$.
To obtain information on the movement of a single particle it is necessary to consider the unitary fluctuations of the signal, that is caused by the entry or exit of a single molecule from the V_{eff}. To observe these fluctuations it is necessary that only a few molecules are present in the V_{eff}: in this way the fluctuations are greater and more easily analyzed [133].
Thanks to the Poisson statistics it is possible to know the average of the rare events (fluorophore in V_{eff}) that are observed, which allows to determine the average number of particles present in the volume. The count of the photons emitted and the construction of the relative photon-counts histogram, allows to determine how many times n molecules enter the V_{eff} (frequency) and provides the average number of molecules $\langle N \rangle$ in the V_{eff}.

The detected fluorescence fluctuations derive from the difference in intensity at a certain instant t and from the average intensity at time t:

$$\delta F(t) = F(t) - \langle F(t) \rangle \qquad \textbf{Equation 26}$$

These fluctuations are analyzed using the autocorrelation function $G(\tau)$, which defines the degree of dependence between the values assumed by a function (i.e. the fluctuations in the intensity of the fluorescence emission) over time. In particular, $G(\tau)$ shows how similar a signal is to itself during the acquisition: the signal is considered at a certain instant t and compared with the value of the signal obtained at a subsequent instant $t + \tau$ [134].

$$G(\tau) = \frac{\langle \delta I(t) \delta I(t+\tau) \rangle}{\langle I(t) \rangle^2} = \frac{\langle I(t) I(t+\tau) \rangle}{\langle I(t) \rangle^2} - 1 \qquad \textbf{Equation 27}$$

Where $\delta I(t) = I(t) - \langle I(t) \rangle$ is the deviation from the average intensity. The normalization used in **Equation 27**, allows to determine at $G(\tau = 0)$ the average number of particles in the measurement volume.

The fluorophores can be excited in the triplet state therefore, for a characteristic time Θ_T, they do not emit photons. Typically Θ_T occurs on a shorter time scale than the diffusion τ_D, but it can be measured and in this case the autocorrelation function becomes [134]:

$$G(\tau) = \frac{1 - \Theta_T + \Theta_T e^{-\tau/\Theta_T}}{1 - \Theta_T} \left[\frac{1}{\langle N \rangle} \left(1 + \frac{4D\tau}{w^2} \right)^{-1} \left(1 + \frac{4D\tau}{z^2} \right)^{-1/2} \right] \qquad \textbf{Equation 28}$$

Where w and z are the dimensions of the effective volume axes.

The trend of the autocorrelation function is shown in **Figure 69**.

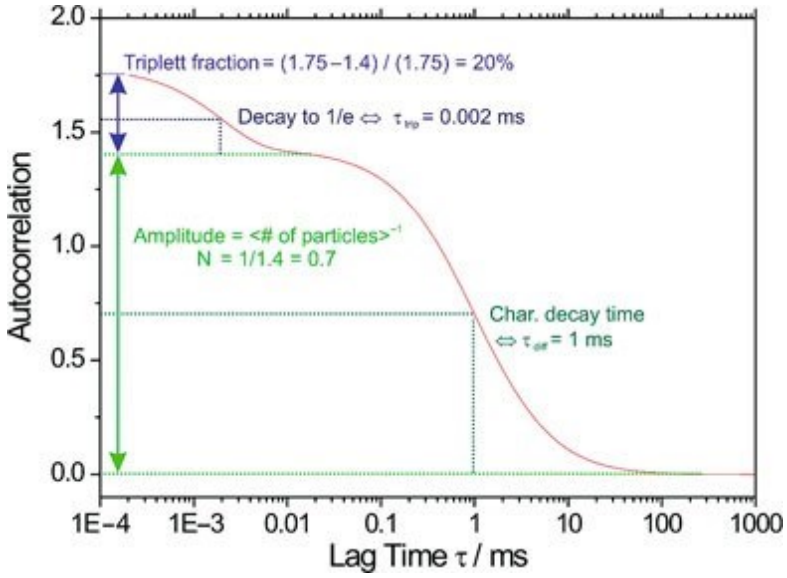

Figure 69. Trend of the autocorrelation function. The autocorrelation function allows to determine the diffusion time of the molecule and therefore to derive the diffusion coefficient. In time scales of µs, a triplet state component may also be present.

The autocorrelation function gives two important parameters: the diffusion time τ_D and the intercept $G(0)$. τ_D increases (the curve shifts to the right) if the fluctuations are slow, that is, if the molecule diffuses slowly, and through this parameter it is possible to determine the diffusion coefficient D of the molecule τ_D:

$$D = \frac{w_{xy}^2}{4\tau_D} \qquad \textbf{Equation 29}$$

$G(0)$ is proportional to the inverse of the number of particles present in the V_{eff}: if the intercept value increases, the number of particles decreases.

As shown in **Figure 70**, the higher the diffusion coefficient (bottom), the wider the trajectory that the particle covers. The slowly diffusing molecules, at low concentrations, produce large signal fluctuations around the

mean fluorescence intensity value; while the fast diffusing molecules, at high concentration, give rise to small signal fluctuations. Also, due to their lower size in the V_{eff} there are more molecule, so the number of photon detected is greater than for a molecule with a lower D (red).

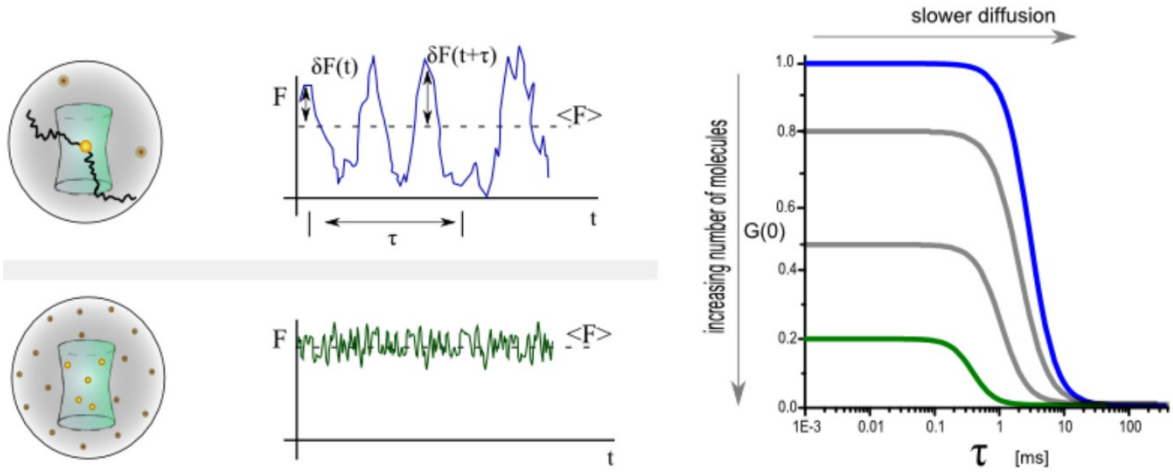

Figure 70. FCS principle. Slow diffusing (top) and fast diffusing (bottom) particles in the effective volume emit fluorescence, the fluctuations of which allow to obtain the autocorrelation function (right). From this function it is possible to derive the diffusion time and the number of particles present in the effective volume. Source: Time-Resolved Fluorescence Wiki - fluorescence correlation spectroscopy, a short introduction.

Laser flash photolysis

LFP, also called transient absorption, is a technique that allows the study of time-resolved processes in the range from nanoseconds to seconds.
A short laser pulse generates, in the sample, transient photo-excited species which can be an intermediate radical or a short-lifetime excited state. When the sample relaxes, returning to the ground state or forming products, the change in absorption is monitored as a function of time.
Typically, this technique uses a pulsed laser (pump) to excite the sample and a continuous light source (probe) that passes through the sample. The pump creates the transient species and acts as "zero time" for the experiment, while the probe (usually a white light) is used to study the temporal evolution of absorption at a given wavelength. To minimize light-scattering from the pump, the monitoring beam is positioned at 90° respect to the pump. In addition, a monochromator is present before the detector and it is advisable to use a dichroic mirror to further reject stray light from the pump beam.

The "kinetic mode", in which the transient absorption is measured as a function of time and at a single detection wavelength, allows to obtain time traces that represent the absorption variation $\Delta A(\lambda, t)$

$$\Delta A(\lambda, t) = \log\left(\frac{I_B(\lambda, t)}{I_S(\lambda, t)}\right) \qquad \textbf{Equation 30}$$

Where I_B is the intensity of the baseline (the signal obtained by illuminating the sample only with the probe and thus blocking the pump), I_S the intensity of the sample (the signal obtained using both the pump and the probe) [110].

Transient species can have a higher or lower absorption than the ground state (ΔA positive or negative, respectively). Greater absorption is associated with triplet-triplet or singlet-singlet transitions, while a reduction is associated with ground state depletion or sample emission [135].

From the transitions, be they triplet-triplet or singlet-singlet, it is possible to derive the lifetime of the transient species. In organic molecules the lifetime of the triplet state is often decreased (depletion phenomenon) by the oxygen present in the sample. The measurements of transient absorption at different oxygen concentrations therefore allow to verify whether the observed transition is triplet-triplet, since as the oxygen concentration decreases the lifetime of the transient species increases [135].

Time-resolved phosphorescence

When a PS is in the triplet state, it can interact with the molecular oxygen present in solution which can be promoted to the excited singlet state: $O_2(^1\Delta_g)$. The quantum yield of singlet oxygen formation Φ_Δ is given by the number of singlet oxygen molecules that are formed for each absorbed photon [136]:

$$\Phi_\Delta = \Phi_T * f_{T\Sigma} * S_\Delta \qquad \textbf{Equation 31}$$

Where Φ_T is the quantum yield of the triplet state formation of the molecule (PS) that excites the molecular oxygen, $f_{T\Sigma}$ is the fraction of molecules in the triplet state trapped by molecular oxygen and takes into account that this is a collision process that must occur within the lifetime of the triplet state of the PS, S_Δ is the fraction of molecules in the triplet state that produce singlet oxygen.
As can be seen, Φ_Δ not only depends on the properties of the PS, but also on the concentration of molecular oxygen, so experimentally the sample is left in equilibrium with the air.

To determine Φ_Δ, the time-resolved (phosphorescence) signal of singlet oxygen in the NIR (at 1275 nm) is measured. This signal typically shows a rise and a decay and can be described through a bi-exponential function [136]:

$$S(t) = S(0)\frac{\tau_\Delta}{\tau_\Delta - \tau_T}\left(e^{-t/\tau_\Delta} - e^{-t/\tau_T}\right) + y_0 \qquad \textbf{Equation 32}$$

Where $S(0)$ is an instrumental quantity which is directly proportional to Φ_Δ and is the amplitude of the signal at "zero" time, τ_Δ is the lifetime of singlet oxygen, τ_T is the lifetime of the triplet state of the PS, y_0 is the background given by the dark counts.
As said $S(0)$ is proportional toΦ_Δ, but it also depends on the absorbance A of the sample:

$$S(0) = k * \Phi_\Delta(1 - 10^{-A}) \qquad \textbf{Equation 33}$$

Where k it is a parameter that takes into account geometric and electronic factors of the system, the refractive index of the solvent, the constant rate of decay of the singlet oxygen and the energy of the pump beam [136].

Using a reference molecule it is possible to determine the Φ_Δ of a PS. For each compound, solutions with different absorbances (in the range 0.01-0.1 at the excitation wavelength) are prepared, and for each of them the phosphorescence signal is measured and $S(0)$ is obtained; plotting $S(0)$ as a function of $1\text{-}10^{-A}$ a linear plot is obtained for each compound, and by comparing slope of the compound with unknown Φ_Δ, with that for a reference compound it is possible to determine Φ_Δ for the sample [136]:

$$\Phi_{\Delta,sample} = \Phi_{\Delta,ref}\frac{S(0)_{sample}}{S(0)_{ref}} \qquad \textbf{Equation 34}$$

For this analysis the compounds must be dissolved in the same solvent and equilibrated in air.

To minimize scattered light from the pump interfering with the detector, the monitoring beam is positioned 90° to the pump. Additionally, filters are used to remove fluorescence and phosphorescence emissions from the PS.

Stochastic optical reconstruction microscopy

STORM is a super-resolution microscopy technique that uses photo-switchable molecules.
In this type of microscopy, the fluorophore molecules are activated individually and stochastically in a "blink" process: fluorophores are activated from a non-emitting (off or dark) state to an emitting (on) state, then rapidly return in the dark state or undergo photobleaching (**Figure 71**).
When the fluorophore is in the triplet T state it can be reduced or oxidized reaching, via intersystem crossing, a dark non-fluorescent state (R·) which, after a characteristic time, returns to the ground state S_0 allowing the fluorophore to restart the cycle. When in the R· state, some molecules can be further reduced to the leuco state, a dark colorless state that is more stable and has a longer lifetime [137].

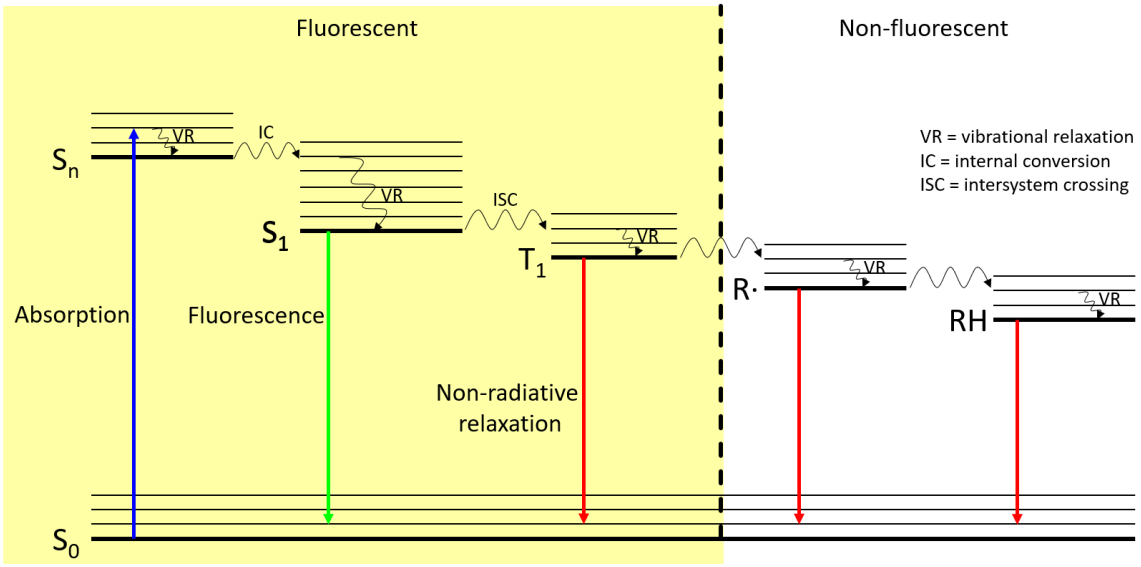

Figure 71. Jablonski diagram applied to STORM microscopy. The triplet state T can be reduced or oxidized to a dark radical state (R·); furthermore, some molecules can be reduced to a colorless (leuco) state (RH).

This ensures that only a small fraction of the fluorophores is detected in each image. After the photons emitted by the excited molecules are detected by the camera, a program precisely reconstructs and locates the point-spread functions of each molecule. By capturing multiple images, each with a random subset of the fluorophores undergoing the blink process and recalculating the central position of the point-spread functions, a super-resolution image of single molecule coordinates can be reconstructed.

Out-of-focus fluorophores cause a higher background which decreases the signal-to-noise ratio resulting in worse accuracy in the determination of the molecules' positions. To reduce out-of-focus contributions, the sample is usually illuminated in a TIRF condition (with the incident angle slightly less than the critical angle) thus exciting only a thin layer of the sample [137].

One type of STORM called direct-STROM (dSTORM) uses ordinary fluorophores and causes them to go through the blink process thanks to an oxygen scavenging buffer that converts the fluorophores to the off state.
These buffers usually contain GLOX (glucose, glucose oxidase and glucose catalase) and reducing agents (such as mercaptoethylamine MEA and β-mercaptoethanol BME).

GLOX is an enzymatic oxygen scavenging system used to scavenge molecular oxygen because when it is present it quenches the triplet state and radicals, shortening the lifetime of the dark state and producing ROS (for STORM the reverse is essential). Glucose oxidase uses molecular oxygen to oxidize glucose producing gluconolactone and hydrogen peroxide (H_2O_2). The latter is a ROS, so glucose catalase is used to decompose it into water and molecular oxygen; note that no oxygen is removed from the system in the overall reaction [137].

MEA and BME are reducing agents containing primary thiol which acts as electron donor, promoting the formation of anionic dark states with longer lifetime [137].

Bibliography

[1] "Antimicrobial resistance." https://www.who.int/news-room/fact-sheets/detail/antimicrobial-resistance.

[2] C. J. Murray *et al.*, "Articles Global burden of bacterial antimicrobial resistance in 2019: a systematic analysis," *Lancet*, 2022, doi: 10.1016/S0140-6736(21)02724-0.

[3] J. O'Neill, "TACKLING DRUG-RESISTANT INFECTIONS GLOBALLY: FINAL REPORT AND RECOMMENDATIONS THE REVIEW ON ANTIMICROBIAL RESISTANCE CHAIRED BY JIM O'NEILL," 2016.

[4] A. Rapacka-Zdończyk *et al.*, "Factors Determining the Susceptibility of Bacteria to Antibacterial Photodynamic Inactivation," *Front. Med.*, vol. 8, p. 642609, May 2021, doi: 10.3389/FMED.2021.642609.

[5] R. Gaynes, "The discovery of penicillin—new insights after more than 75 years of clinical use," *Emerg. Infect. Dis.*, vol. 23, no. 5, pp. 849–853, May 2017, doi: 10.3201/eid2305.161556.

[6] M. Klausen, M. Ucuncu, and M. Bradley, "Design of Photosensitizing Agents for Targeted Antimicrobial Photodynamic Therapy," *Molecules*, vol. 25, no. 22, p. 5239, Nov. 2020, doi: 10.3390/molecules25225239.

[7] B. Spellberg *et al.*, "The epidemic of antibiotic-resistant infections: A call to action for the medical community from the infectious diseases society of America," *Clin. Infect. Dis.*, vol. 46, no. 2, pp. 155–164, Jan. 2008, doi: 10.1086/524891.

[8] J. L. Martinez, "General principles of antibiotic resistance in bacteria," *Drug Discov. Today Technol.*, vol. 11, no. 1, pp. 33–39, Mar. 2014, doi: 10.1016/J.DDTEC.2014.02.001.

[9] R. M. Humphries, A. N. Abbott, and J. A. Hindler, "Understanding and Addressing CLSI Breakpoint Revisions: a Primer for Clinical Laboratories," *J. Clin. Microbiol.*, vol. 57, no. 6, pp. e00203-19, Jun. 2019, doi: 10.1128/JCM.00203-19.

[10] J. M. A Blair, M. A. Webber, A. J. Baylay, D. O. Ogbolu, and L. J. V Piddock, "Molecular mechanisms of antibiotic resistance," *Nat Rev Microbiol.*, vol. 13, no. 1, pp. 42–51, 2015, doi: 10.1038/nrmicro3380.

[11] D. G. J. Larsson and C.-F. Flach, "Antibiotic resistance in the environment," *Nat. Rev. Microbiol.*, pp. 1–13, Nov. 2021, doi: 10.1038/S41579-021-00649-X.

[12] Z. Jian *et al.*, "Antibiotic resistance genes in bacteria: Occurrence, spread, and control," *J. Basic Microbiol.*, vol. 61, no. 12, pp. 1049–1070, 2021, doi: 10.1002/JOBM.202100201/FORMAT/PDF.

[13] B. Aslam *et al.*, "Antibiotic Resistance: One Health One World Outlook," *Front. Cell. Infect. Microbiol.*, vol. 11, p. 1153, Nov. 2021, doi: 10.3389/FCIMB.2021.771510/BIBTEX.

[14] R. Yin and M. Hamblin, "Antimicrobial Photosensitizers: Drug Discovery Under the Spotlight," *Curr. Med. Chem.*, vol. 22, no. 18, pp. 2159–2185, Jul. 2015, doi: 10.2174/0929867322666150319120134.

[15] R. Laxminarayan, "The overlooked pandemic of antimicrobial resistance," *Lancet*, Jan. 2022, doi: 10.1016/S0140-6736(22)00087-3.

[16] N. Ahmad-Mansour *et al.*, "Staphylococcus aureus Toxins: An Update on Their Pathogenic Properties and Potential Treatments," *Toxins (Basel).*, vol. 13, no. 10, p. 677, Oct. 2021, doi: 10.3390/TOXINS13100677.

[17] M. Kawada-Matsuo, M. N. T. Le, and H. Komatsuzawa, "Antibacterial Peptides Resistance in Staphylococcus aureus: Various Mechanisms and the Association with Pathogenicity," *Genes (Basel).*, vol. 12, no. 10, p. 1527, Oct. 2021, doi: 10.3390/GENES12101527.

[18] J. Y. Park and K. S. Seo, "Staphylococcus aureus," in *Food Microbiology: Fundamentals and Frontiers*, wiley, 2019, pp. 555–584.

[19] G. Y. C. Cheung, J. S. Bae, and M. Otto, "Pathogenicity and virulence of Staphylococcus aureus," *Virulence*, vol. 12, no. 1, pp. 547–569, 2021, doi: 10.1080/21505594.2021.1878688.

[20] T. J. Foster, "Antibiotic resistance in Staphylococcus aureus. Current status and future prospects," *FEMS Microbiol. Rev.*, vol. 41, no. 3, pp. 430–449, May 2017, doi: 10.1093/FEMSRE/FUX007.

[21] N. A. Turner *et al.*, "Methicillin-resistant Staphylococcus aureus: an overview of basic and clinical research," *Nat. Rev. Microbiol.*, vol. 17, no. 4, pp. 203–218, Apr. 2019, doi: 10.1038/s41579-018-0147-4.

[22] X.-J. Fu, Y. Fang, and M. Yao, "Antimicrobial Photodynamic Therapy for Methicillin-Resistant

Staphylococcus aureus Infection," *Biomed Res. Int.*, vol. 2013, p. 159157, 2013, doi: 10.1155/2013/159157.
[23] C. Pérez, T. Zúñiga, and C. E. Palavecino, "Photodynamic therapy for treatment of Staphylococcus aureus infections," *Photodiagnosis Photodyn. Ther.*, vol. 34, p. 102285, Jun. 2021, doi: 10.1016/J.PDPDT.2021.102285.
[24] W. E. Sause, P. T. Buckley, W. R. Strohl, A. S. Lynch, and V. J. Torres, "Antibody-Based Biologics and Their Promise to Combat Staphylococcus aureus Infections," *Trends Pharmacol. Sci.*, vol. 37, no. 3, pp. 231–241, Mar. 2016, doi: 10.1016/j.tips.2015.11.008.
[25] J. Chen, H. Zhou, J. Huang, R. Zhang, and X. Rao, "Virulence alterations in staphylococcus aureus upon treatment with the sub-inhibitory concentrations of antibiotics," *J. Adv. Res.*, vol. 31, pp. 165–175, Jul. 2021, doi: 10.1016/J.JARE.2021.01.008.
[26] R. Laxminarayan *et al.*, "Access to effective antimicrobials: a worldwide challenge," *Lancet*, vol. 387, no. 10014, pp. 168–175, Jan. 2016, doi: 10.1016/S0140-6736(15)00474-2.
[27] C. Willyard, "The drug-resistant bacteria that pose the greatest health threats," *Nature*, vol. 543, no. 7643, p. 15, Feb. 2017, doi: 10.1038/NATURE.2017.21550.
[28] N. Kashef and M. R. Hamblin, "Can microbial cells develop resistance to oxidative stress in antimicrobial photodynamic inactivation?," *Drug Resist. Updat.*, vol. 31, p. 31, Mar. 2017, doi: 10.1016/J.DRUP.2017.07.003.
[29] M. Tampa *et al.*, "Photodynamic therapy: A hot topic in dermato-oncology (Review)," *Oncol. Lett.*, vol. 17, no. 5, pp. 4085–4093, May 2019, doi: 10.3892/ol.2019.9939.
[30] A. Wiehe, J. M. O'brien, and M. O. Senge, "Trends and targets in antiviral phototherapy," *Photochem. Photobiol. Sci. 2019 1811*, vol. 18, no. 11, pp. 2565–2612, Oct. 2020, doi: 10.1039/C9PP00211A.
[31] L. M. Baltazar, A. Ray, D. A. Santos, P. S. Cisalpino, A. J. Friedman, and J. D. Nosanchuk, "Antimicrobial photodynamic therapy: An effective alternative approach to control fungal infections," *Front. Microbiol.*, vol. 6, no. MAR, p. 202, Mar. 2015, doi: 10.3389/FMICB.2015.00202/BIBTEX.
[32] L. Benov, "Photodynamic therapy: Current status and future directions," *Med. Princ. Pract.*, vol. 24, no. Suppl 1, pp. 14–28, Apr. 2015, doi: 10.1159/000362416.
[33] T. C. Zhu and J. C. Finlay, "The role of photodynamic therapy (PDT) physics," *Med. Phys.*, vol. 35, no. 7, pp. 3127–3136, 2008, doi: 10.1118/1.2937440.
[34] A. P. Castano, T. N. Demidova, and M. R. Hamblin, "Mechanisms in photodynamic therapy: Part two - Cellular signaling, cell metabolism and modes of cell death," *Photodiagnosis Photodyn. Ther.*, vol. 2, no. 1 SPEC. ISS., pp. 1–23, 2005, doi: 10.1016/S1572-1000(05)00030-X.
[35] K. Lang, J. Mosinger, and D. M. Wagnerová, "Photophysical properties of porphyrinoid sensitizers non-covalently bound to host molecules; models for photodynamic therapy," *Coord. Chem. Rev.*, vol. 248, no. 3–4, pp. 321–350, Feb. 2004, doi: 10.1016/j.ccr.2004.02.004.
[36] A. B. Ormond and H. S. Freeman, "Dye sensitizers for photodynamic therapy," *Materials (Basel).*, vol. 6, no. 3, pp. 817–840, 2013, doi: 10.3390/ma6030817.
[37] J. F. Algorri, M. Ochoa, P. Roldán-Varona, L. Rodríguez-Cobo, and J. M. López-Higuera, "Light Technology for Efficient and Effective Photodynamic Therapy: A Critical Review," *Cancers (Basel).*, vol. 13, no. 14, p. 3484, Jul. 2021, doi: 10.3390/CANCERS13143484.
[38] K. Plaetzer, B. Krammer, J. Berlanda, F. Berr, and T. Kiesslich, "Photophysics and photochemistry of photodynamic therapy: Fundamental aspects," *Lasers Med. Sci.*, vol. 24, no. 2, pp. 259–268, Mar. 2009, doi: 10.1007/s10103-008-0539-1.
[39] A. P. Castano, T. N. Demidova, and M. R. Hamblin, "Mechanisms in photodynamic therapy: Part one - Photosensitizers, photochemistry and cellular localization," *Photodiagnosis Photodyn. Ther.*, vol. 1, no. 4, pp. 279–293, 2004, doi: 10.1016/S1572-1000(05)00007-4.
[40] P. R. Ogilby, "Singlet oxygen: There is indeed something new under the sun," *Chem. Soc. Rev.*, vol. 39, no. 8, pp. 3181–3209, Jul. 2010, doi: 10.1039/b926014p.
[41] M. C. Derosa and R. J. Crutchley, "Photosensitized singlet oxygen and its applications," *Coord. Chem. Rev.*, vol. 233–234, pp. 351–371, 2002.

[42] R. W. Redmond and I. E. Kochevar, “Spatially Resolved Cellular Responses to Singlet Oxygen,” *Photochem. Photobiol.*, vol. 82, no. 5, p. 1178, 2006, doi: 10.1562/2006-04-14-ir-874.
[43] D. Osiro, R. B. Filho, O. B. G. Assis, L. A. de C. Jorge, and L. A. Colnago, “Measuring bacterial cells size with AFM,” *Brazilian J. Microbiol.*, vol. 43, no. 1, p. 341, Jan. 2012, doi: 10.1590/S1517-838220120001000040.
[44] T. Dai, Y. Y. Huang, and M. R. Hamblin, “Photodynamic therapy for localized infections-State of the art,” *Photodiagnosis Photodyn. Ther.*, vol. 6, no. 3–4, pp. 170–188, Sep. 2009, doi: 10.1016/j.pdpdt.2009.10.008.
[45] M. J. Davies, “Singlet oxygen-mediated damage to proteins and its consequences,” *Biochem. Biophys. Res. Commun.*, vol. 305, no. 3, pp. 761–770, Jun. 2003, doi: 10.1016/S0006-291X(03)00817-9.
[46] H. Sies and C. F. M. Menck, “Singlet oxygen induced DNA damage,” *Mutat. Res. DNAging*, vol. 275, no. 3–6, pp. 367–375, 1992, doi: 10.1016/0921-8734(92)90039-R.
[47] J. Cadet, J. L. Ravanat, G. W. Helen, H. C. Yeo, and B. N. Ames, “Singlet oxygen DNA damage: Chromatographic and mass spectrometric analysis of damage products,” *Methods Enzymol.*, vol. 234, no. C, pp. 79–88, Jan. 1994, doi: 10.1016/0076-6879(94)34079-X.
[48] N. Watabe, Y. Ishida, A. Ochiai, Y. Tokuoka, and N. Kawashima, “Oxidation decomposition of unsaturated fatty acids by singlet oxygen in phospholipid bilayer membranes.,” *J. Oleo Sci.*, vol. 56, no. 2, pp. 73–80, 2007, doi: 10.5650/jos.56.73.
[49] R. D. Nielsen, K. Che, M. H. Gelb, and B. H. Robinson, “A ruler for determining the position of proteins in membranes,” *J. Am. Chem. Soc.*, vol. 127, no. 17, pp. 6430–6442, May 2005, doi: 10.1021/JA042782S/SUPPL_FILE/JA042782SSI20050310_090526.PDF.
[50] I. O. L. Bacellar and M. S. Baptista, “Mechanisms of Photosensitized Lipid Oxidation and Membrane Permeabilization,” *ACS Omega*, vol. 4, no. 26, pp. 21636–21646, Dec. 2019, doi: 10.1021/acsomega.9b03244.
[51] B. Rodríguez-Amigo *et al.*, “A Double Payload Complex between Hypericin and All-trans Retinoic Acid in the β-Lactoglobulin Protein,” *Antibiotics*, vol. 11, no. 2, Feb. 2022, doi: 10.3390/ANTIBIOTICS11020282/S1.
[52] P. J. L. Crugeira, H. H. S. Almeida, L. G. Teixeira, and M. F. Barreiro, “Photodynamic inactivation of Staphylococcus aureus by ecological antibacterial solutions associating LED (ʎ 450 ± 10 nm) with curcumin and olive leaf extracts,” *J. Photochem. Photobiol. B.*, vol. 238, Jan. 2023, doi: 10.1016/J.JPHOTOBIOL.2022.112626.
[53] I. Nieves, C. Hally, C. Viappiani, M. Agut, and S. Nonell, “A porphycene-gentamicin conjugate for enhanced photodynamic inactivation of bacteria,” *Bioorg. Chem.*, vol. 97, Apr. 2020, doi: 10.1016/J.BIOORG.2020.103661.
[54] R. Bresolí-Obach *et al.*, “Triphenylphosphonium cation: A valuable functional group for antimicrobial photodynamic therapy,” *J. Biophotonics*, vol. 11, no. 10, Oct. 2018, doi: 10.1002/JBIO.201800054.
[55] S. AR *et al.*, “The Remarkable Effect of Potassium Iodide in Eosin and Rose Bengal Photodynamic Action against Salmonella Typhimurium and Staphylococcus aureus,” *Antibiot. (Basel, Switzerland)*, vol. 8, no. 4, p. 211, Dec. 2019, doi: 10.3390/ANTIBIOTICS8040211.
[56] V. Pérez-Laguna *et al.*, “Bactericidal Effect of Photodynamic Therapy, Alone or in Combination with Mupirocin or Linezolid, on Staphylococcus aureus,” *Front. Microbiol.*, vol. 8, no. MAY, May 2017, doi: 10.3389/FMICB.2017.01002.
[57] M. Wainwright *et al.*, “Photoantimicrobials—are we afraid of the light?,” *Lancet Infect. Dis.*, vol. 17, no. 2, pp. e49–e55, Feb. 2017, doi: 10.1016/S1473-3099(16)30268-7.
[58] M. Levine, “Differentiation of B. Coli and B. Aerogens on a Simplified Eosin-Methylene Blue Agar,” *J. Infect. Dis.*, vol. 23, no. 1, pp. 43–47, Jul. 1918, doi: 10.1086/INFDIS/23.1.43.
[59] C. S. A. Caires *et al.*, “Photoinactivation effect of eosin methylene blue and chlorophyllin sodium-copper against Staphylococcus aureus and Escherichia coli,” *Lasers Med. Sci.*, vol. 32, no. 5, pp. 1081–1088, Jul. 2017, doi: 10.1007/S10103-017-2210-1.
[60] B. M and L. J, “The photodynamic effect: the comparison of chemiexcitation by luminol and phthalhydrazide,” *Luminescence*, vol. 26, no. 6, pp. 410–415, Nov. 2011, doi: 10.1002/BIO.1245.

[61] K. H, K. K, N. Y, I. T, and K. T, “Xanthene dyes induce membrane permeabilization of bacteria and erythrocytes by photoinactivation,” *Photochem. Photobiol.*, vol. 88, no. 2, pp. 423–431, Mar. 2012, doi: 10.1111/J.1751-1097.2012.01080.X.

[62] E. Bonin *et al.*, “Photodynamic inactivation of foodborne bacteria by eosin Y,” *J. Appl. Microbiol.*, vol. 124, no. 6, pp. 1617–1628, Jun. 2018, doi: 10.1111/JAM.13727.

[63] G. A. Johnson, N. Muthukrishnan, and J.-P. Pellois, “Photoinactivation of Gram Positive and Gram Negative Bacteria with the Antimicrobial Peptide (KLAKLAK) 2 Conjugated to the Hydrophilic Photosensitizer Eosin Y,” *Bioconjug. Chem*, vol. 24, no. 1, pp. 114–23, 2013, doi: 10.1021/bc3005254.

[64] G. A. Johnson, E. Ann Ellis, H. Kim, N. Muthukrishnan, T. Snavely, and J.-P. Pellois, “Photoinduced Membrane Damage of E. coli and S. aureus by the Photosensitizer-Antimicrobial Peptide Conjugate Eosin-(KLAKLAK) 2,” *PLoS One*, vol. 9, no. 3, p. e91220, 2014, doi: 10.1371/journal.pone.0091220.

[65] G. Sabarees, V. Velmurugan, G. P. Tamilarasi, V. Alagarsamy, and V. Raja Solomon, “Recent Advances in Silver Nanoparticles Containing Nanofibers for Chronic Wound Management,” *Polymers (Basel).*, vol. 14, no. 19, Oct. 2022, doi: 10.3390/POLYM14193994.

[66] N. Maldonado-Carmona, T. S. Ouk, and S. Leroy-Lhez, “Latest trends on photodynamic disinfection of Gram-negative bacteria: photosensitizer’s structure and delivery systems,” *Photochem. Photobiol. Sci. 2021 211*, vol. 21, no. 1, pp. 113–145, Nov. 2021, doi: 10.1007/S43630-021-00128-5.

[67] S. R. G. Fernandes, R. Fernandes, B. Sarmento, P. M. R. Pereira, and J. P. C. Tomé, “Photoimmunoconjugates: novel synthetic strategies to target and treat cancer by photodynamic therapy,” *Org. Biomol. Chem.*, vol. 17, no. 10, pp. 2579–2593, Mar. 2019, doi: 10.1039/C8OB02902D.

[68] P. M. R. Pereira, B. Korsak, B. Sarmento, R. J. Schneider, R. Fernandes, and J. P. C. Tomé, “Antibodies armed with photosensitizers: From chemical synthesis to photobiological applications,” *Org. Biomol. Chem.*, vol. 13, no. 9, pp. 2518–2529, Mar. 2015, doi: 10.1039/c4ob02334j.

[69] J. Sandland and R. W. Boyle, “Photosensitizer Antibody-Drug Conjugates: Past, Present, and Future,” *Bioconjug. Chem.*, vol. 30, no. 4, pp. 975–993, Apr. 2019, doi: 10.1021/acs.bioconjchem.9b00055.

[70] E. Ben-Hur and I. Rosenthal, “Photohemolysis of human erythrocytes induced by aluminum phthalocyanine tetrasulfonate,” *Cancer Lett.*, vol. 30, no. 3, pp. 321–327, Mar. 1986, doi: 10.1016/0304-3835(86)90057-1.

[71] A. J. Bullous, C. M. A. Alonso, and R. W. Boyle, “Photosensitiser-antibody conjugates for photodynamic therapy,” *Photochem. Photobiol. Sci.*, vol. 10, no. 5, pp. 721–750, May 2011, doi: 10.1039/c0pp00266f.

[72] C. M. A. Alonso, A. Palumbo, A. J. Bullous, F. Pretto, D. Neri, and R. W. Boyle, “Site-specific and stoichiometric conjugation of cationic porphyrins to antiangiogenic monoclonal antibodies,” *Bioconjug. Chem*, vol. 21, no. 2, pp. 302–312,.

[73] F. Giuntini, C. M. A. Alonso, and R. W. Boyle, “Synthetic approaches for the conjugation of porphyrins and related macrocycles to peptides and proteins,” *Photochem. Photobiol. Sci.*, vol. 10, no. 5, pp. 759–791, May 2011, doi: 10.1039/c0pp00366b.

[74] M. L. Embleton, S. P. Nair, B. D. Cookson, and M. Wilson, “Antibody-Directed Photodynamic Therapy of MethicillinResistant Staphylococcus aureus,” *Microb Drug Resist.*, vol. 10, no. 2, pp. 92–97, Aug. 2004, doi: 10.1089/1076629041310000.

[75] G. Kim, M. Karbaschi, M. Cooke, A. Gaitas, and P. P. Author, “Light-based Methods for Whole Blood Bacterial Inactivation Enabled by a Recirculating Flow System HHS Public Access Author manuscript,” *Photochem Photobiol*, vol. 94, no. 4, pp. 744–751, 2018, doi: 10.1111/php.12899.

[76] S. Khan, S. N. Khan, R. Meena, A. M. Dar, R. Pal, and A. U. Khan, “Photoinactivation of multidrug resistant bacteria by monomeric methylene blue conjugated gold nanoparticles,” *J. Photochem. Photobiol. B Biol.*, vol. 174, pp. 150–161, Sep. 2017, doi: 10.1016/J.JPHOTOBIOL.2017.07.011.

[77] A. Cantelli, F. Piro, P. Pecchini, M. Di Giosia, A. Danielli, and M. Calvaresi, “Concanavalin A-Rose Bengal bioconjugate for targeted Gram-negative antimicrobial photodynamic therapy,” *J. Photochem. Photobiol. B Biol.*, vol. 206, p. 111852, May 2020, doi: 10.1016/J.JPHOTOBIOL.2020.111852.

[78] S. P, K. S, G. R, D. T, and Y. M, “Targeted delivery of a photosensitizer to Aggregatibacter actinomycetemcomitans biofilm,” *Antimicrob. Agents Chemother.*, vol. 54, no. 6, pp. 2489–2496, Jun. 2010, doi: 10.1128/AAC.00059-10.
[79] “PATIENT INFORMATION SHEET Eosin.” www.whatsinsidescjohnson.com.
[80] “Introduction to Amine Modification—Section 1.1 - IT.”
[81] X. F. Zhang, J. Zhang, and L. Liu, “Fluorescence properties of twenty fluorescein derivatives: Lifetime, quantum yield, absorption and emission spectra,” *J. Fluoresc.*, vol. 24, no. 3, pp. 819–826, Feb. 2014, doi: 10.1007/s10895-014-1356-5.
[82] A. Penzkofer, A. Beidoun, and M. Daiber, “Intersystem-crossing and excited-state absorption in eosin Y solutions determined by picosecond double pulse transient absorption measurements,” *J. Lumin.*, vol. 51, no. 6, pp. 297–314, May 1992, doi: 10.1016/0022-2313(92)90059-I.
[83] F. Wilkinson, W. P. Helman, and A. B. Ross, “Quantum Yields for the Photosensitized Formation of the Lowest Electronically Excited Singlet State of Molecular Oxygen in Solution,” *J. Phys. Chem. Ref. Data*, vol. 22, no. 1, pp. 113–262, Jan. 1993, doi: 10.1063/1.555934.
[84] G. Porter, E. S. Reid, and C. J. Tredwell, “Time resolved fluorescence in the picosecond region,” *Chem. Phys. Lett.*, vol. 29, no. 3, pp. 469–472, Dec. 1974, doi: 10.1016/0009-2614(74)85147-X.
[85] F. Sperandio, Y.-Y. Huang, and M. Hamblin, “Antimicrobial Photodynamic Therapy to Kill Gram-negative Bacteria,” *Recent Pat. Antiinfect. Drug Discov.*, vol. 8, no. 2, pp. 108–120, Aug. 2013, doi: 10.2174/1574891x113089990012.
[86] “Methylene Blue Monograph for Professionals - Drugs.com.” https://www.drugs.com/monograph/methylene-blue.html?references=1#r1.
[87] J. P. Tardivo *et al.*, “Methylene blue in photodynamic therapy: From basic mechanisms to clinical applications,” *Photodiagnosis Photodyn. Ther.*, vol. 2, no. 3, pp. 175–191, Sep. 2005, doi: 10.1016/S1572-1000(05)00097-9.
[88] W. S. and J. R. Sutter, “Kinetic study of the monomer-dimer equilibrium of methylene blue in aqueous solution,” *J. Phys. Chem.*, vol. 83, no. 12, pp. 1573–1576, 1979, doi: DOI: 10.1021/j100475a004.
[89] L. R. R. Santin *et al.*, “Study between solvatochromism and steady-state and time-resolved fluorescence measurements of the Methylene blue in binary mixtures,” *Dye. Pigment.*, vol. 119, pp. 12–21, Aug. 2015, doi: 10.1016/J.DYEPIG.2015.03.004.
[90] B. S. Fujimoto, J. B. Clendenning, J. J. Delrow, P. J. Heath, and M. Schurr, “Fluorescence and Photobleaching Studies of Methylene Blue Binding to DNA,” *J. Phys. Chem*, vol. 98, no. 26, pp. 6633–6643, 1994.
[91] E. I. Alarcon, M. González-Béjar, P. Montes-Navajas, H. Garcia, E. A. Lissi, and J. C. Scaiano, “Unexpected solvent isotope effect on the triplet lifetime of methylene blue associated to cucurbit[7]uril,” *Photochem. Photobiol. Sci.*, vol. 11, no. 2, pp. 269–273, Jan. 2012, doi: 10.1039/C1PP05227F.
[92] V. Y. Gak, V. A. Nadtochenko, and J. Kiwi, “Triplet-excited dye molecules (eosine and methylene blue) quenching by H2O2 in aqueous solutions,” *J. Photochem. Photobiol. A Chem.*, vol. 116, no. 1, pp. 57–62, Jun. 1998, doi: 10.1016/S1010-6030(98)00230-5.
[93] G. A. Da Collina *et al.*, “Controlling methylene blue aggregation: a more efficient alternative to treat Candida albicans infections using photodynamic therapy,” *Photochem. Photobiol. Sci.*, vol. 17, no. 10, pp. 1355–1364, 2018, doi: 10.1039/C8PP00238J.
[94] S. VA, N. SD, M. AP, G. ML, and L. VB, “Antiviral photodynamic therapy: Inactivation and inhibition of SARS-CoV-2 in vitro using methylene blue and Radachlorin,” *Photodiagnosis Photodyn. Ther.*, vol. 33, p. 102112, Mar. 2021, doi: 10.1016/J.PDPDT.2020.102112.
[95] L. Chaiet and F. J. Wolf, “The properties of streptavidin, a biotin-binding protein produced by Streptomycetes,” *Arch. Biochem. Biophys.*, vol. 106, no. C, pp. 1–5, 1964, doi: 10.1016/0003-9861(64)90150-X.
[96] T. G. M. Schmidt *et al.*, “The role of changing loop conformations in streptavidin versions engineered for high-affinity binding of the Strep-tag II peptide,” *J. Mol. Biol.*, vol. 433, no. 9, p. 166893, Apr. 2021, doi: 10.1016/j.jmb.2021.166893.

[97] F. Liu, J. Z. H. Zhang, and Y. Mei, “The origin of the cooperativity in the streptavidin-biotin system: A computational investigation through molecular dynamics simulations,” *Sci. Rep.*, vol. 6, no. 1, pp. 1–11, Jun. 2016, doi: 10.1038/srep27190.
[98] “Biotinylation | Thermo Fisher Scientific - IT.” https://www.thermofisher.com/it/en/home/life-science/protein-biology/protein-biology-learning-center/protein-biology-resource-library/pierce-protein-methods/biotinylation.html.
[99] E. D. Lobo, R. J. Hansen, and J. P. Balthasar, “Antibody pharmacokinetics and pharmacodynamics,” *J. Pharm. Sci.*, vol. 93, no. 11, pp. 2645–2668, Nov. 2004, doi: 10.1002/jps.20178.
[100] G. Vidarsson, G. Dekkers, and T. Rispens, “IgG subclasses and allotypes: From structure to effector functions,” *Front. Immunol.*, vol. 5, no. OCT, p. 520, Oct. 2014, doi: 10.3389/fimmu.2014.00520.
[101] W. Choe, T. A. Durgannavar, and S. J. Chung, “Fc-Binding Ligands of Immunoglobulin G: An Overview of High Affinity Proteins and Peptides,” *Mater. (Basel, Switzerland)*, vol. 9, no. 12, p. 994, 2016, doi: 10.3390/MA9120994.
[102] A. Rita Cruz *et al.*, “Staphylococcal protein A inhibits complement activation by interfering with IgG hexamer formation,” *bioRxiv*, p. 2020.07.20.212118, Jul. 2020, doi: 10.1101/2020.07.20.212118.
[103] L. A. Marraffini, A. C. DeDent, and O. Schneewind, “Sortases and the Art of Anchoring Proteins to the Envelopes of Gram-Positive Bacteria,” *Microbiol. Mol. Biol. Rev.*, vol. 70, no. 1, pp. 192–221, Mar. 2006, doi: 10.1128/mmbr.70.1.192-221.2006.
[104] A. C. DeDent, M. McAdow, and O. Schneewind, “Distribution of protein A on the surface of Staphylococcus aureus,” *J. Bacteriol.*, vol. 189, no. 12, pp. 4473–4484, Jun. 2007, doi: 10.1128/JB.00227-07.
[105] Sigma!Aldrich, “CONCANAVALIN A.” https://www.sigmaaldrich.com/deepweb/assets/sigmaaldrich/product/documents/220/377/c2010pis.pdf.
[106] W. J. Reeder and R. D. Ekstedt, “Study of the Interaction of Concanavalin A with Staphylococcal Teichoic Acids,” *J. Immunol.*, vol. 106, no. 2, pp. 334–40, 1971.
[107] F. S. Coulibaly and B. B. C. Youan, “Concanavalin A - Polysaccharides Binding Affinity Analysis Using A Quartz Crystal Microbalance,” *Biosens. Bioelectron.*, vol. 59, pp. 404–411, Sep. 2014, doi: 10.1016/J.BIOS.2014.03.040.
[108] T. J. Silhavy, D. Kahne, and S. Walker, “The Bacterial Cell Envelope,” *Cold Spring Harb. Perspect. Biol.*, vol. 2, no. 5, p. a000414, 2010, doi: 10.1101/CSHPERSPECT.A000414.
[109] P. C. J. Leijh, T. L. Van Zwet, and R. Van Furth, “Effect of concanavalin A on intracellular killing of Staphylococcus aureus by human phagocytes.,” *Clin. Exp. Immunol.*, vol. 58, no. 3, p. 557, 1984.
[110] S. Abbruzzetti, S. Bruno, S. Faggiano, E. Grandi, A. Mozzarelli, and C. Viappiani, “Time-resolved methods in Biophysics. 2. Monitoring haem proteins at work with nanosecond laser flash photolysis,” *Photochem. Photobiol. Sci.*, vol. 5, no. 12, pp. 1109–1120, Dec. 2006, doi: 10.1039/B610236K.
[111] S. Abbruzzetti, S. Sottini, C. Viappiani, and J. E. T. Corrie, “Acid-induced unfolding of myoglobin triggered by a laser pH jump method,” *Photochem. Photobiol. Sci.*, vol. 5, no. 6, pp. 621–628, Jun. 2006, doi: 10.1039/B516533D.
[112] S. Lee and H. Kim, “Crosslinking of Streptavidin–Biotinylated Bovine Serum Albumin Studied with Fluorescence Correlation Spectroscopy,” *Bull. Korean Chem. Soc.*, vol. 42, no. 1, pp. 80–86, Jan. 2021, doi: 10.1002/BKCS.12164.
[113] M. Levitus, “Tutorial: Measurement of fluorescence spectra and determination of relative fluorescence quantum yields of transparent samples,” *Methods Appl. Fluoresc.*, vol. 8, no. 3, p. 033001, Jul. 2020, doi: 10.1088/2050-6120/ab7e10.
[114] O. Ciocirlan and O. Iulian, “Density, viscosity and refractive index of the dimethyl sulfoxide + o-xylene system,” *J. Serb. Chem. Soc*, vol. 74, no. 3, pp. 317–329, 2009, doi: 10.2298/JSC0903317C.
[115] V. T. Hoang *et al.*, “Optical Properties of Buffers and Cell Culture Media for Optofluidic and Sensing Applications,” *Appl. Sci.*, vol. 9, no. 6, p. 1145, Mar. 2019, doi: 10.3390/app9061145.
[116] G. R. Fleming, A. W. E. Knight, J. M. Morris, R. J. S. Morrison, and G. W. Robinson, “Picosecond Fluorescence Studies of Xanthene Dyes,” *J. Am. Chem. Soc.*, vol. 99, no. 13, pp. 4306–4311, 1977,

doi: 10.1021/ja00455a017.
[117] T. Gensch, C. Viappiani, and S. E. Braslavsky, “Laser Induced Optoacoustic Spectroscopy,” *Encycl. Spectrosc. Spectrom.*, pp. 1288–1296, Jan. 1999, doi: 10.1016/B978-0-12-374413-5.00361-4.
[118] L. Song, C. A. G. 0 Varma, A. J. W. Verhoeven, and H. J. Tanke, “Influence of the Triplet Excited State on the Photobleaching Kinetics of Fluorescein in Microscopy,” *Biophys. J.*, vol. 70, pp. 2959–2968, 1996, doi: 10.1016/S0006-3495(96)79866-1.
[119] R. W. Redmond and J. N. Gamlin, “A compilation of singlet oxygen yields from biologically relevant molecules,” *Photochem. Photobiol.*, vol. 70, no. 4, pp. 391–475, Oct. 1999, doi: 10.1111/j.1751-1097.1999.tb08240.x.
[120] I. E. B. Lucimara P.F. Aggarwal, Mauricio S. Baptista, “Effects of NaCl upon TPPS4 triplet state characteristics and singlet oxygen formation,” *J. Photochem. Photobiol. A Chem.*, vol. 186, no. 2–3, pp. 187–193, 2007.
[121] H. LG, F. SJ, and R. RG, “An introduction to Staphylococcus aureus, and techniques for identifying and quantifying S. aureus adhesins in relation to adhesion to biomaterials: review,” *Eur. Cell. Mater.*, vol. 4, pp. 39–60, 2002, doi: 10.22203/ECM.V004A04.
[122] A. Matsuhisa, Y. Saito, H. Ueyama, M. Yamamoto, T. Ohono, and A. Matsuhisa, “Binding of Streptavidin to Bacteria or Fungi and Its Applications in Detecting These Microbes,” *Microbiol. Immunol.*, vol. 37, no. 10, pp. 765–772, 1993, doi: 10.1111/j.1348-0421.1993.tb01703.x.
[123] R. Alon, E. A. Bayer, and M. Wilchek, “Streptavidin contains an RYD sequence which mimics the RGD receptor domain of fibronectin,” *Biochem. Biophys. Res. Commun.*, vol. 170, no. 3, pp. 1236–1241, Aug. 1990, doi: 10.1016/0006-291X(90)90526-S.
[124] ATTO-TEC, “ATTO MB2.” https://www.atto-tec.com/fileadmin/user_upload/Katalog_Flyer_Support/ATTO_MB2.pdf.
[125] M. D. Laramie, M. K. Smith, F. Marmarchi, L. R. McNally, and M. Henary, “Small Molecule Optoacoustic Contrast Agents: An Unexplored Avenue for Enhancing In Vivo Imaging,” *Molecules*, vol. 23, no. 11, p. 2766, Oct. 2018, doi: 10.3390/MOLECULES23112766.
[126] Megazyme, “Concanavalin A.” https://www.megazyme.com/documents/Data_Sheets/L-CONA-200MG_DATA.pdf.
[127] A. Gollmer, A. Felgenträger, W. Bäumler, T. Maisch, and A. Späth, “A novel set of symmetric methylene blue derivatives exhibits effective bacteria photokilling - A structure-response study,” *Photochem. Photobiol. Sci.*, vol. 14, no. 2, pp. 335–351, Feb. 2015, doi: 10.1039/C4PP00309H/METRICS.
[128] M. Bostad *et al.*, “Light-triggered, efficient cytosolic release of IM7-saporin targeting the putative cancer stem cell marker CD44 by photochemical internalization,” *Mol. Pharm.*, vol. 11, no. 8, pp. 2764–2776, Aug. 2014, doi: 10.1021/MP500129T.
[129] D. Gao *et al.*, “A near-infrared phthalocyanine dye-labeled agent for integrin αvβ6-targeted theranostics of pancreatic cancer,” *Biomaterials*, vol. 53, pp. 229–238, Jun. 2015, doi: 10.1016/J.BIOMATERIALS.2015.02.093.
[130] A. R. Santos *et al.*, “Application of Response Surface Methodology to Evaluate Photodynamic Inactivation Mediated by Eosin Y and 530 nm LED against Staphylococcus aureus,” *Antibiot. (Basel, Switzerland)*, vol. 9, no. 3, Mar. 2020, doi: 10.3390/ANTIBIOTICS9030125.
[131] M. L. Embleton, S. P. Nair, B. D. Cookson, and M. Wilson, “Selective lethal photosensitization of methicillin-resistant Staphylococcus aureus using an IgG-tin (IV) chlorin e6 conjugate,” *J. Antimicrob. Chemother.*, vol. 50, no. 6, pp. 857–864, Dec. 2002, doi: 10.1093/JAC/DKF209.
[132] P. Dharmaratne *et al.*, “Contemporary approaches and future perspectives of antibacterial photodynamic therapy (aPDT) against methicillin-resistant Staphylococcus aureus (MRSA): A systematic review,” *Eur. J. Med. Chem.*, vol. 200, Aug. 2020, doi: 10.1016/J.EJMECH.2020.112341.
[133] J. R. Lakowicz, *Principles of fluorescence spectroscopy*. Springer, 2006.
[134] P. Schwille and E. Haustein, “Fluorescence Correlation Spectroscopy An Introduction to its Concepts and Applications,” *Spectroscopy*, vol. 94, no. 22, 2001.
[135] Edinburgh Photonics, “Laser Flash Photolysis Spectrometer.” .
[136] S. Nonell and S. E. Braslavsky, “Time-resolved singlet oxygen detection,” in *Methods in enzymology*,

vol. 319, Methods Enzymol, 2000, pp. 37–49.
[137] M. W. D. John R. Allen, Joel S. Silfies, Stanley A. Schwartz, “Single-Molecule Super-Resolution Imaging | Nikon’s MicroscopyU.”

Index of figures

Index of tables

List of publications

Published paper directly related to the thesis

- Mussini A, Uriati E, Hally C, Nonell S, Bianchini P, Diaspro A, Pongolini S, Delcanale P, Abbruzzetti S, Viappiani C. *Versatile Supramolecular Complex for Targeted Antimicrobial Photodynamic Inactivation*. Bioconjug Chem. 2022 Apr 20; 33(4): 666-676. doi:10.1021/acs.bioconjchem.2c00067

Other published papers and short paper

- Delcanale P, Uriati E, Mariangeli M, Mussini A, Moreno A, Lelli D, Cavanna L, Bianchini P, Diaspro A, Abbruzzetti S, Viappiani C. *The Interaction of Hypericin with SARS-CoV-2 Reveals a Multimodal Antiviral Activity*. ACS Appl Mater Interfaces. 2022 Mar 30; 14(12): 14025–32. doi:10.1021/ACSAMI.1C22439
- Mussini A, Uriati E, Bianchini P, Diaspro A, Cavanna L, Abbruzzetti S, Viappiani C. *Targeted photoimmunotherapy for cancer*. Biomol Concepts. 2022 Mar 19; 13(1): 126–47. doi:10.1515/BMC-2022-0010
- Mussini A, Hally C, Viappiani C, Nonell S, Agut Bonsfills M, Abbruzzetti S. *Photosensitizing proteins for a targeted antibacterial photodynamic inactivation*. Nuovo Cimento C. 2021 Aug 13; 4-5. doi: 10.1393/ncc/i2021-21122-6

Poster communication at congresses

- Mussini A, Uriati E, Hally C, Nonell S, Bianchini P, Diaspro A, Pongolini S, Delcanale P, Abbruzzetti S, Viappiani C. *Protein based targeted delivery system for antimicrobial PDT*. 6th Photobiology School, Brixen (Italy), August 21st-27th 2022
- Mussini A, Delcanale P, Abbruzzetti S, Viappiani C, Uriati E, Mariangeli M, Bianchini P, Diaspro A, Lelli D, Moreno A. *Binding of hypericin against SARS-CoV-2*. XXV Congresso Nazionale SIBPA 2021, Parma (Italy) June 28th – July 21st 2021
- Mussini A, Uriati E, Hally C, Nonell S, Bianchini P, Diaspro A, Pongolini S, Delcanale P, Abbruzzetti S, Viappiani C. *Protein based targeted delivery system for antimicrobial PDT*. 13th European Biophysics Conference, Vienna (Austria), July 24th-28th 2021
- Mussini A, Uriati E, Hally C, Nonell S, Bianchini P, Diaspro A, Pongolini S, Delcanale P, Abbruzzetti S, Viappiani C. *Protein based targeted delivery system for antimicrobial PDT*. 19th Congress of the European Society for Photobiology, Salzburg (Austria), August 30th – September 3rd 2021

Acknowledgements

I want to thank the University of Parma and the IQS (Chemical Institute of Sarriá, School of Engineering University Ramon Llull) for having been able to participate in the co-tutelle program. I also thank Azienda USL di Piacenza and Fondazione di Piacenza e Vigevano for the financial support of the PhD project.
I sincerely thank the Biophysics group of the University of Parma and the Applied Photobiological Chemistry group of IQS. I also really want to thank my supervisors Professor Cristiano Viappiani and Professor Santi Nonell Marrugat for being incredibly helpful, for all the support they gave me and for everything they taught me.
Most of the photophysical characterization was carried out at the University of Parma, Department of Mathematical, Physical and Computer Sciences, group of Biophysics under the supervision of Professors Cristiano Viappiani and Stefania Abbruzzetti and the collaboration of the Researcher Pietro Delcanale and the PhD student Manuela Maria Alampi.
The singlet oxygen and the bacterial photoinactivation experiments were conducted at the IQS School of Engineering (Ramon Llull University), Department of Analytical and Applied Chemistry, group of Applied Photobiological Chemistry under the supervision of the Professor Santi Nonell Marrugat and the collaboration of the PhD students Cormac Hally Garcia and Mireia Jordà Redondo.
The microscopy measurements were conducted at the Italian Institute of Technology (Genoa), group of Nanoscopy under the supervision of the Professors Alberto Diaspro and Paolo Bianchini by the PhD students Eleonora Uriati and Matteo Mariangeli.

«A long time ago the atoms in your body were spread across trillions of kilometers of otherwise empty space. Billions of years in the past there was no hint that they would eventually come to be configured as your eyes, your skin, your hair, your bones, or the eighty-six billion neurons of your brain. Many of these atoms came from deep inside a star—perhaps several stars, themselves separated by many trillions of kilometers. As these stars exploded, they hurled matter outward in a flood of scorching gas that filled a small part of one galaxy out of hundreds of billions of other galaxies, arrayed throughout a gaping maw of space and time almost a trillion kilometers across.

[...]

They've been in the shell of a trilobite, perhaps thousands of trilobites. They've been in tentacles, roots, feet, wings, blood, and trillions, quadrillions of bacteria in between. Some have floated in the eyes of creatures that once looked out across the landscapes of a hundred million years ago. Yet others have nestled in the yolks of dinosaur eggs or hung in the exhaled breath of a panting creature in the depths of an ice age. For other atoms this is their first time settling into a living organism, having drifted through eons in oceans and clouds, part of a trillion raindrops or a billion snowflakes.

Now, at this instant, they are all here, making you.»

Scharf, Caleb A.; illustrations by Ron Miller (2017). *The Zoomable Universe: An Epic Tour Through Cosmic Scale, from Almost Everything to Nearly Nothing*. New York: Scientific American / Farrar, Straus and Giroux.